Light responsive polymers : from molecule to device

Light Responsive Polymers

From Molecule to Device

PROEFSCHRIFT

ter verkrijging van de graad van doctor aan de Technische Universiteit Eindhoven, op gezag van de rector magnificus prof.dr.ir. F.P.T. Baaijens, voor een commissie aangewezen door het College voor Promoties, in het openbaar te verdedigen op woensdag 18 april 2018 om 16:00 uur

door

Jeroen ter Schiphorst

Geboren te Arnhem

Dit proefschrift is goedgekeurd door de promotoren en de samenstelling van de promotiecomissie is als volgt:

Voorzitter:	prof. dr. N.A.J.M. Sommerdijk
1e promotor:	prof. dr. A.P.H.J. Schenning
2e promotor:	prof. dr. D.J. Broer
Onafhankelijke leden:	prof. dr. D. Diamond (Dublin City University)
	dr. ir. L.M.W. Scheres (Surfix B.V.)
	prof. dr. ir. J.M.J. den Toonder
Overig lid	dr. R. Klajn (Weizmann Institute of Science)
Adviseur	dr. D. Liu

Het onderzoek of ontwerp dat in dit proefschrift wordt beschreven is uitgevoerd in overeenstemming met de TU/e Gedragscode Wetenschapsbeoefening.

A catalogue record is availible from the Eindhoven University of Technology Library.

ISBN: 978-94-6233-913-2

The research described in this thesis has been financially supported under the European Union's Seventh Framework Programme for research, technological development and demonstration, through the NAPES project grant agreement no. 604241.

Summary

Light Responsive Polymers

From Molecule to Device

Light provides the energy necessary for life on our planet. Light is also an important and powerful tool in science, for instance for measuring and for changing substances. Light responsive materials can change their shape, size, or appearance under the influence of illumination. In this thesis, light is used as a tool to set matter into motion.

The research described in this thesis is based on two different materials; hydrogels and liquid crystal networks. Hydrogels are soft materials where motion is based on absorbance and release of water. They are known for their capability to induce large changes in size when switching from a hydrophilic state to hydrophobic state and are of particular interest for drug delivery, microfluidic applications, and switchable surfaces. The light responsive behavior in hydrogels can be achieved using spiropyran based molecules. These molecules are capable of switching between predominantly hydrophilic and hydrophobic states using light, changing the overall character of the hydrogel, allowing reversible and repeatable swelling and shrinking. In contrast, the used liquid crystal materials are glassy polymers in which the motion is based on the generation of stresses, disorder, and free volume in the coating. Liquid crystal networks are most known for their use in display applications, but are found to be very interesting scaffolds for bio-materials, allowing cell culturing. In contrast to hydrogels, liquid crystal networks can operate in a solvent free environment and are relatively inert. However, due to their glassy nature, motion is limited, requiring strong light sources to deform. The light responsive behavior can be achieved by incorporating azobenzene molecules in the network, pushing and pulling harmoniously on the materials, thus generating structures.

In this thesis, Chapter 1 provides an overview of the development of light responsive polymers with a focus on hydrogel based materials for microfluidic applications.

In Chapter 2, the process of molecular design is described to achieve micro valves that are capable of switching on and off a specific flow in microfluidic devices. For this, spiropyran molecules are selected that have isomerization kinetics in similar ranges, allowing the gel to shrink and swell in similar time frames, in strong contrast to previously reported systems that opened within seconds, but closing took hours.

In Chapter 3, the optimized molecule developed in Chapter 2 is used to create hydrogel valves that can be opened rapidly, kept open at a certain flow rate and quickly closed again. Solely due to the correct molecular kinetics of both the forward and backward reaction of

the isomerization, a forced oscillation is generated using pulsed light frequencies in the timeframe of seconds, which can be sustained for an extended period of time (hours).

In Chapter 4, the need of micromixers is illustrated. Mixing of two water streams is often considered to be relatively easy, but in microfluidics, due to the non-chaotic behavior of fluids, two separate fluids can be remain separated over several meters in a channel. To induce mixing, structured surfaces are found to be useful, but are always static. This chapter describes a responsive hydrogel filled structures capable of switching from a mixing state to a non-mixing state, allowing the user to determine whether or not the fluids should be mixed or kept separated.

Chapter 5 shows that hydrogel based materials are not limited to microfluidic applications, but can be also grafted from a cotton fiber, by first modifying the cotton fiber with an initiator and subsequently using ARGET-ATRP to form a polymer from this reactive center. Hydrogels are generated that are able to absorb considerable amounts of water, which can be released either by illumination with artificial light sources, or simply by non-focused irradiation of the sun. Here the challenge is to graft polymers using metal based catalysts in the presence of spiropyran, a molecule that is known to bind ions.

Chapter 6 describes liquid crystalline polymer coatings that are of interest for cell manipulation. In detail, a hierarchical structured pillared surface is made that shows the capability of cell adhesion and alignment. The nano-roughness is playing a subtle but key role in the cell movement rate and experiments are successfully performed to switch this material in nano-roughness in the presence of living cells.

Chapter 7 is the technology assessment, discussing the impact of the research in more detail. In this chapter, the advantages, limitations, and improvements of the materials studied are discussed, as well as the market readiness level of hydrogel valves. Furthermore, additional directions for future work based on a molecule to device approach are presented.

Table of Content

Chapter 1

General introduction

This chapter is partially reproduced from:

'Photoresponsive Polymer Hydrogel Coatings that Change Topography' J.E. Stumpel, J. ter Schiphorst and A.P.H.J. Schenning, Book chapter 7, *Wiley-WCH*, 2017, 159-173. ISBN: 978-3-527-33869-6.

and

'Light-responsive polymers for microfluidic applications' J. ter Schiphorst, J. Saez, D. Diamond, F. Benito-Lopez and A.P.H.J. Schenning, *Lab Chip*, 2018, **18**, 699-709.

1.1 Introduction

Polymer materials play an important role in our society by providing us with the opportunity to create, protect and decorate everyday objects. Their properties are often determined by the surface topography, chemistry and composition of the material. Recently, the development of stimulus-responsive polymer materials received considerable attention.[1–4] In this category of materials, the properties change in response to an external stimulus, for instance temperature,[4–6] light,[7–12] or pH.[6,13] The properties can be adjusted depending on the needs of the user or by environmental changes. It is expected that these materials will play an important role in meeting societal challenges in the field of sustainable energy, health care, food safety and water management. For instance, stimuli responsive polymers that change shape are attractive for microfluidic based analytica platforms to monitor water quality. By using such polymers as low cost components for instance as a valve allows strong reduction in the costs of these devices (*vide infra*).

An appealing stimulus for these polymers is light, as it can be applied locally in a non-contact fashion. The immediate chemical environment of the polymer films doesn't need to change and integration of complex electrodes or heating elements, in case of electricity or temperature as a stimulus, is not required. Especially the latter is increasing the complexity and costs when these elements are embedded in a device. In particular, photo-induced volumetric changes, surface roughness and polarity of the material are of interest, as this opens a wide field of applicability, especially for microfluidics, which operate in a compatible size regime.[14,15] For preparing light responsive polymers often photochromic dyes are embedded in the polymer matrix. Two popular dyes that have been used are spiropyrans and azobenzenes. The photochromic molecule determines the responsive character of the material and can be chemically modified to change the required wavelength needed to actuate the material, or to enhance the kinetics. As responsive polymers, hydrogels and liquid crystals have been used. This chapter will focus on hydrogel based materials as this is the main part of this PhD research, while for light responsive liquid crystalline polymers the reader is refered to a recent review.[16,17]

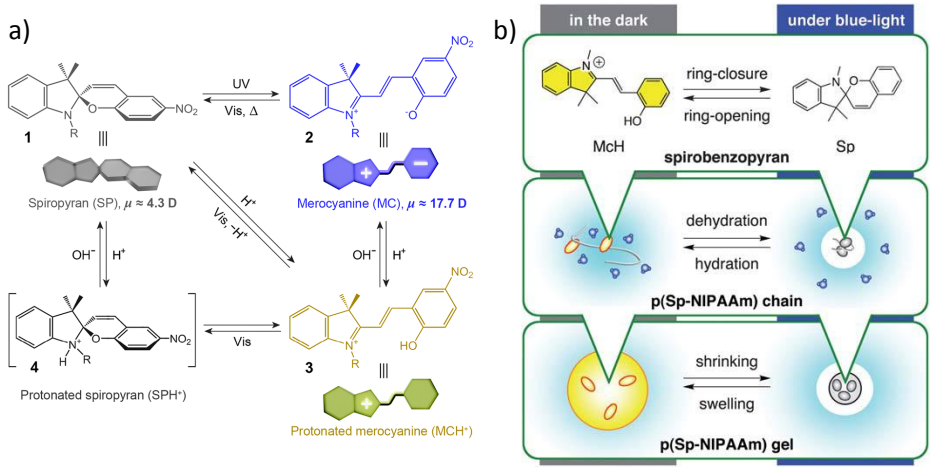

Figure 1.1. a) Different isomerisation mechanisms of a spiropyran (gray) to the merocyanine (blue), protonated merocyanine (orange) and protonated spiropyran (black). For the work of this thesis, the pathway from protonated merocyanine to spiropyran is used. b) Effect of the protonated merocyanine and spiropyran on a NIPAM polymer, showing the posibility to switch the hydration state with light. This effect can be translated to for instance valves, mixers and cotton. a) Copyright 2014, b) copyright 2011, Royal Society of Chemistry.

Volumetric and dimensional changes in hydrogels are caused by swelling and shrinkage due to absorption or release of water. To induce photoresponsivity into a hydrogel, metal nanoparticles, *e.g.* gold nanoparticles, which can transfer light into heat, or photochromic dyes which change their properties upon light exposure can be incorporated in the material.[15,18–21] Dyes are interesting as they can result in changes in the material, without large changes in the temperature, which is important for analytical and biological applications. The most commonly used dyes in photoresponsive materials are azobenzene derivatives, undergoing *trans-cis* isomerisation which changes the shape of the molecule, and hydrophobic spiropyran derivatives, which isomerise into the hydrophilic merocyanine form, changing the polarity of the system (Figure 1.1a). When spiropyran is added to a hydrogel, isomerisation of the photochromic dye (molecule) leads to an alteration of the materials properties as a result of a polarity change of the dye, causing water uptake or release and therefore a volumetric change (material) (Figure 1.1b).
In this chapter, a brief overview of the principles and potential applications of photoresponsive hydrogels is provided. In the first part of this chapter, the operating mechanisms in light responsive hydrogels will be discussed. In the second part the potential microfluidic applications of light responsive hydrogels will be presented as this is also the main part of this thesis. The final section sets out the aim and structure of the thesis.

1.2 Light responsive hydrogels

Hydrogels are polymer networks that are swollen with water and possess properties similar to natural tissue due to their large water content. In general, this results in the possibility of

large dimensional changes, but also relativly poor mechanical properties due to this large water content. The ability of hydrogels to absorb water arises from hydrophilic functional groups attached to the polymeric backbone. These three-dimensional cross-linked hydrophilic polymer networks are capable of swelling or de-swelling reversibly in water. A commonly used monomer for the preparation of photoresponsive polymer hydrogel networks is N-isopropylacrylamide (NIPAM), of which the corresponding polymer (pNIPAM) possesses well-studied thermoresponsive changes in hydrophilicity. Depending on the temperature, this polymer will either form intermolecular hydrogen bonds with water (hydrophilic polymer) or intramolecular hydrogen bonds with itself or other polymer chains (hydrophobic polymer). This transition is called the lower critical solution temperature (LCST) and occurs around 30-35°C. Several methods have been developed in order to make hydrogel photoresponsive. This can be divided into two main principles: transferring light into heat or inducing molecular alteration *e.g.* isomerisation of a photochromic dye.

A facile and elegant method to prepare films which indirectly responds to light is by selecting a substrate that can transfer light into heat. pNIPAM films have been prepared on a substrate with light-absorbing CrO_2-patterns which convert light into heat.[22] In these materials, photo-exposure results in local heating of the substrate, which causes the partial shrinkage of the films and therefore changes in the surface topography (Figure 1.2). Since the thermal effect is initiated from the bottom of the films, the response of the surface topography strongly depends on the thickness of the hydrogel layer. Conversion of light into heat has been used more regularly in pNIPAM hydrogel films, by implementing inorganic nanomaterial into the hydrogel, leading to, for instance photoresponsive valves in microfluidic devices or photo-induced buckling in films (*vide infra*).[23–25]

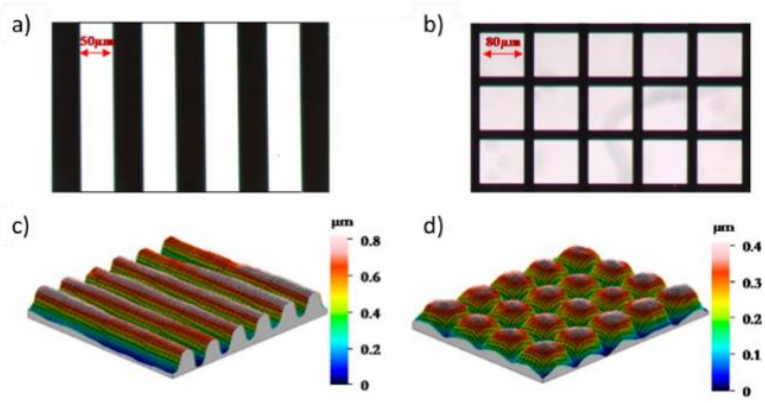

Figure 1.2. Images of light responsive surfaces consisting of patterned CrO_2 in a) striped and b) square configurations. The dark lines represent CrO_2. Before actuation, both surfaces were coated with polyNIPAM films, of which the thickness upon immersion in water was 4 and 16 μm, respectively. The corresponding 3D surface topographic images during the photo actuation of these films are shown in c) and d), respectively. Copyright 2013, American Chemical Society.

A second method to create photoresponsive hydrogels is the incorporation of a photochromic dye. Early investigations of the incorporation of spiropyran in pNIPAM, immersed in slightly acidic media, resulted in the development of photoresponsive hydrogel films.[7,9] The working mechanism for the swelling and shrinkage observed in the hydrogel is shown schematically in Figure 1.1b. In an acidic environment, the hydrophobic UV-absorbing spiropyran spontaneously isomerizes into hydrophilic visible light absorbing protonated merocyanine (McH^+). Exposure to visible light leads to the formation of spiropyran. When the source of actuation is removed, the in an acidic environment more stable McH^+ is formed again. By incorporation in a linear NIPAM polymer chain, spiropyran and McH^+ can induce the dehydration and hydration of the entire polymer chain, caused by the large difference in polarity between the two isomers. A crosslinker can be copolymerized to obtain a polymer network which forms the hydrogel. The photochromic behavior *e.g.* kinetics and absorption wavelengths of spiropyran can be fine-tuned by adding electron-donating or electron-withdrawing groups on the benzene rings of the molecule or by making adjustments in the molecular composition of the hydrogels.[10,26]

Photoresponsive polymer hydrogels are also used for biomedical applications. These materials are used to control biological activity and the immobilization of proteins and antibodies. They could also be used to modulate the growth of bacteria and cells and, indeed, photoresponsive hydrogel structures have been used for controlled cell culturing, which requires closely-controlled conditions as cells are highly sensitive to changes in their surroundings.[3,27] The hydrophilicity and surface topography of substrates used for cell growth are therefore of crucial importance. A material which can reversibly switch its properties between cell-attractive and cell-repellent properties is interesting as a functional substrate for tissue engineering.[28] Poly(spiropyran-NIPAM) hydrogel films have been reported with the possibility to control cell adhesion.[28] The spiropyran form is the most stable isomer at neutral pH. UV exposure results in the isomerization of spiropyran into the zwitterionic merocyanine. Patterned illumination results in a difference of cell adhesion at the different areas (Figure 1.3 a-c). After a subsequent washing step, the majority of the cells are left on the UV-exposed areas of the surface and the cell population is 20 times higher than in the non-exposed areas. This effect is most probably caused by the zwitterionic merocyanine causing more hydrophilic regions, which have a higher affinity to the cells, although the exact mechanism is not yet fully understood. To improve on the mechanical stability of hydrogels, a copolymer of acrylamide (AAm), 2-vinyl-4,6-diamino-1,3,5-triazine (VDT), spiropyran and poly(ethylene glycol) (PEG) was created where AAm and VDT can form hydrogen bonds, increasing the stiffness. Repeated illumination with visible and UV-light gives cell adhesion and detachment as well as a change in contact angle (Figure 1.3d-e). Interestingly, the hydrogen bonds of VDT also allowed complexes of PolyVDT/pDNA to be bound and released under influence of light, allowing reverse gene transfection.[29]

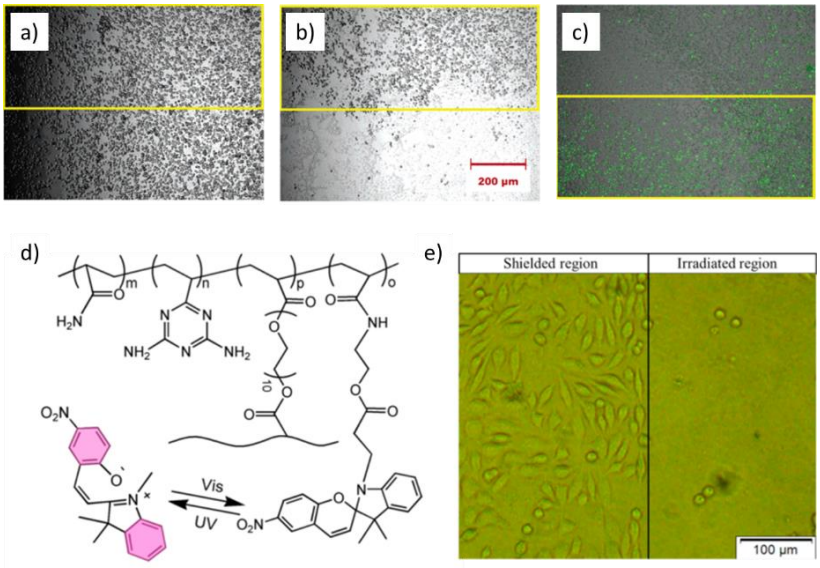

Figure 1.3. Microscopic images of a photoresponsive culture surface a) before and b) after regional UV irradiation and c) after a second regional UV irradiation. Yellow rectangles indicate UV-irradiated regions. d) Molecular structure of P(AAm-co-VDT-co-SPAA) hydrogels and e) microscopy images of mouse fibroblast L929 cells on the PAVSP hydrogel surface after regional cell detachment. (a-c) Copyright 2005, (d-e) copyright 2014, American Chemical Society.

1.3 Light responsive polymers for microfluidic applications

Microfluidic devices have been the subject of intense research activities during recent years. They perform complex measurements faster, with less waste generation and at lower cost. This is achieved through miniaturization and parallelization of processes, resulting in highly efficient, high throughput, accurate, and controllable analytical measurements.[30–33] However, these devices typically require external components to fulfil critical functions, resulting in a chip-in-a-lab, rather than a lab-on-a-chip (Figure 1.4). This makes these devices limited for use in hand-held devices or in-situ measurements, where interest is more towards large scale deployment with high sample frequency, rather than achieving the highest possible accuracy. A good example is the need for in-situ monitoring of water quality in lakes or rivers, which at present is performed by manual sampling, typically once every 3 months, often missing spikes in pollution or giving misleading information when sampling at a temporary point of high or low pollution. The ideal scenario is to deploy sensors at multiple locations to provide information for citizens through the internet. At present, this is limited by the high cost of the measuring platforms, which can be more than €20.000 per unit. Clearly there is a need to drive down unit costs significantly, towards a more acceptable €2000 or less. In order to achieve this, new materials and concepts for microfluidic devices are required.[34]

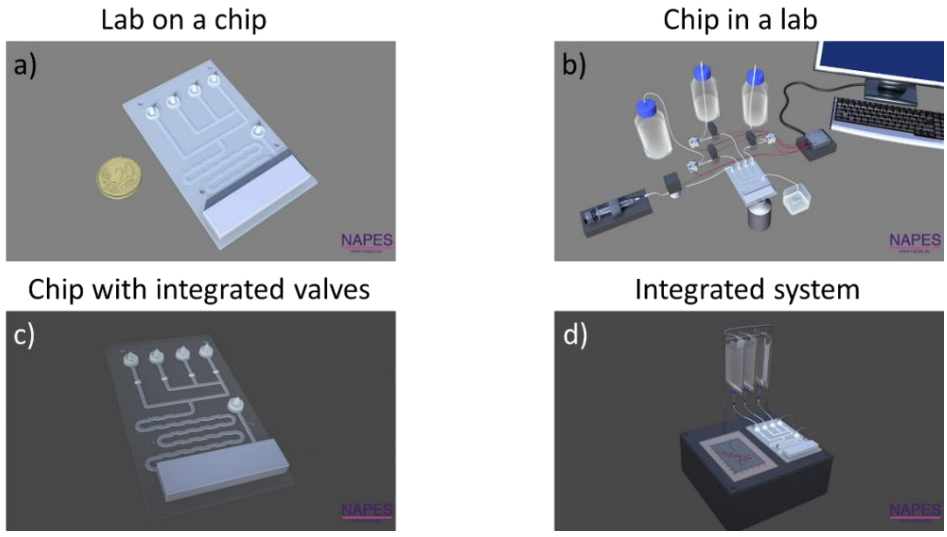

Figure 1.4. a) Example of a microfluidic chip set-up, consisting of several inlets, a mixing unit, an optical detection system and an outlet for reagent based measurements, b) connected to a measuring system, resulting in a chip in a lab. Multiple pumps and valves are required to adjust the flow rates. Chip with integrated valves c), allowing local illumination to modify the flow rate resulting in a completely d) integrated hand-held system. Copyright 2018, Royal Society of Chemistry.

Often, while the microfluidic device itself may be small, the equipment required to use the device itself is large, *e.g.* pumps, valves and mixing components. Moreover, the requirement of microscopes or other sophisticated optical or electronical elements for detection are drawbacks for the practical use of microfluidic technology outside the laboratory. Therefore, the combination of detection units with conventional valves, pumps and mixers components, limits the scalability and prospects for the generation of relevant products based on microfluidics. Another key factor to be considered for autonomous devices placed in remote locations is the total energy consumption of the device. That energy should be as low as possible in order to develop battery powered devices, capable of functioning indefinitely through localized energy scavenging.

An important factor to be considered, which is common for all the already cited requirements, is the limited use of new approaches to overcome these drawbacks, which unfortunately continue to appear in most of the microfluidic devices published in the literature. For instance, valves are often located off-chip, which is not scalable to more complex fluidic designs, and approaches that integrate large numbers of valves tend to require off-chip connections for actuation (*e.g.* pressure source).[35] Combining fully integrating valves inside the channel with simple actuation control is therefore a very attractive option for advancing microfluidics (Figure 1.4c-d).

Recent research has shown that the integration of responsive materials within microfluidic devices can lead to the development of novel in-situ, microscale mechanical components with the potential to produce vastly simplified and highly efficient fluidic chip

configurations.[7,15,36,37] The use of integrated responsive materials requires less energy for operation and less dead volume through the elimination of significant amounts of tubing and inter-connects. The development of such smart devices reduces the unit cost, platform dimensions and complexity, in comparison to existing microfluidic devices. Such advances also open the way to a more modular approach to creating microfluidic devices, where the chip can be redesigned and replaced on the platform, allowing exchange of the chip unit and/or components in a cartridge form.

In analytical applications, microfluidic platforms typically perform several key operations. At the device front end, sampling, sample preparation, valving, mixing and transport is performed, while at the back end, analyte detection takes place. Stimuli-responsive materials can be used for several of these functions, and increasing interest in this topic is reflected in the rising number of publications in recent years, emerging since 2004. To actuate these materials, several stimuli have been used e.g. temperature, pH, magnetic fields, electricity, and light. Light is particularly interesting, as it allows control over the components, without changing the interior conditions of the channel. Furthermore, light and temperature effects can be strongly linked, as light can also be used to induce a localized thermal response.

Over the recent years, several reviews on responsive materials for microfluidics have been published.[15,19,38–42] The most recent overview of responsive materials for microfluidics was given by Hilber[43] in 2016, entitled "Stimulus-active polymer actuators for next-generation microfluidic devices". In this excellent overview of materials, similar unsolved problems that are currently still relevant are stated e.g. "studies addressing this issue identified the lack of standardization and integration as the main barriers of acceptance by the end user and thus to commercial breakthrough" and "The operator may face difficulties in connecting the microfluidic device to ancillary hardware, such as external supplies, valves, pumps and other microfluidic devices". This is in agreement with the current vision of generating an integrated microfluidic device, where all parts such as valves and mixers are inside the chip, rather than having these components as external pieces.

1.3.1 Microvalves

Valves are used to ensure that liquids are at the correct place, at the correct time, within the microchannel network of a microfluidic device. Valves regulate fluid movement inside the microfluidic channel, determining whether or not a fluid is allowed to pass, as well as the amount of fluid that passes per unit time. Often, a microfluidic device is set-up in such a way, that fluids from different sources (e.g. sample, reagent) must be thoroughly mixed to enable subsequent detection by optical techniques. To achieve this, a microfluidic chip will require multiple valves and as the complexity of the system increases (*e.g.* multistage reagent addition, multicomponent analysis), valving requirements also become more demanding. Several valve configurations currently in common use are *e.g.* solenoid valves, screw valves, pneumatic valves[35] and recently hydrogel valves.[7,10] Depending on the applied pressures, desired accuracy, actuation speed, and price that the user is willing to pay, a suitable valve

can be selected for the desired application. When for instance a single use sensor is used and multiple measurements through time are required, already 30 valves for one measurement per day for a month are required. To achieve this high degree of parallelization, a price of only a couple of cents per valve is allowed when the price of the device is decisive. To drive down the cost and energy consumption of the device, pneumatic and hydrogel valves are particularly interesting as they can be applied cheaply and allow parallelization without driving the price up too much. Especially hydrogel valves are interesting, as the valve is closed when not being addressed and can be opened using low energy consumption light emitting diode (LED) illumination. Recently big steps have made to implement these valves in a microfluidic set-up for advanced flow control.

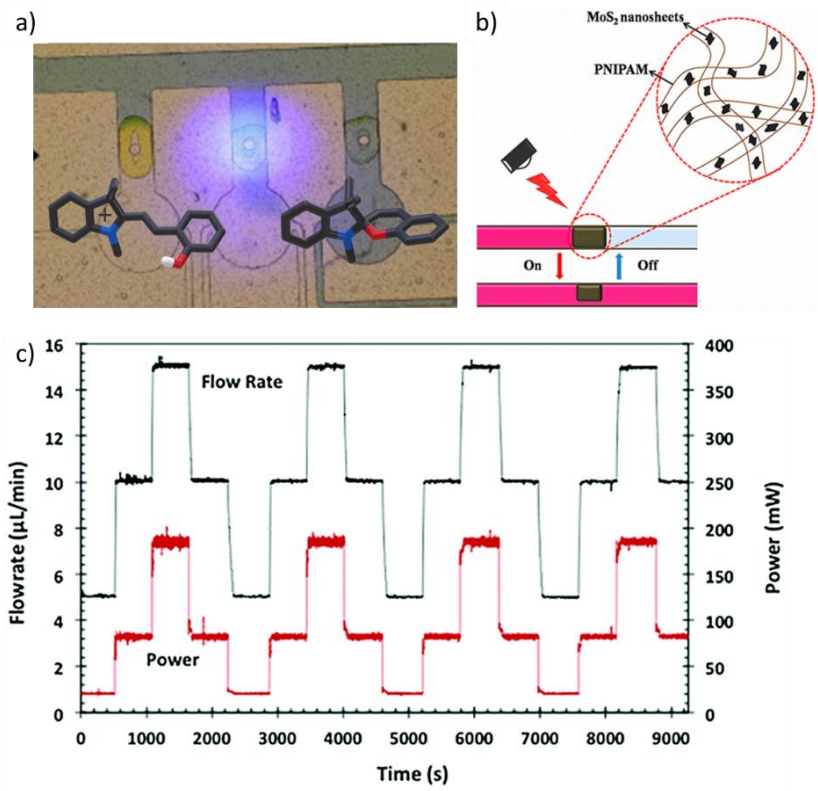

Figure 1.5. Light responsive hydrogels for microfluidic applications. a) Light responsive valves based on pNIPAM and spiropyran, showing rapid opening upon illumination with blue light, but require several hours to close, working in an acidic environment. b) Light responsive pNIPAM valve containing MoS_2 nanosheets, resulting in light induced thermal actuation of the valve. c) Hydrogel valve containing a fast light responsive spiropyran moiety, operating in a neutral environment, allowing precise control over the flow rate using a feedback loop. a) Copyright 2007, Elsevier, b) copyright 2016, American Chemical Society, c) copyright 2017 Royal Society of Chemistry.

As implementing local heating units requires complex on-chip set-ups, making a modular approach of a microfluidic chip on a platform harder, a different stimulus is desired, which can be applied ex-situ and in a non-contact fashion. This can be achieved by using photo-thermal components [25,44,45] (Figure 1.5b) or by incorporating photochromic dyes that change

polarity.[21] In 2007, Sugiura and co-workers[7] showed an elegant way of generating a photoresponsive microvalve that can be controlled by local irradiation of light (Figure 1.5a). By incorporating a spiropyran based moiety in the hydrogel and flowing acidic water through the channel, the protonated hydrophilic merocyanine is formed. This results in a swollen hydrogel due to the absorption of water and therefore closing of the microchannel. By illumination with either blue or white light, the hydrophobic spiropyran is formed leading to shrinkage of the hydrogel and a valve was achieved that opened within seconds, but closes in several hours, limiting the practical use of these valves. Furthermore, an acidic environment might be not always desired and many biological processes occur at neutral pH's. Ziółkowski and co-workers[46] showed in 2013 that incorporation of acrylic acid in the backbone of the hydrogel allowed usage of these materials at neutral pH, as the acid acts as an internal proton donor, providing the required protons to stabilize the protonated merocyanine. Furthermore, in 2011, Satoh and co-workers[26,47] showed that the swelling of the hydrogel (and closing of the channel) can be sped up enormously by chemically modifying the spiropyran dye, whereby now the isomerization kinetics in both directions are within the same order of magnitude. This study together with the work of Ziółkowski [46] and Sugiura[7] where the foundation of the development of the current state of the art light responsive hydrogels that allow manipulation of fluid within a timescale of seconds at high accuracy. Combined with the recent developments on computer platforms e.g. Raspberry Pi and Arduino systems, powerful tools to individually address, register and control the LED sources, as well as implementation of feedback loops, allow the user to manipulate the flux of light, making it possible to address valves individually and with high accuracy for a relatively low cost. This resulted in the recent work (2017) of Delaney and co-workers,[10] who showed that these materials can be used for precision control of the flow rate in microfluidic channels. In this work, a modular platform is build, containing multiple LED's that are all individually addressable (Figure 1.5c). By placing a chip containing the light responsive valves on top of these LED's combined with a proportional integral-derivative controller and a graphical user interface, a dial-in set-up that allowed the user to set the desired flow-speed is achieved. This system shows surprisingly high stability for the hydrogel and LED, showing that several hours of constant operation did not result in drifting of the flow rate as well as the power. Using these valves to control water based systems results in a large decrease in valve cost, as these valves can be generated for <€0.10 a piece, in contrast to other valves, which even have to be connected using external tubing, as the valve is not integrated inside the system.

1.3.2 Micromixers

Valves and mixing in microfluidics often come hand in hand as many processes inside microfluidics involve joining multiple channels to combine fluids, and mixing these to a homogeneous state. In microchannels, laminar flow dominates and mixing occurs mostly by diffusion. For many assays, and particularly bioassays where large molecules are often

involved, diffusion coefficients are low, with ineffective mixing resulting in poorly optimized processes and/or over-long assays. To overcome these problems, micromixers are used to more effectively mix laminar flows from merging channels. Efficient mixers based on active structures (i.e. structures that can be controlled) external to the microfluidic chip are well known in the literature. The ability to incorporate this function within the channels is obviously an attractive option. However, these systems often require complex external equipment. Simulations and experimental evidence show that simple asymmetric structures inside a channel also results in efficient mixing of laminar streams. Stroock and co-workers[48] showed that a staggered herringbone structure causes asymmetric circulation of the liquid. By alternating the asymmetric structure every cycle, an efficient micromixer was created that allowed fluids to be mixed within two centimeters, compared to a meter in the absence of this mixer. This work inspired many scientists to generate other micromixer designs for their specific set-up. However, as these structures are typically static, it does not allow the user to vary the structure configuration, unlike active micromixers. By incorporating responsive materials into channel walls/surface, passive based switching mixers can be integrated into microfluidics systems, enabling the user to determine the degree of mixing. This was demonstrated by Prettyman and coworkers[13] who showed that stimuli responsive hydrogels can be used to switch mixing on and off. They used pH responsive hydrogel posts arranged in a hexagonal oriented fashion. The diameter of the posts varied according to the fluid pH, resulting in switching of mixing efficiency.

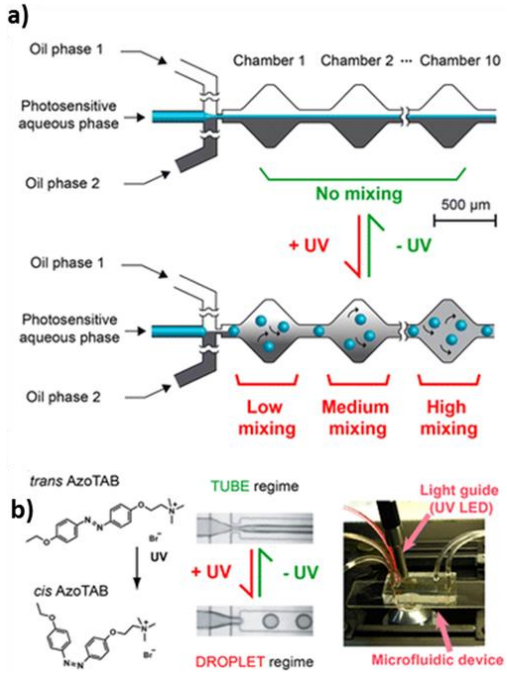

Figure 1.6. a) Light responsive micromixer based on the capability to switch between a jetting and drop making system, caused by the isomerization of azobenzene b). The photoswitch is dissolved in the middle aqueous phase. Copyright 2013, American Chemical Society.

In 2012, the group of Baigl showed that it is possible to switch a stream of liquid from a tubing phase to a drop making phase. Shortly after, in 2013, Venacio-Marques[49] and co-workers showed that mixing can also be achieved using the photoisomerization of azobenzene (Figure 1.6). In this case, a flow focus device was created, wherein two oil phases (one containing a dye for visualization) and an aqueous phase were brought in contact. The aqueous phase contained the light switchable chromophore, a water soluble trans-azobenzene. When not illuminated, the stable regime of the flow concentrator was tubing, in which the water phase was injected inside the oil phase. However, when illuminated with UV light, the azobenzene isomerized to the *cis* form, resulting in a droplet regime. Due to the design of the channel, the droplets moved around chaotically, mixing the dyed and transparent streams. Continuing on this, Nurdin and co-workers [50] showed that a similar system could be used to generate a high throughput switching system, capable of going from drop generation, to fusion and mixing, using a dual flow focusing device, showing the versatility of this system.

1.3.3 Transport

An example where light responsive hydrogels can be implemented in microfluidics, is the transport of particles by sheet-like poly(spiropyran-NIPAM) hydrogel films, exposed locally with light to obtain restricted shrinkage. Illumination trough a mask or light focused at a small area allows local shrinkage of the material and multiple illuminations using a variety of masks allows the formation of more complex structures, by changing the illumination time or position. This technique has been used to move spherical objects (glass beads) over a hydrogel surface (Figure 1.7a-b).[8,47]

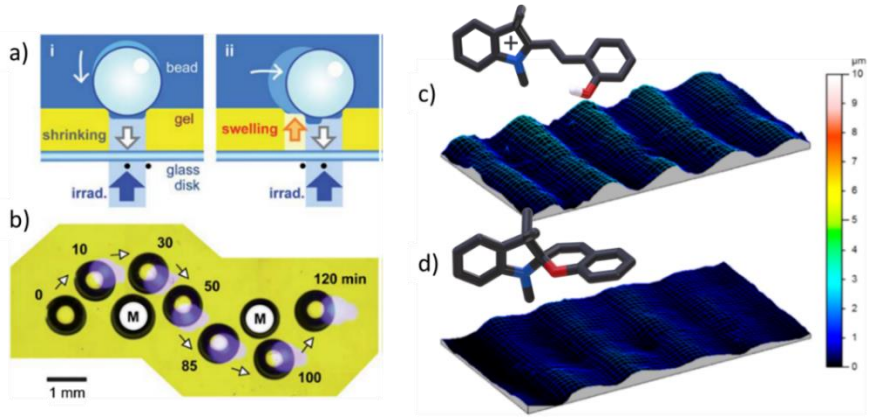

Figure 1.7. a,b) Schematic illustration showing the mechanism of light-controllable micro-conveying system composed of a sheet-like poly(spiropyran-NIPAM)-based hydrogel. Light-irradiation forms a pit into which a glass bead is trapped. The region partly overlapped with the first pit is irradiated to form a next pit. Disappearance of the first pit by reswelling of the gel results in transportation of the bead to the second pit. c) Poly(spiropyran-NIPAM) hydrogel ratchet structure in its swollen state and collapsed state d), allowing the formation of asymmetric structures by polymerizing this material on an asymmetric surface. (a,b) Copyright 2011, Royal Chemical Society, (c,d) copyright 2014, American Chemical Society.

Local exposure with light, shrinks the gel, causing the bead to get trapped in the pit. When the light source is moved slowly over the surface, the bead is being conveyed over the surface. Again, the formation of the structure (size and speed) depends on the molecular structure of the spiropyran implemented in the gel, as different spiropyran molecules have different kinetics, predominantly for the swelling event.

Spiropyran containing pNIPAM hydrogels similar to the previously discussed sheet-like films have also been used for the development of photo switchable surface topographies.[51] The working mechanism of these materials is based on either pre-structured surfaces or a non-uniform crosslink density, resulting in programmed shrinkage of the hydrogel.[52] Polymerization-induced diffusion, a technique where diffusion of the fast reacting monomer occurs due to depletion of this monomer during the process, has been used as a tool to fabricate films with a spatial difference in crosslink density throughout the film.[53,54] Light exposure results in shrinkage of the film, predominantly in the less crosslinked regions as there is less confinement of the gel. A decrease in the height difference of the relief structure is observed during shrinkage, resulting in smoothening of the surface topography. Recently, poly(spiropyran-NIPAM-acrylic acid) hydrogels which operate in a pH-neutral environment were created.[46,55] With this material photo responsive ratchet-like topographies have been developed on pre-structured substrates.[56] These ratchets decreased in steepness or even form opposite ratchet structures after photo-exposure (Figure 1.7c-d). These type of films can be of interest in self-cleaning surfaces and in microfluidic devices, as the flow and mixing behavior in such a device is dependent on the structure inside the channels. An alteration in the channel's interior can therefore lead to a change in the performance of the microfluidic system.

1.4 Aim and outline of this thesis

The aim of this work is to fabricate light responsive polymer with programmed properties that can be integrated in prototype devices to display their functionality. For this a molecule to device approach is used, whereby new photochromic molecules are synthesized and incorporated in polymers. The application of the light/responsive polymers in microfluidic devices, smart textile and regenerative medicine are investigated.

In Chapter 2, molecular design of the photochromes leads to improvement of the limiting kinetic step for shape changing hydrogels. These gels are used as a valve in a microfludic device, operating at neutral pH's and can be switched within 5 minutes, using blue light. In Chapter 3, the valves described in Chapter 2 are use to control the flow in a microfluidic channel. When using pulses of light, the size of the gel osscilates, allowing precise control over the flow behavior. In Chapter 4, light responsive micromixers are created, that mix fluids efficiently when not being illuminated. Upon illuminating these structures, collapse of the scaffold filled hydrogel results in decrease in efficiency of mixing. In Chapter 5, it is shown that these materials are not only applicable for microfluidic applications, but can also

be grown from the reactive sites formed on the cotton material. Hereby, the material shows reversible absorption and release of humidity by light making these polymers suited for water collecting. In Chapter 6, structured liquid crystal materials are used for cell culturing, showing that these materials can be used for tissue engineering. The benefit of these materials is that they do not require a water based environment, but forming structure in these material require stronger illumination methods. In Chapter 7, a technology assesment for the developped materials is performed, showing the benefits, but also the limitations of the used materials in this thesis.

1.5 References

1 B. C. Alexander and K. M. Shakesheff, *Adv. Mater.*, 2006, **18**, 3321–3328.
2 R. Byrne, F. Benito-lopez and D. Diamond, *Mater. Today*, 2010, **13**, 16–23.
3 T. Sun and G. Qing, *Adv. Healthc. Mater.*, 2011, **23**, H57–H77.
4 F. D. Jochum and P. Theato, *Chem. Soc. Rev.*, 2013, **42**, 7468–7483.
5 C.-L. Mou, X.-J. Ju, L. Zhang, R. Xie, W. Wang, N.-N. Deng, J. Wei, Q. Chen and L.-Y. Chu, *Langmuir*, 2014, **30**, 1455–1464.
6 Z. Li, J. Shen, H. Ma, X. Lu, M. Shi, N. Li and M. Ye, *Mater. Sci. Eng. C. Mater. Biol. Appl.*, 2013, **33**, 1951–1957.
7 S. Sugiura, K. Sumaru, K. Ohi, K. Hiroki, T. Takagi and T. Kanamori, *Sensors Actuators A Phys.*, 2007, **140**, 176–184.
8 A. Szilágyi, K. Sumaru, S. Sugiura, T. Takagi, T. Shinbo, M. Zrínyi and T. Kanamori, *Chem. Mater.*, 2007, **19**, 2730–2732.
9 S. Sugiura, A. Szilágyi, K. Sumaru, K. Hattori, T. Takagi, G. Filipcsei, M. Zrínyi and T. Kanamori, *Lab Chip*, 2009, **9**, 196–198.
10 C. Delaney, P. Mccluskey, S. Coleman, J. Whyte, N. Kent and D. Diamond, *Lab Chip*, 2017, **17**, 2013–2021.
11 G. Chen, F. Svec and D. R. Knapp, *Lab Chip*, 2008, **8**, 1198–1204.
12 J. E. Stumpel, D. J. Broer and A. P. H. J. Schenning, *Chem. Commun.*, 2014, **50**, 15839–15848.
13 J. B. Prettyman and D. T. Eddington, *Sensors Actuators, B Chem.*, 2011, **157**, 722–726.
14 D. H. Kang, S. M. Kim, B. Lee, H. Yoon and K.-Y. Suh, *Analyst*, 2013, **138**, 6230–6242.
15 L. Florea, D. Diamond and F. Benito-Lopez, *Macromol. Mater. Eng.*, 2012, **297**, 1148–1159.
16 D. Liu and D. J. Broer, *Responsive Polymer Surfaces: Dynamics in Surface Topography*, Wiley-VCH, 1st edn., 2017.
17 M. Hendrikx, A. P. H. J. Schenning, M. G. Debije and D. J. Broer, *Crystals*, 2017, **2**, 1–20.
18 F. Ercole, T. P. Davis and R. E. Evans, *Polym. Chem.*, 2009, **1**, 37–54.
19 R. Klajn, *Chem. Soc. Rev.*, 2014, **43**, 148–184.
20 N. S. Satarkar, W. Zhang, R. E. Eitel and J. Z. Hilt, *Lab Chip*, 2009, **9**, 1773–1779.
21 E. Lee, H. Lee, S. Il Yoo and J. Yoon, *ACS Appl. Mater. Interfaces*, 2014, **6**, 16949–16955.
22 D. Liu, C. W. M. Bastiaansen, J. M. J. den Toonder and D. J. Broer, *Langmuir*, 2013, **29**, 5622–5629.
23 A. W. Hauser, A. A. Evans, J. Na and R. C. Hayward, *Soft Matter*, 2015, **54**, 5434–5437.
24 S. R. Sershen, G. A. Mensing, M. Ng, N. J. Halas, D. J. Beebe and J. L. West, *Adv. Mater.*, 2005, **17**, 1366–1368.
25 J. Zhang, P. Du, D. Xu, Y. Li, W. Peng, G. Zhang, F. Zhang and X. Fan, *Ind. Eng. Chem. Res.*, 2016, **55**, 4526–4531.
26 T. Satoh, K. Sumaru, T. Takagi, K. Takai and T. Kanamori, *Phys. Chem. Chem. Phys.*, 2011, **13**, 7322–7329.
27 P. M. Mendes, *Chem. Soc. Rev.*, 2008, **37**, 2512–2529.
28 J.-I. Edahiro, K. Sumaru, Y. Tada, K. Ohi, T. Takagi, M. Kameda, T. Shinbo, T. Kanamori and Y. Yoshimi, *Biomacromolecules*, 2005, **6**, 970–974.
29 N. Wang, Y. Li, Y. Zhang, Y. Liao and W. Liu, *Langmuir*, 2014, **30**, 11823–11832.
30 G. M. Whitesides, *Nature*, 2006, **442**, 368–373.
31 C.-Y. Lee, C.-L. Chang, Y.-N. Wang and L.-M. Fu, *Int. J. Mol. Sci.*, 2011, **12**, 3263–3287.
32 E. A. Mansur, M. Ye, Y. Wang and Y. Dai, *Chinese J. Chem. Eng.*, 2008, **16**, 503–516.
33 H. E. H. Meijer, M. K. Singh, T. G. Kang, J. M. J. den Toonder and P. D. Anderson, *Macromol. Symp.*, 2009, **279**, 201–209.

34 D. Diamond, R. Byrne, F. B. Lopez, J. Cleary, D. Maher, J. Healy, J. Kim and K. Lau, *IEEE SENSORS 2010 Conf.*, 2010, 1079–1082.
35 M. A. Unger, H. P. Chou, T. Thorsen, A. Scherer and S. R. Quake, *Science*, 2000, **288**, 113–116.
36 D. J. Beebe, J. S. Moore, J. M. Bauer, Q. Yu, R. H. Liu, C. Devadoss and B. Jo, *Nature*, 2000, **404**, 588–590.
37 J. ter Schiphorst, S. Coleman, J. E. Stumpel, A. Ben Azouz, D. Diamond and A. P. H. J. Schenning, *Chem. Mater.*, 2015, **27**, 5925–5931.
38 D. Eddington, *Adv. Drug Deliv. Rev.*, 2004, **56**, 199–210.
39 C. Zhang, D. Xing and Y. Li, *Biotechnol. Adv.*, 2007, **25**, 483–514.
40 I. Tomatsu, K. Peng and A. Kros, *Adv. Drug Deliv. Rev.*, 2011, **63**, 1257–1266.
41 D. Baigl, *Lab Chip*, 2012, **12**, 3637–3653.
42 A. Döring, W. Birnbaum and D. Kuckling, *Chem. Soc. Rev.*, 2013, **42**, 7391–7420.
43 W. Hilber, *Appl. Phys. A Mater. Sci. Process.*, 2016, **122**, 1–39.
44 A. D. Jadhav, B. Yan, R. Luo, L. Wei and X. Zhen, *Biomicrofluidics*, 2015, **9**, 34114.
45 C. Zhu, Y. Lu, J. Peng, J. Chen and S. Yu, *Adv. Funct. Mater.*, 2012, **22**, 4017–4022.
46 B. Ziółkowski, L. Florea, J. Theobald, F. Benito-Lopez and D. Diamond, *Soft Matter*, 2013, **9**, 8754–8760.
47 T. Satoh, K. Sumaru, T. Takagi and T. Kanamori, *Soft Matter*, 2011, **7**, 8030–8034.
48 A. D. Stroock, S. K. W. Dertinger, A. Ajdari, I. Mezic, H. A. Stone and G. M. Whitesides, 2002, **295**, 647–652.
49 A. Venancio-Marques, F. Barbaud and D. Baigl, *J. Am. Chem. Soc.*, 2013, **135**, 3218–3223.
50 L. Nurdin, A. Venancio-Marques, S. Rudiuk, M. Morel and D. Baigl, *Comptes Rendus Chim.*, 2015, **19**, 199–206.
51 J. E. Stumpel, D. Liu, D. J. Broer and A. P. H. J. Schenning, *Chemistry*, 2013, **19**, 10922–10927.
52 J. Kim, J. A. Hanna, M. Byun, C. D. Santangelo and R. C. Hayward, 2012, **335**, 1201–1206.
53 C. M. Leewis, A. M. De Jong, L. J. Van Ijzendoorn and D. J. Broer, *J. Appl. Phyrics*, 2004, **95**, 8352–8356.
54 D. Liu, C. W. M. Bastiaansen, J. M. J. den Toonder and D. J. Broer, *Soft Matter*, 2013, **9**, 588–596.
55 B. Ziółkowski, L. Florea, J. Theobald, F. Benito-Lopez and D. Diamond, *J. Mater. Sci.*, 2016, **51**, 1392–1399.
56 J. E. Stumpel, B. Ziółkowski, L. Florea, D. Diamond, D. J. Broer and A. P. H. J. Schenning, *ACS Appl. Mater. Interfaces*, 2014, **6**, 7268–7274.

Chapter 2

Molecular design of light-responsive hydrogels for microvalve applications

Abstract. Reversible light-responsive hydrogel valves with response characteristics compatible for microfluidics have been obtained by optimization of molecular design of spiropyran photoswitches and gel composition. Self-protonating gel formulations were exploited, wherein acrylic acid is copolymerized in the hydrogel network as an internal proton donor, to achieve a swollen state of the hydrogel in water at neutral pH. Light-responsive properties were endowed upon the hydrogels by copolymerization of spiropyran chromophores, using electron withdrawing and donating groups to tune the gel-swelling and shrinkage behavior. In all cases the shrinkage is determined by the water diffusion rate, while for the swelling the isomerization kinetics is the rate determining step. For one hydrogel reversible and reproducible volume changes were observed. Finally, gel-valves integrated within microfluidic channels were fabricated allowing reversible and repeatable operation, with opening and closing of the valve in minutes.

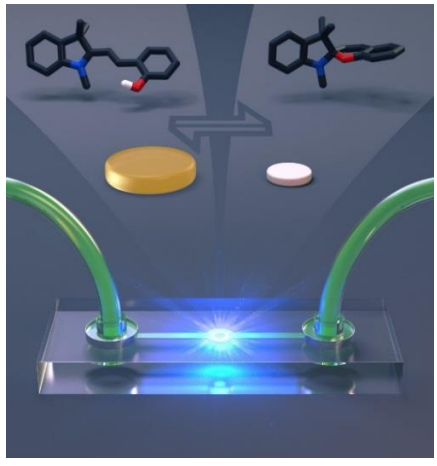

This chapter is partially reproduced from:
'Molecular design of light-responsive hydrogels, for in situ generation of fast and reversible valves for microfluidic applications' J. ter Schiphorst, S. Coleman, J. E. Stumpel, A. Ben Azouz, D. Diamond, A. P. H. J. Schenning, *Chem. Mater.* 2015, **27**, 5925−5931.

2.1 Introduction

Light-responsive coatings and materials have been an attractive field of research in recent years.[1–5] Photoswitching allows alteration in the dimensional and structural composition of the material with highly precise and localized actuation, without direct contact between the material and the actuating stimulus, and with minimum impact on environmental conditions.[6–11] This approach is appealing for optical data storage,[12] actuators[1] and valves in microfluidics.[13–21] In particular, the latter application ideally requires fast and reversible actuation of the valve structure in order to work efficiently. Key requirements for successful adoption are manufacturability combined with reliability, durability and low cost, particularly when employing these fluidic systems in analytical instruments at remote locations.[22] However, up to now, most examples are based on temperature responsive systems, which are not readily implementable in microfluidics.[18,20,22,23] Hydrogel based materials in which a photochrome is covalently incorporated in the polymer backbone can exhibit significant volume changes using light as the actuation stimulus (see also chapter 1).[24] Various photochromes have been studied that exhibit light-induced isomerization *e.g.* azobenzenes[25,26] and spiropyrans (Sp).[1] Significantly larger changes in dimensionality of a gel can be achieved using Sp-derivatives, as there is a large change in polarity when isomerizing this molecule. In an acidic environment, the stable hydrophilic isomer merocyanine-H^+ (McH^+) is formed, which can be switched using light, to the ring-closed hydrophobic spiropyran form changing the overall character of a hydrogel from predominantly hydrophilic to predominantly hydrophobic, allowing repeatable swelling and shrinkage of the material, due to accompanying water uptake and release (Figure 2.1).

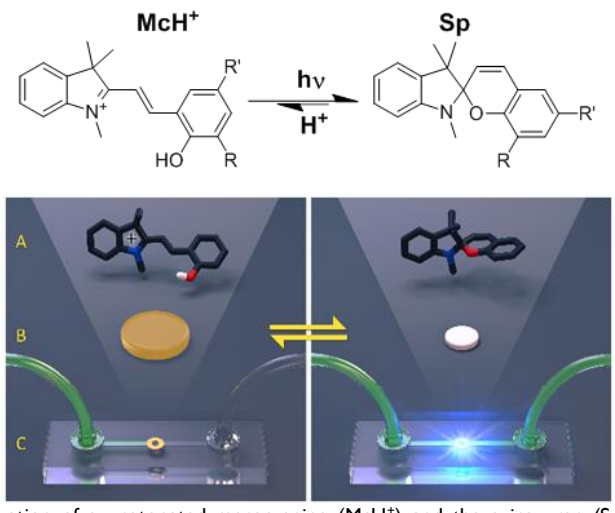

Figure 2.1. Isomerization of a protonated merocyanine (McH^+) and the spiropyran (Sp) form (A) with the corresponding effect on the size of a hydrogel by irradiation with light (B), implemented as light-responsive valve in microfluidics (C).

Recently, several approaches involving light-responsive poly(N-isopropylacrylamide) (pNIPAM)-based hydrogels containing a photochromic compound, that isomerizes and therefore contracts and swells the gels, have been reported.[9,25,27–29] Nevertheless, valves have only rarely been investigated using light-responsive hydrogels. Only a reversible spiropyran-based hydrogel valve with fast opening has been demonstrated. However, the time required to close this valve by reswelling was found to be in the order of one hour, thus essentially limiting the potential applications to single use devices (see also chapter 1).[7]

A possible solution for obtaining reversible and repeatable operation with fast opening and closing speed, is to modify the chemical nature of the photochromic molecule. Isomerization rates of Sp are strongly dependent on the substituents (Figure 2.2) as shown by Satoh *et al.*[27,30] Not only the kind of substituent (electron withdrawing or donating) but also the position was found to change the kinetics in an acidic environment, where an electron donating group at the 8' position was the fastest of the molecules compared. However, an acidic environment is not always acceptable, as neutral pHs are frequently required in many analytical methods.[7] Therefore, inspired by the work of Ziółkowski *et al.*,[9] the following study employed a self-protonating system wherein acrylic acid is copolymerized into the hydrogel to provide an internalized source of protons.

In the present work the molecular structure of the Sp is optimized (Figure 2.2) showing improved photoresponsive characteristics that is manifested also by reversible volume changes and a good valve function in microfluidic applications. In a structure property relationship study the effect of various substituents on the photo-isomerization speed of spiropyran derivatives and the corresponding macroscopic impact on hydration and dehydration of a hydrogel incorporating these derivatives is presented. The molecular kinetics of various Sp derivatives is coupled to the corresponding shrinking/swelling kinetics of small hydrogel disks as a model study and subsequently the incorporation of the gel with the fastest actuation properties into a microfluidic chip is realized to show the reversibility and reusability. The photo-actuation process is performed under neutral, aqueous conditions by illumination with a low-cost light-emitting diode (LED). This study and configuration opens up new opportunities to integrate low-cost valving functions within microfluidic systems using compact, low-cost and low-energy irradiation sources.

2.2 Experimental

A detailed description of the experiments can be found in the corresponding publication.[31] Chip design and manufacturing was performed by S. Coleman and A. Ben Azouz.

Synthesis.

Sp-8'-OH was synthesized according to a procedure reported by Stumpel *et al.*[10] condensing 1,3,3-trimethyl-2-methleneindoline with 2,3-dihydroxybenzaldehyde. ^{1}H-NMR (400 MHz, $CDCl_3$, 25°C, TMS): δ = 7.18 (t, J = 7.7 Hz, 1H CH Ar), 7.07 (d, J = 6.9 Hz, 1H, CH Ar), 6.90 – 6.81 (m, 2H CH Ar), 6.81 – 6.70 (m, 2H CH Ar and NCCH=CH), 6.64 (d, J = 7.3 Hz, 1H, CH Ar), 6.53 (d, J = 7.7 Hz, 2H, CH Ar), 5.69 (d, J = 10.3 Hz, 1H, NCCH=CH), 5.23 (s, 1H, OH), 2.75 (s, 3H, NCH_3), 1.30 (s, 3H, CCH_3), 1.18 (s, 3H, CCH_3). ^{13}C-NMR (100 MHz, $CDCl_3$, 25°C, TMS): δ = 147.85, 143.11, 140.72, 136.43, 129.42, 127.65, 121.60, 120.30, 119.58, 119.26, 118.90, 118.03, 115.39, 106.89, 105.32, 51.72, 28.81, 25.93, 19.92. MALDI-ToF MS: m/z calcd for $C_{19}H_{19}NO_2$ $(M+H)^+$: 294.15, found: 294.17.

1 was synthesized according to a procedure reported by Stumpel *et al.*,[10] reacting 6-bromohexyl acrylate with the corresponding SP-8'-OH. The crude product was pre-purified by subjection to a silica column using 10% ethylacetate in heptane, before injection in a recycle GPC column, using 256 and 360 nm as detection wavelengths. For later chapters, purification was performed using an alumina oxide column.^{1}H-NMR (400 MHz, $CDCl_3$, 25°C, TMS): δ = 7.12 (t, J = 7.6, 1H, CH Ar), 7.04 (d, J = 6.3 Hz, 1H, CH Ar), 6.84 (d, J = 10.2 Hz, 1H, NCCH=CH), 6.82 – 6.76 (m, 2H, CH Ar), 6.72 (d, J = 4.9 Hz, 2H, CH Ar), 6.47 (d, J = 7.7 Hz, 1H, CH Ar), 6.41 (dd, J = 17.3, 1.4 Hz, 1H, *trans*-HC=C), 6.13 (dd, J = 17.3, 10.4 Hz, 1H, H_2C=CH), 5.82 (dd, J = 10.4, 1.4 Hz, 1H, *cis*-HC=C), 5.70 (d, J = 10.2 Hz, 1H, NCCH-CH), 4.09 (t, J = 6.7 Hz, 2H, OCH_2), 3.89 – 3.65 (m, 2H, Ar OCH_2), 2.71 (s, 3H, NCH_3), 1.58-1.43 (m, 4H, CH_2 alkane), 1.32 (s, 3H, CCH_3) 1.29-1.05 (m, 4H, CH_2 alkane), 1.18 (s, 3H, CCH_3). ^{13}C-NMR (100 MHz, $CDCl_3$, 25°C, TMS): δ = 166.32, 148.09, 146.20, 145.14, 136.92, 130.40, 129.45, 128.68, 127.33, 121.30, 120.16, 120.02, 119.58, 119.22, 118.98, 118.38, 106.62, 104.12, 70.75, 64.68, 51.37, 29.36, 28.95, 28.42, 25.74, 25.56, 25.36, 20.19. MALDI-ToF MS: m/z calcd for $C_{28}H_{33}NO_4$ $(M+H)^+$: 448.25, found: 448.29. Yield: 50%

Sample preparation.

For the fabrication of the hydrogels, a 2:1 dioxane and water mixture was prepared containing 91 mol% NIPAM, 5 mol% acrylic acid, 2 mol% *N,N'*-

methylenebisacrylamide (MBIS), 1 mol% Irgacure 819 as white light photo initiator and 1 mol% of the corresponding Sp (0.5 mg/µL, Figure 2.2).
To monitor the isomerization kinetics, thin films of the photoresponsive gels were prepared and attached to a glass slide, using a cell composed of 50 micron thick pressure sensitive adhesive spaced glass slides filled each with monomer solution. The internal surface of the bottom slide of this cell was functionalized with 3-(trimethoxysilyl)propyl methacrylate to ensure covalent attachment of the gel to maintain a flat film for UV-Vis spectroscopy. For easy removal of the top glass slide of the cell, the corresponding glass plate was functionalized with a fluorinated compound (*1H,1H,2H,2H*-Perfluorodecyl-triethoxysilane). Subsequently the filled cell was illuminated with white light for 15 seconds to achieve a cross-linked network. The fluorinated glass was removed and the samples were allowed to dry before being submerged in water overnight, to ensure a fully equilibrated hydrated state.
To investigate the volume changes of the light-responsive hydrogels, disks were prepared using a cell consisting of a non-functionalized microscope glass slide and a 192 micron thick pressure sensitive adhesive spacer capped with a microscope cover glass slide with an attached mask having 1 mm diameter holes. The material was illuminated for 15 seconds using a broadband spectrum (400-750 nm) white LED lamp at 1 cm above the mask to form the disks. The capping slide/mask was then removed and the disks mimicking valves were carefully rinsed and transferred into a container filled with distilled water and left overnight to swell and ensure an equilibrium hydrated state. It is assumed that the isomerization kinetics in the covalently attached material is similar to the isomerization kinetics in the hydrogel disks.

Microfluidic valve preparation and actuation.

Valves were polymerized in-situ within microfluidic channels situated within PMMA chips. The two-layer chips were prepared from 1.5 mm thick PMMA sheets. The microfluidic microchannels, liquid inlet and an outlet, and a circular feature with central pillar (for housing the valve) were micromilled on the base layer and then sealed to the top capping layer. The microchannel dimensions were 1 mm wide and 0.150 mm deep, while the circular chamber and pillar were 2.6 mm and 1 mm in diameter, respectively. The microchannel was filled initially with the monomer solution and the valve was created by irradiation of the solution with blue LED light at 450 nm peak wavelength, using a suitable mask to define the valve dimensions. After creation of the valve structure in-situ, the microfluidic system was rinsed using deionized water to ensure a fully hydrated state. An in-house developed blue LED (430-470 nm) system was subsequently used for actuation of the valves. The channels are filled with water overnight to allow the valves to fully swell and prime the chip.
Valve performance was assessed using an in-house designed constant head platform to generate a constant flow through the system. Valve opening was achieved via

exposure to blue LED light (peak wavelength at 450 nm) for one minute, while closure occurred spontaneously when the LED light source was turned off, as thermal equilibrium favors formation of the McH^+ isomer. Liquid flow through the chip was monitored as the valve opened and closed using a Fluigent L FRP Flow Meter and FRP Flowboard.

2.3 Results and discussion

Molecular design and synthesis of the spiropyran.

Sp derivatives (Figure 2.2) were synthesized with an ester or an ether moiety at the 6' position (**2** and **3**) or an ether moiety at the 8' position (**1**), whereby the ester is an electron withdrawing substituent and the ether as an electron donating substituent.[30] The Sp-based derivatives **2** and **3** were synthesized according to procedures reported earlier,[9–11] whereas the Sp-8' derivative **1** is a novel compound. For synthesizing this derivative, a Fisher base and the corresponding salicylaldehyde are condensed to form the spiropyran derivative with a hydroxyl group at the desired 8' position. Subsequently, a Williamson ether synthesis of the Sp with 6-bromohexyl acrylate under Finkelstein conditions using potassium iodine and potassium carbonate in 2-butanone results in the corresponding Sp-ether derivative **1**. After purification **1** is fully characterized (see experimental section).

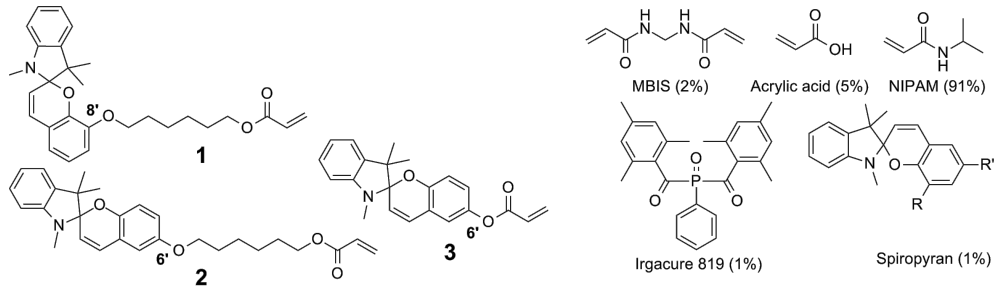

Figure 2.2. Left: the synthesized structures used for this study with an ester (**3**) or ether (**2**) at the 6' position and an ether (**1**) at the 8' position. Right: the materials used for preparing the light-responsive hydrogels.

Synthesis and characterization of the hydrogels.

To accurately monitor the isomerization kinetics of the hydrogels, the photoresponsive hydrogels (91 mol% NIPAM, 5 mol% acrylic acid, 2 mol% MBIS, 1 mol% Irgacure 819 and 1 mol% **1**, **2** or **3**) were attached to a glass slide. Subsequently these slides were positioned inside a custom fabricated PMMA-based cuvette containing water to keep the hydrogel hydrated. Hydrogel **1** shows a single strong absorbance band at λ_{max} = 403 nm while **2** shows two absorbance peaks at λ_{max} = 376 and 467 nm. Hydrogel **3** shows absorbance peak at λ_{max} = 425 nm. It should be noted

that no absorption peaks were observed at longer wavelength, indicating the absence of the non-protonated merocyanine form (*vide supra*). These spectral characteristics are typical for protonated merocyanine (McH^+) and the observed red shift of the absorption maximum for the different derivatives is in agreement with previous reported spiropyran substituted linear pNIPAM polymers.[30]

Before switching the material with light, the amount of protonated merocyanine (McH^+) in the hydrogels is estimated using UV-Vis spectrophotometry at various concentrations of HCl ranging from 0.05M to 1M.[30] At a concentration of 1M HCl, it is assumed that Sp is completely in the McH^+ form. Subsequently, 0.2M triethylamine in water is brought in contact with the hydrogel to produce both the Sp and Mc form, as indicated by the appearance of an additional absorbance peak at higher wavelengths,[31] characteristic of merocyanine.[30]

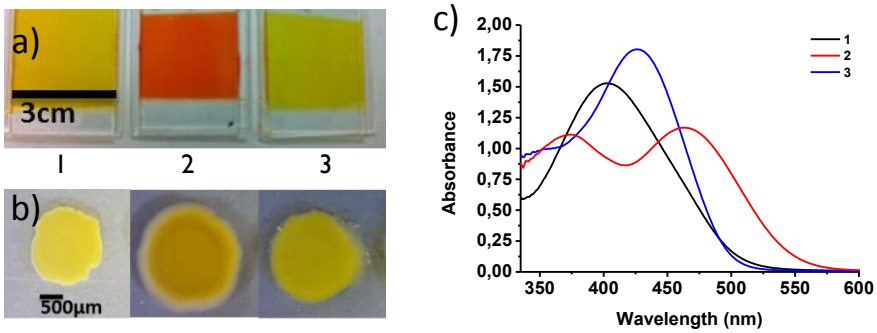

Figure 2.3. a) Photographs of the surface attached hydrogels used for the kinetics measurements. b) Hydrogel disks made to measure the swelling effects. c) UV-Vis spectra the surface attached hydrogels based on compounds 1, 2 and 3.

Upon exposure to increasing concentrations of HCl, the absorbance intensity at 403 nm of hydrogel **1** increases (1M HCl). After 150 minutes of exposure to this HCl concentration, no further increase is observed.[31] This reveals that around 84% of the spiropyran is in the McH^+ form. A similar procedure is used to determine the McH^+ fraction in hydrogels **2** and **3**, resulting in 78% and near 100% respectively. The fraction of McH^+ in **3** is surprisingly high, as one would expect this value to be lower due to the electron withdrawing nature of the ester which should destabilize the positively charged protonated mercocyanine.

To determine the volume change in the hydrogels, free standing hydrogel disks, with dimensions similar to the valves (*vide infra*), were prepared having an initial diameter of 1 mm and thickness of 192 µm before storing in deionized water. The size of the gel disk (Figure 2.3) in deionized water is measured as the average of 3 disks. The largest disk is obtained with compound **2** (2.32 mm^2). Compound **3** had an average size of 2.00 mm^2 and compound **1** an average size of 1.22 mm^2 calculated by measuring the amount of pixels in a microscope photograph using ImageJ software (Table 2.1). Remarkably, there is no correlation between the amount of McH^+ and

the initial size of the hydrogel disks. This shows that other factors such as the presence of a difference in crosslink density is possible, as the white light polymerizes and isomerizes the mixture at the same time. It should be noted that the difference in initial size of the hydrogel disks is most likely not a determining factor for volume changes, as the thickness (z) for all gels is far smaller than the area (x-y plane) i.e. z<<x,y.

Table 2.1. Properties of the hydrogel disks and surface attached hydrogels.

	λ_{max} (nm)	Concentration merocyanine in the gel exposed to pure water (%)	Initial area/size (mm^2/mm)**
1	403	84	1.22 mm^2, d=1.250 mm
2	376 467	78	2.32 mm^2, d=1.719 mm
3	425	Near 100*	2.00 mm^2, d=1.596 mm

* Fluctuations were observed.
** Calculated as the average of 3 gels using the area in pixels. 1 pixel = 5 x 5 μm^2, circle is assumed for calculating the diameter d.

Photoswitching and actuation of hydrogels.

To measure the isomerization kinetics of McH^+ to Sp, the surface attached hydrogels were illuminated with white light for 300 seconds. Upon illumination, the absorbance measured at the peak maximum decreased rapidly, indicating that the isomerization of McH^+ is fast. The resulting UV-Vis absorption spectrum indicates the formation of the Sp form.[1] The absorbance at the photo-stationary state (pss) is in all cases close to zero, pointing to a quantitative conversion of the McH^+ to the Sp form. Compound **3** requires ~12 seconds before reaching the pss, while **2** and **1** require ~75 and ~90 seconds, respectively (Figure 2.4). This indicates that **3** has the fastest molecular closing kinetics, which is what one would expect, due to the electron withdrawing nature of the ester units.
When the free-standing gels were exposed to white light, rapid shrinkage of the disk occurs. A stereomicroscope is used to track the degree of shrinkage every 30 seconds, and the surface area is calculated. Upon plotting the disk area versus time, one can see that the slope of the shrinkage is very similar in all situations. All gel disks shrink to ca. 60% of their original area. The minimal size of the gel after 300 seconds illumination is 65, 58 and 54% of the initial area of the hydrogels **1**, **2** and **3,** respectively (Figure 2.4). These results show that the volume shrinkage is relatively independent of the spiropyran derivative used. When comparing the McH^+ isomerization and gel swell kinetics (Figure 2.4), it is clear that the shrinking of the

gel is the rate limiting step since the pss is already reached after maximal 90 seconds, while the gel still does not show maximum shrinkage even after 300 seconds of illumination.

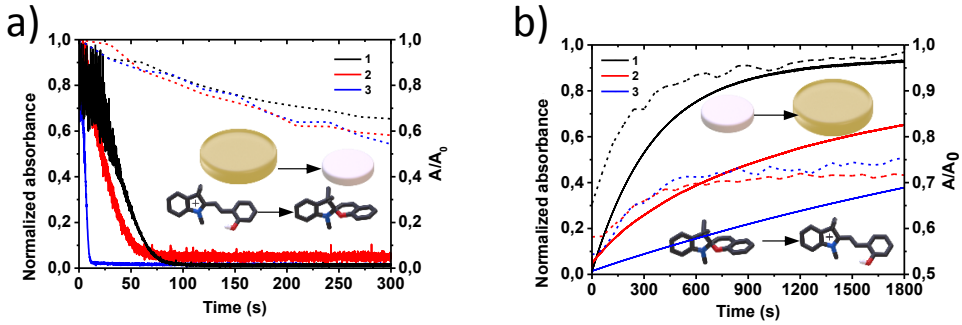

Figure 2.4. (a) The isomerization of McH^+ to Sp in both the surface attached hydrogel (solid line) and the corresponding shrinkage (dashed line) of the hydrogel disks during 300 seconds irradiation with white light. (b). The isomerization of Sp to McH^+ in both the surface attached hydrogel (solid line) and the corresponding swelling (dashed line) of the hydrogel disks during 1800 seconds in the dark. The absorbance is measured at λ_{max}; 403, 467 and 425 nm for **1**, **2** and **3** respectively.

When the material is allowed to reswell in the dark for 1800 seconds, the formation of McH^+ can be tracked over time using UV-Vis spectroscopy. The conversion of Sp to McH^+ appeared to follow 1st order kinetics in all three cases. In Figure 2.4, the normalized absorbance of the McH^+ versus time plot shows that **1** has the fastest ring opening kinetics indicated by the slope. After 1800 seconds, **1** recovered to 92% of the original protonated merocyanine absorbance, while **3** and **2** only recovered to 65% and 38% of the original absorbance, respectively. The isomerization rate coefficient $k_{Sp \rightarrow McH}$ of **1** is found to be $2{,}78 \times 10^{-3}$ s^{-1}, while **2** is $1{,}08 \times 10^{-3}$ s^{-1} and **3** is $2{,}77 \times 10^{-4}$ s^{-1} making the rate constant of **1** ca. 2.5 times faster than **2**, and ca. 10 times faster than **3**. The rate of isomerization and the trend is comparable to earlier reported result in acidic media[11,30] where it is shown that electron donating groups at the 8' position increase the isomerization to McH^+.

The volume changes in the hydrogel disks were also monitored over the same time period and the area is measured every minute (Figure 2.4). Upon reswelling, only the gel containing **1** recovered its approximate initial size (99%), while the gels containing **2** and **3** recovered only 72% and 75%, respectively. When comparing the Sp isomerization and gel swell kinetics, the data suggests that the isomerization kinetics is the rate limiting step since the pss is still not reached after the allocated 1800 seconds recovery time. Remarkably only in the case of hydrogel **1,** the reswelling kinetics track the isomerization kinetics, until an almost full volume recovery of the hydrogel disk is reached within the 1800 seconds recovery time.

Photoswitching and actuation of hydrogels: reversibility.

The illumination followed by recovery in the dark is repeated three times to investigate the reversibility of the light induced volume changes of the hydrogels. UV-Vis spectroscopy show that the fraction of McH^+ and Sp formed is constant. In addition, the isomerization kinetics is not changing, revealing full reversibility of the isomerization process. Gels containing **1** exhibited swell recovery and only exhibited minor loss of original size (Figure 2.5). In contrast, the gel containing **2** and **3** decrease in size upon the second and third illumination cycle, indicating that (i) the minimal size is not reached and (ii) the swelling kinetics are slower than in the gel containing compound **1**.
After three cycles of 300 seconds illuminating and 1800 seconds recovering, the size of the gel calculated using the data in Figure 2.5 is 99, 58 and 66% of the initial area for **1**, **2** and **3** respectively. This data is summarized in Table 2.2.

Table 2.2. Kinetic properties of the used hydrogel disks and surface attached hydrogels.

Gel containing spiropyran:	Photo stationary state (s)	$K_{Sp \rightarrow McH^+}$ 10^3 s^{-1}	Swollen after 1800 s*
1	~90	2.78	99%
2	~75	1.08	58%
3	~12	0.277	66%

*Calculated by the average of 3 gels in the last run using the data in Figure 2.5a.

The hydrated gel size of derivatives **2** and **3** is observed to decrease upon multiple illuminations (Figure 2.5) which could potentially present a challenge when this material is used in a valve configuration, since it could potentially result in leaking through the valve after a number of switching cycles. In contrast, the equivalent data for gels incorporating **1** suggest that swelling and contracting behavior is reproducible and valves based on this gel formulation should be capable of repetitive switching between open/closed configurations.

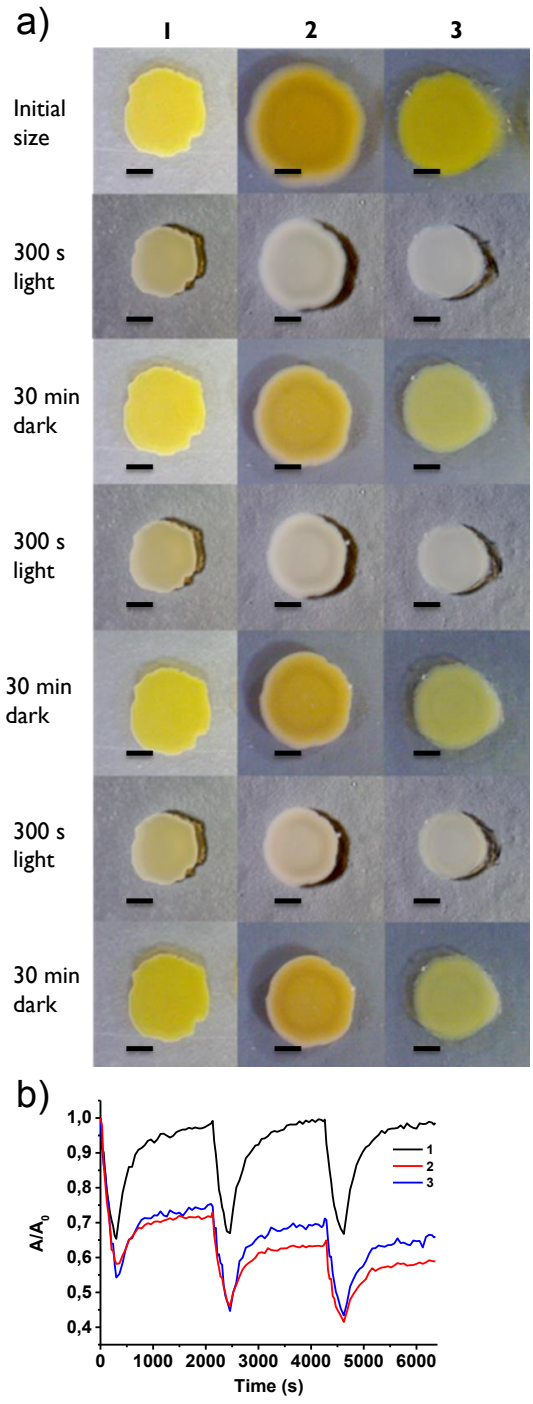

Figure 2.5. a) Photographs of the disks at the initial size and after three runs of 300 s of illumination with white light and subsequently recovering in the dark for 1800 s. The scale bar represents 500 μm. b) Normalized plot of the area of the disk depicting the macroscopic swelling effects upon three consecutive illumination and relaxation runs.

Isomerization kinetics versus swelling kinetics.

There are two scenarios that can occur when correlating the isomerization kinetics of the Sp derivative to the swelling and shrinking behavior of the hydrogels:

1. The kinetics of the isomerization of Sp is **faster** than the swelling kinetics: Diffusion limitation.
2. The kinetics of the isomerization of Sp is **slower** than the swelling kinetics: Isomerization limitation.

To improve the swelling speed of the material, in the first scenario the material can be dimensionally scaled down, as there is a dependence of diffusion on the radius squared of the material. In the second scenario, improvements can be obtained by designing the molecular structure of the Sp derivative, so as to enhance the isomerization kinetics. When plotting the normalized Sp isomerization kinetics and gel swell kinetics in one plot (Figure 2.4), one can clearly see that the shrinking of the gel is diffusion process limited. Upon reswelling, in the case of both Sp-6' derivatives (**2** and **3**), the material does not return to its original size in the measured time window. The isomerization kinetics are slower than the recovery of the material, indicating that there is an isomerization kinetics limitation. **1** however exhibits full recovery of its initial swollen size in the measured timespan but it is debatable whether the kinetics of isomerization for **1** are in the same range or slower than the swelling kinetics. The slope of both the swelling and isomerization curve is very similar, indicating that these two observables are directly connected to each other *i.e.* the hydrophilicity changes which occur upon isomerization are being translated to a change in hydrophilicity of the entire material.

When examining the swelling profile in Figure 2.4 in more detail, two separate situations are observed. For derivatives **2** and **3**, the initial swelling seems very steep and suddenly reaches a plateau. Therefore, an initial diffusion limitation followed by isomerization limitation seems to be occurring. This is not the case for the **1** where a gradual increase in both the kinetics and extent of swelling is observed.

From the results above, it is clear that **1** exhibits the greatest potential as a fast, reusable valve for implementation due to its (almost) complete recovery.

Performance of hydrogel based microvalves.

Hydrogel-based valves were produced to examine the applicability of the macroscopic results observed above as a practical application for fluid control. Since derivative **1** exhibited the fastest isomerization kinetics and reversible swell/shrink profile, light-switchable valves based on this gel are created. The valve has similar dimensions as obtained for the hydrogel disks in Figure 2.5, and the only difference is a pillar in the middle to ensure that the valve stays in place. When the valve is placed in the microfluidic device, no flow is observed in the channel (Figure 2.6). However

when the valve is locally illuminated using a blue LED, flow is observed in the channel within a few seconds, indicating that the hydrogel valve rapidly shrinks due to photoisomerization of the McH^+ moiety. When the light is turned off the flow decreased and stopped, suggesting that the valve spontaneously returned to its original size and blocks the channel.

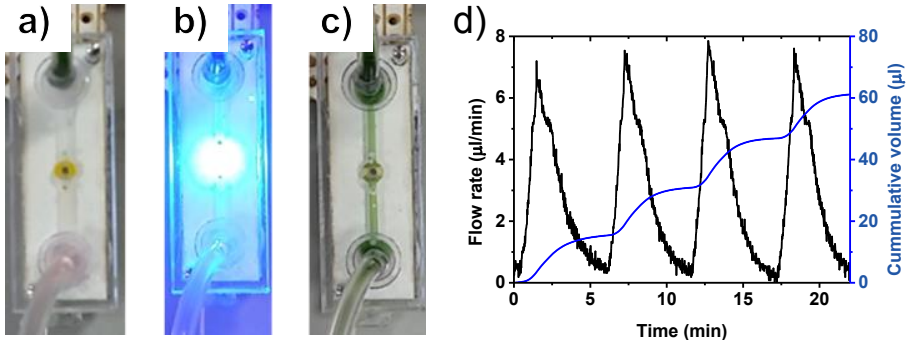

Figure 2.6. Valve action of a gel containing derivative **I**, polymerized in-situ within a sealed PMMA chip. a) No flow is observed with the valve fully swollen and channel sealed. b) Illumination with a blue LED results in shrinking of the valve. c) Open valve after 1 min illumination showing flow. The fluid passing thought the valve is colored green for visualization. The channel is filled with clear water before attaching the tubing to ensure a swollen state of the gel. d) Flow profile of water in a chip containing a gel valve with spiropyran derivative **I**, upon illumination with blue light for 1 minute followed by not illuminating for 5 minutes. Reproducible opening and closing is observed indicated by the flow profile (black) as well as the cumulative flow volume profile (blue).

The light induced flow changes are monitored over time by illuminating the valve with a blue (450 nm peak wavelength) LED for one minute, followed by switching off the LED for 5 minutes. Upon illumination, flow of liquid is observed almost immediately, reaching ca. 7 µL/min after one minute (Figure 2.6). After switching off the LED, the flow decreased to nearly zero within 5 minutes suggesting that valve closure is essentially complete within this time. During the open/close cycle, around 15 µL of the liquid passed. For hydrogel **I** a 10% shrinkage occurs during the illumination period (Figure 2.4) while after 5 minutes in the dark complete recovery to the original size is observed. Interestingly the opening and closing of the valves can at least be repeated four times, showing that the valve actuation is reversible (Figure 2.6). These results show the potential of photoresponsive hydrogels based valves to provide flexible flow control within microfluidic chips.

2.4. Conclusion

In this chapter, it is demonstrated that molecular design of the photochromic compound is important for optimizing the responsive properties of associated hydrogels. Changing the spiropyran derivative produces significant improvement of the isomerization speed and the reversible swelling/shrinking behavior of the hydrogels. These hydrogels can be applied as an efficient valve in a microfluidic device.

The in-situ photo-polymerization of these valving gels opens up a new and flexible way to control liquid flow in microfluidics that can be widely employed in analytical devices. The simplified, compact configuration and non-contact operation with LED illumination also allows flow control in completely sealed fluidic units. This is in contract to electro-switched valves, where direct connection between the energy source and the device is required. These results are not only interesting for microfluidics, but can be applied as a general concept, in which switching speed and reversibility are crucial.

2.5 References

1 R. Klajn, *Chem. Soc. Rev.*, 2014, **43**, 148–184.
2 I. Tomatsu, K. Peng and A. Kros, *Adv. Drug Deliv. Rev.*, 2011, **63**, 1257–1266.
3 S. Dai, P. Ravi and K. C. Tam, *Soft Matter*, 2009, **5**, 2513–2533.
4 F. D. Jochum and P. Theato, *Chem. Soc. Rev.*, 2013, **42**, 7468–7483.
5 L. Florea, D. Diamond and F. Benito-Lopez, *Macromol. Mater. Eng.*, 2012, **297**, 1148–1159.
6 S. Sugiura, A. Szilágyi, K. Sumaru, K. Hattori, T. Takagi, G. Filipcsei, M. Zrínyi and T. Kanamori, *Lab Chip*, 2009, **9**, 196–198.
7 S. Sugiura, K. Sumaru, K. Ohi, K. Hiroki, T. Takagi and T. Kanamori, *Sensors Actuators A Phys.*, 2007, **140**, 176–184.
8 A. Szilágyi, K. Sumaru, S. Sugiura, T. Takagi, T. Shinbo, M. Zrínyi and T. Kanamori, *Chem. Mater.*, 2007, **19**, 2730–2732.
9 B. Ziółkowski, L. Florea, J. Theobald, F. Benito-Lopez and D. Diamond, *Soft Matter*, 2013, **9**, 8754–8760.
10 J. E. Stumpel, D. Liu, D. J. Broer and A. P. H. J. Schenning, *Chemistry*, 2013, **19**, 10922–10927.
11 J. E. Stumpel, B. Ziółkowski, L. Florea, D. Diamond, D. J. Broer and A. P. H. J. Schenning, *ACS Appl. Mater. Interfaces*, 2014, **6**, 7268–7274.
12 J. E. Stumpel, D. J. Broer and A. P. H. J. Schenning, *Chem. Commun.*, 2014, **50**, 15839–15848.
13 G. M. Whitesides, *Nature*, 2006, **442**, 368–373.
14 L. Dong and H. Jiang, *Soft Matter*, 2007, **3**, 1223–1230.
15 M. R. Romero, R. D. Arrua, C. I. Alvarez Igarzabal and E. F. Hilder, *Sensors Actuators B Chem.*, 2013, **188**, 176–184.
16 D. Eddington, *Adv. Drug Deliv. Rev.*, 2004, **56**, 199–210.
17 C. Zhang, D. Xing and Y. Li, *Biotechnol. Adv.*, 2007, **25**, 483–514.
18 K.-F. K. Arndt, D. Kuckling and A. Richter, *Polym. Adv. Technol.*, 2000, **11**, 496–505.
19 S. Park, D. Kim, S. Y. Ko, J.-O. Park, S. Akella, B. Xu, Y. Zhang and S. Fraden, *Lab Chip*, 2014, **14**, 1551–1563.
20 D. Kim and D. J. Beebe, *Lab Chip*, 2007, **7**, 193–198.
21 D. J. Beebe, J. S. Moore, J. M. Bauer, Q. Yu, R. H. Liu, C. Devadoss and B. Jo, *Nature*, 2000, **404**, 588–590.
22 M. E. Harmon, M. Tang and C. W. Frank, *Polymer*, 2003, **44**, 4547–4556.
23 Q. Luo, S. Mutlu, Y. B. Gianchandani, F. Svec and J. M. J. Fréchet, *Electrophoresis*, 2003, **24**, 3694–3702.
24 M. Czugala, C. O'Connell, C. Blin, P. Fischer, K. J. Fraser, F. Benito-Lopez and D. Diamond, *Sensors Actuators B Chem.*, 2014, **194**, 105–113.
25 M.-M. Russew and S. Hecht, *Adv. Mater.*, 2010, **22**, 3348–3360.
26 E. Merino and M. Ribagorda, *Beilstein J. Org. Chem.*, 2012, **8**, 1071–1090.
27 T. Satoh, K. Sumaru, T. Takagi and T. Kanamori, *Soft Matter*, 2011, **7**, 8030–8034.
28 G. Filipcsei, K. Sumaru, T. Takagi, T. Kanamori and M. Zrinyi, *J. Mol. Liq.*, 2014, **189**, 63–67.
29 N. Wang, Y. Li, Y. Zhang, Y. Liao and W. Liu, *Langmuir*, 2014, **30**, 11823–11832.
30 T. Satoh, K. Sumaru, T. Takagi, K. Takai and T. Kanamori, *Phys. Chem. Chem. Phys.*, 2011, **13**, 7322–7329.
31 J. ter Schiphorst, S. Coleman, J. E. Stumpel, A. Ben Azouz, D. Diamond and A. P. H. J. Schenning, *Chem. Mater.*, 2015, **27**, 5925–5931.

Chapter 3

Tuning microfluidic flow by pulsed light oscillating spiropyran-based polymer hydrogel valves

Abstract. A method for microfluidic flow control based on polymer hydrogel valves with rapid and reversible actuation properties is described. The platform allows for contactless optical flow control based upon pulsing light, resulting in a forced oscillating and control over the valve through photo-isomerization of a spiropyran derivative, co-polymerized within a N-isopropylacrylamide (NIPAM) hydrogel. Illuminating with pulsed light (450 nm) allows the valves to be held at an intermediate position for extended periods of time. Varying the pulse sequence of the light source enables the flow rate to be regulated within a microfluidic flow rate range of 0–27 μL/min. Due to the pulsed light, a small period change in the flow rate is observed that corresponds to the pulse sequence as a corresponding oscillation in the hydrogel valve.

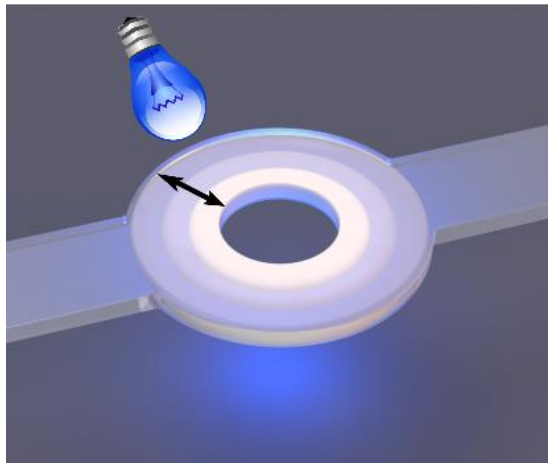

This chapter is partially reproduced from:
'Tuning microfluidic flow by pulsed light oscillating spiropyran-based polymer hydrogel valves' S. Coleman, J. ter Schiphorst, A. Ben Azouz, S. Bakker, A. P. H. J. Schenning and D. Diamond, *Sensors Actuators B Chem.*, 2017, **245**, 81–86.

3.1 Introduction

The integration of stimuli-responsive materials within microfluidic devices as a mean of non-contact microfluidic flow control,[1–6] has resulted in the development of novel in-situ, microscale mechanical components.[7–16] These components have the potential to produce vastly simplified and highly efficient fluidic chip configurations (see also Chapter 1). This requires less energy for operation and less dead volume between chips through elimination of significant amounts of tubing. The development of these biomimetic microfluidic flow systems; fluidic channels with integrated functionality similar to the human body such as the vascular system, allows for the production of microfluidic chips with in-situ generated valves, reducing the platform dimensions and complexity. This contrasts greatly with externally located mechanical valves, which are not readily scalable due to their large dimensions relative to the microfluidic platform, forcing fluidic handling to occur off chip.

Hydrogels within which a photochrome is covalently incorporated have been found to exhibit significant volume changes using light as the non-invasive stimulus, resulting in potential uses in microfluidics.[2,17,18] A popular approach to the production of light responsive swell/shrink hydrogels has been the co-polymerization of molecular photoswitches within poly(N-isopropylacrylamide) (pNIPAM).[4,18–22] Several photochromes that exhibit light-induced isomerization have been investigated, particularly azobenzenes[22,23] and spiropyrans (Sp).[24–26] Until now, the implementation of these light responsive gels for valve applications has been rarely reported.[2,18] Furthermore, tuning the flow control rather than an on/off function with these gel-based valves has not yet been reported. The latter is influenced by the fact that the photo-responsive molecules employed only has two states that are accessible by switching on/off a stimulus. Intermediate states, such as possible with mechanical valves, have not been reported. The ability to control flow, as well as stop/start flow via photoresponsive hydrogel valves having intermediate states would be appealing.

In the previous chapter a reversible light-responsive hydrogel valve that is inherently compatible with microfluidics is developed. The valve structures can be easily created in-situ after fabrication of the microfluidic platform.[18] In this self-protonating pNIPAM hydrogel, acrylic acid acts as a proton source in solution/polymer to stabilize the yellow colored hydrophilic isomer merocyanine-H^+ (McH^+), which forms spontaneous in water. This can be switched using blue light, to the ring-closed, colorless hydrophobic spiropyran form, changing the overall character of a hydrogel *i.e.* from predominantly hydrophilic (swollen) to predominantly hydrophobic (contracted), allowing repeatable swelling and shrinkage of the material, due to accompanying water uptake and release.[18] Using a Sp that is fast in both isomerization directions allowed gel-valves integrated within microfluidic channels for reversible and repeatable operation, now with opening and closing of the valve in minutes.[18]

This chapter describes the application of this photoresponsive hydrogel valve for tunable flow control within a microfluidic chip. By using a pulsing blue light source, an oscillating polymer hydrogel valve having intermediate sizes is formed, that is able to regulate the microfluidic flow rate.

3.2. Experimental

Sample preparation.

The hydrogel valves (Figure 3.1a) were produced using the following formulation (Figure 3.1 b): 500 µL 2:1 dioxane and water mixture containing 229.8 mg solid content (0.45 mg/µL); consisting of 91 mol% N-isopropylacrylamide (NIPAM), 5 mol% acrylic acid (AA), 2 mol% N,N'-methylenebisacrylamide (MBIS), 1 mol% Irgacure 819 as white light photo initiator and 1 mol% of Spiropyran derivative **1**. All materials except **1** were purchased from Sigma Aldrich and used without further purification. **1** was synthesized as described in Chapter 2 and the corresponding article.[18]

Pulsed light experiments on hydrogel disks.

The hydrogel disks generated to determine the effect of longer exposure of pulsed light were made by photopolymerizing the hydrogel monomer mixture between 150 µm spaced glass slides using an Exfo Omnicure S2000 lamp. This results in a stronger crosslinked network than using the previously method described in Chapter 2, therefore less shrinkage is observed. Subsequently, the formed film was swollen overnight in water, dried overnight (small amount of residual water is retained to prevent the material from becoming too brittle to handle) and small disks were manually punched using a 1.2 mm diameter hole puncher. Dimensional variations between disks used for the hydrogel size regulation experiments arises from variations in the amount of residual water being present in the gel during hole punching and therefore each disk must be individually characterized and the data is normalized for comparison. The gels were swollen between two glass slides spaced 250 µm apart. The area of the gels was determined by using a Leica M80 stereo microscope equipped with a Leica DFC420C camera. Images of the gel were taken after pulsing/constant illumination (Kingbright HB Blue 450nm 600mW, 3.5V), operated at 150 mA for pulsing. The capture time of each image was 10-15 s. Images were taken every 5 min during illumination, to ensure that the formation of McH^+ and resulting gel swelling when the light was off for image capture, had minimal impact on the overall gel dimensions as the time required for gel imaging was far shorter than that of illumination during actuation. The images were analyzed using Otsu Auto local thresholding with manual corrections in ImageJ software.[27] A light filter was used to block the blue light region of the spectrum to minimize shifts in the SP equilibrium and shrinking of the gel through generation of the SP form due to illumination required for microscope imaging. All microscope images were taken at 32x magnification.

Microfluidic chip design.

Valves were polymerized in-situ within microfluidic channels created in polymethylmethacrylate (PMMA) chips. The two-layer chips were prepared using a 1.5 mm thick PMMA layer for inlets and channels and a 1 mm thick capping layer to seal the chip. The microfluidic channels, liquid inlet and outlet, and a circular feature with central pillar (for housing the valve) were micro milled on the bottom layer and then sealed to the top capping layer using a dichloromethane exposure for 7 minutes.[28] The microchannel dimensions were 1 mm wide and 0.200 mm deep, while the circular valve chamber and pillar were 2.6 mm and 1 mm in diameter, respectively (Figure 3.1a).

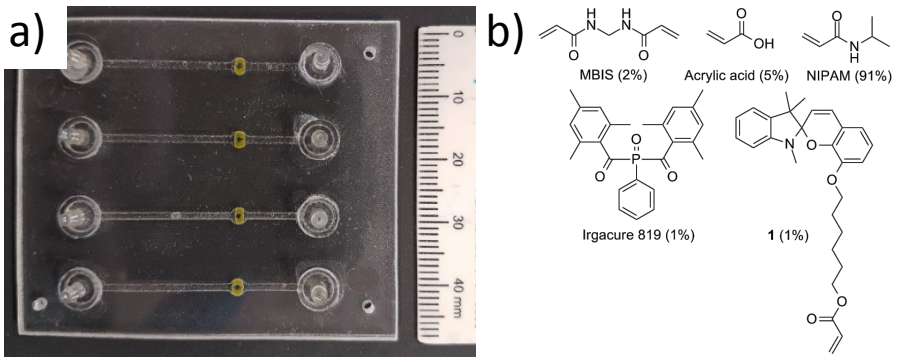

Figure 3.1: a) The chip used for performing the flow measurements, showing the possibility to form multiple valves on a single chip. b) The composition of the hydrogel used to form the microvalves.

Microfluidic valve preparation and performance.

After completing chip fabrication, the microchannel was filled with the monomeric hydrogel formulation. The valve was created in-situ by irradiation of the solution with blue LED light (Kingbright HB Blue 450nm 600mW, 3.5V) for 3 s, using an in-house fabricated LED illumination platform (same as used for later actuation) and mask to define the valve dimensions in the valve chamber. After polymerization, the microfluidic system was rinsed using deionized water to remove any unreacted monomer and the valve was allowed to briefly swell to seal the channel (monitored using Fluigent S flow sensor). Following this, the gel was illuminated for a further 60 s to complete polymerization. The valves were then left for 24h prior to usage to ensure complete hydration and swelling of the material.
Valve performance was assessed using the in-house designed LED system for actuation. Valve opening was achieved by exposure to blue LED light (Kingbright HB Blue 450nm 600mW, 3.5V) at full power for varying lengths of time, controlled by a Texas Instruments MSP430f5529 controller board. Closure of the valve occurred spontaneously as soon as the LED light source is switched off. Flow rates were monitored using either a Fluigent S (range 0-7 μL/min) or M (range 0-80 μL/min) flow rate sensor connected to a Fluigent FRP

Flowboard. It should be noted that the flow experiments reveal that these valves do not show fatigue after 10 hours of operation and continuously switching.[29]
To ensure a constant pressure was applied to the system to maintain regular liquid flow, a "constant head of pressure" method was employed using an in-house built platform. The set-up involved the use of two cylinder containers (R1 and R2), large enough that the pressure can be considered constant during the experiment. 500 ml (R1) and 300 ml (R2) water was added to the reservoirs resulting in water column heights (of 62.75 mm (R1) and 29.80 mm (R2) allowing the valve to seal the channel completely and therefore block the flow when being in the swollen form, while also providing a flow rate range (0 - 5.5 µL/min) compatible with the Fluigent S sensor without failure of the valve in the contracted form. A total volume of 241 µL of water was calculated to have passed through the chip during the entire experimental run (5500 s) and this value was assumed small enough to have insignificant effect upon the overall pressures during the experiments.

3.3 Results and Discussion

To investigate if it is possible to tune the size of the hydrogels by pulsed light, free standing hydrogel disks are exposed to a range of illumination conditions, using different pulse sequences, (1-1, 1-2 and 1-3) over longer time periods, whereby the first number denotes the time on, while the second number denoted the time off *i.e.* 1-1 stands for a sequence of 1 s illumination and 1 s darkness.

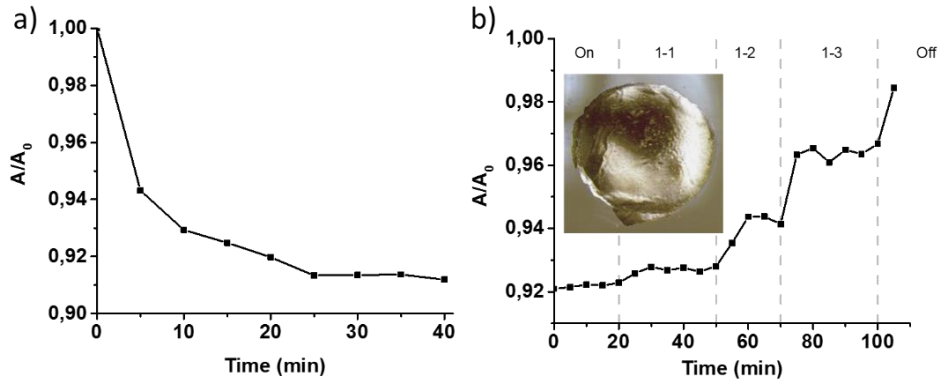

Figure 3.2. a) Normalized effect of continuous illumination by blue light on the size of the hydrogel, reaching the minimal size after roughly 25 minutes. b) Normalized effect of various pulse frequencies (on, 1-1, 1-2, 1-3, off) on hydrogel dimensions. Switching from constant illumination to a pulse sequence results in increased sizes of the hydrogel. After switching off the LED, the gel recovers towards its initial size. Inset: visual enhanced photograph of the hydrogel in the shrunk state during constant illumination (on).

First, a fully swollen gel disk is illuminated continuously with blue light to contract the gel to its minimal size (Figure 3.2a) and subsequently maintained at this size for 20 min. (Figure 3.2b, 92% initial area, 0-20 min). After this period, various pulse sequences are used to create a gel of intermediate size (Figure 3.2b). The gel is first illuminated with a pulse

sequence of 1-1 for 30 min. During the first 10 min of this period, the size of the gel increased slightly (93% initial area). For the remainder of this period, the area is relatively stable. Transitioning to the 1-2 pulse (after 50 min) produced a larger increase in the gel size and eventual stabilization of gel diameter at 94% of the initial area. After switching to a 1-3 pulse sequence, a stable gel size of 96% of the initial area is generated. From this experiment it is clear that changing the pulse frequency from 1-1 to 1-3 leads to the establishment of an increasingly swollen gel, reflecting an increasing shift in the pseudo-equilibrium towards the McH^+ due to the longer light off period. The pulsed light sequence controls the light flux per unit time reaching the gel. These experiments show that the gel size can be controlled by a light pulse sequence and suggest that stable tunable flow rates can be achieved that are unique to this pulse sequence. This is in great contrast to previously used spiropyrans, where there is a mismatch between the two isomerization processes.[30,31]
Finally the effect of various illumination methods is tested using a programmable LED platform. A Fluigent flow sensor S is used to keep the flow rates between 0-7 µL/min and the polymer valve is illuminated using two LED programmed sequences to induce varying degrees of valve actuation. A continuous, single experimental run with the polymer valve illuminated using four LED programs is also performed and a fully detailed description of these experiment can be found in the corresponding article.[32]
Following the successful application of the hydrogels as on-off valves, as shown in the corresponding article[32] and Chapter 2, the ability to induce regulated flow by holding the polymer gels to intermediate states between 'fully open' and 'fully closed' for prolonged periods of time is investigated by pulsing of the light source (Figure 3.3). It is found that under conditions of 1 s illumination and 2 s darkness (1-2 pulse sequence) a relatively stable flow rate could be maintained for the higher flow rates, as shown in Figure 3.3. The gel is first illuminated with 60 s of constant light followed by the 1-2 pulse for 180 s and finally 180 s of darkness to allow for valve closure (Figure 3.3a). In the first 60 s a similar increase in the flow rate was found as seen before.[32] Upon changing the pulsed light exposure it is observed that while a stable, regulated flow rate is achieved (4.20 ±0.05 µL/min), an initial relaxation period of approx. 90 s is required to reach this flow rate. The relaxation from peak flow rate to stable flow resulted in a drop to 4.02 µL/min. An oscillation in the flow rate with a small amplitude (0.05 µL/min,) and a frequency similar to the pulse sequence is observed, but far less pronounced as in Figure 3.4. After switching off the LED, the valve closes in a similar fashion as observed the other pulse experiments.
Following the successful control of a single flow rate, it is demonstrated that the valves can also act as reproducible variable flow rate regulators during continuous operation *i.e.* changing flow rates during operation (Figure 3.3b) using a program where the valve is first opened slightly, kept at this flow, followed by further opening. During the first flow rate control event, the 30 s constant illumination resulted in a peak flow rate of 2.61±0.08 µL/min. This is, approximately 50% of the maximum flow that can be achieved, which is as expected since the illumination period was half that of the single flow control event (Figure

3.3a). When switched to 1-2 pulsed light, a slight decrease in flow is initially observed in the first 90 s, which becomes more stable but with a gradual increase in flow over time. After a period of time (approx. 90 s), the flow rate stabilizes. However, since the pulsed light sequence maintains the pseudo-equilibrium further towards the McH^+, the flow rate slowly increases. This would continue to increase over time towards the steady-state flow rate, which is ca. 4 µL/min according to Figure 3.3a. Nevertheless, since the time to create the equilibrium is larger than the time used in this experiment, repeatable and relatively stable plateau's can be formed. Following the initial 1-2 pulsed light sequence a further 30 s illumination opens the valve and increases the flow rate. A peak flow of 4.66 ±0.08 µL/min is generated following this illumination phase with a gradual reduction to 3.99 µL/min ±0.03 during the 1-2 pulsed light sequence. Once again, similar effects are found during this second flow control phase whereby 30 s constant illumination resulted in rapid opening of the valve followed by reduction in flow rate to a more stable flow. In this case after the 90 s reduction towards the steady-state condition (ca. 4.0 µL/min) is found. Hence, these experiments are in agreement with the experiments found in Figure 3.3, showing that the flow depends on the pulsed light sequence and in the case of short exposure, also on the initial value.

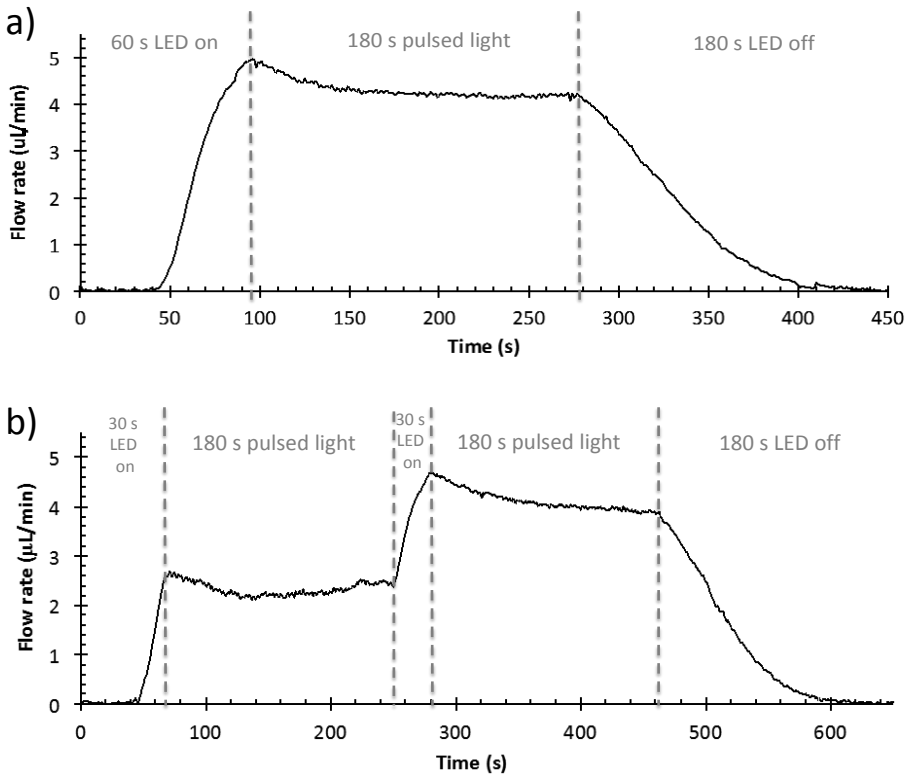

Figure 3.3. a) Effect of a pulsed light (1-2) illumination on the flowrate of the microfluidic device. b) Effect of constant illumination, followed by pulsed light on a microfluidic valve. After pulsing, additional constant illumination results in an increased flow rate. Switching off the illumination results in rapid closing of the valve.

To show that the flow rate is controlled by the pulsed sequence and that this concept is more general, a set of experiments is performed. In these experiments the hydrogel valve is illuminated using a 2-2, 2-3 and 2-4 pulsed light sequences for an extended period. The flow is measured using a Fluigent M flow sensor which has a much larger flow range, ranging from 0 to 80 µL/min. When starting the illumination using a 2-3 pulse, it takes roughly 300 seconds to reach a constant flow of 25 µL/min (Figure 3.4a) that can be kept for at least 10 minutes. In addition, an oscillation in the flow rate with an amplitude of roughly 3 µL/min is achieved (Figure 3.4a and b). This amplitude is the largest, when the flow rate reaches a pseudo equilibrium state. The frequency of the oscillation correspond to the pulse sequence with an increase in the flow rate during illumination and a decrease when not illuminating. This reveals that during the pulsed light irradiation, an oscillation in the dimensions of the hydrogel valve takes place. Interestingly when the pulse sequence is changed the flow rate is also changing. A shorter non-illumination time (2-2) leads to a higher flow of 27 µL/min and a longer non-illumination time (2-4) result in a flow of 20 µL/min whereby, the oscillation frequency is the same as the pulse frequency. It should be noted, however, that there is no systematic change in amplitude of the flow oscillation when change the pulse sequence. The amplitude at these higher flow rates are more pronounced than in the case of the experiments in Figure 3.3, due to the larger flow sensor, restricting the flow less, as well as waiting longer between the pulses.

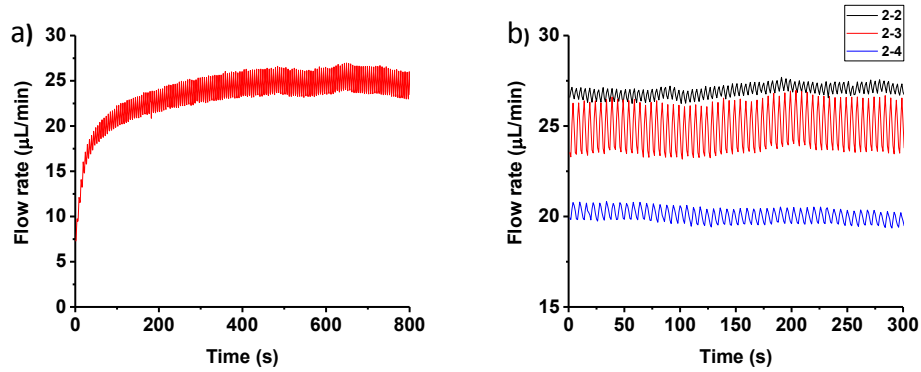

Figure 3.4. a) Effect of pulsed light (2-3 sequence) on the measured flow speed of a hydrogel valve, showing a stable flow speed of 25 µL/minute. b) Arbitrary selected part of the measurement of flow rate for pulse sequences of 2-2, 2-3 and 2-4. In all cases, the oscillation follows the pulse sequence used.

These experiments are followed up by a recent publication the group of Diamond, where a proportional integral derivative (PID) system is used. This closed feedback loop allows measuring the flow rate in real time and adjusting the pulse frequency and illumination intensity accordingly, to achieve the dialed in flow rate.[29]

3.4 Conclusion

It is shown that reproducible actuation for flow control within practical timescales can be achieved using a photoresponsive polymeric hydrogel. By using a pulsing blue light source, an oscillating polymer hydrogel valve having intermediate sizes is formed. It is able to regulate the flow in a microfluidic channel, similar to multi stage controllable mechanical valves. These hydrogel materials demonstrate the initial steps towards the creation of truly biomimetic fluidics platforms. In this, the entire regulatory processes of the system is fully integrated, protected from the external environment, and inherently scalable. This is in contrast to existing mechanical valves, whose integration on chip is limited by size, making parallelization of valves difficult. These mechanical valve arrays are located off-chip, resulting in the requirement of extensive interconnectivity, producing significant dead volumes. The production of chips with integrated valves therefore provides the foundation for the development of chips with much more sophisticated fluid handling capabilities. The use of millimeter dimension surface mounted LEDs in combination with similarly sized gel valves creates the opportunity to create arrays of valves without any significant increase in platform dimensions. This allows more complex functions, such as multi-stage chemical processes or large scale arrays of "single shot" assays while remaining compact, affordable and portable. Our results not only demonstrate the potential application of these gels within microfluidic platforms as microscale valves for the production of low-cost flow control. It also allows the characterization of the photoresponsive hydrogel dimensions using pulsed light. Furthermore, with the recent improvements of this system, full control over the flow in these microchannels with operating times of seconds are now realized.

3.5 References

1 S. Sugiura, A. Szilágyi, K. Sumaru, K. Hattori, T. Takagi, G. Filipcsei, M. Zrínyi and T. Kanamori, *Lab Chip*, 2009, **9**, 196–198.
2 S. Sugiura, K. Sumaru, K. Ohi, K. Hiroki, T. Takagi and T. Kanamori, *Sensors Actuators A Phys.*, 2007, **140**, 176–184.
3 A. Szilágyi, K. Sumaru, S. Sugiura, T. Takagi, T. Shinbo, M. Zrínyi and T. Kanamori, *Chem. Mater.*, 2007, **19**, 2730–2732.
4 B. Ziółkowski, L. Florea, J. Theobald, F. Benito-Lopez and D. Diamond, *Soft Matter*, 2013, **9**, 8754–8760.
5 J. E. Stumpel, D. Liu, D. J. Broer and A. P. H. J. Schenning, *Chemistry*, 2013, **19**, 10922–10927.
6 J. E. Stumpel, B. Ziółkowski, L. Florea, D. Diamond, D. J. Broer and A. P. H. J. Schenning, *ACS Appl. Mater. Interfaces*, 2014, **6**, 7268–7274.
7 G. M. Whitesides, *Nature*, 2006, **442**, 368–373.
8 L. Dong and H. Jiang, *Soft Matter*, 2007, **3**, 1223–1230.
9 M. R. Romero, R. D. Arrua, C. I. Alvarez Igarzabal and E. F. Hilder, *Sensors Actuators B Chem.*, 2013, **188**, 176–184.
10 D. Eddington, *Adv. Drug Deliv. Rev.*, 2004, **56**, 199–210.
11 C. Zhang, D. Xing and Y. Li, *Biotechnol. Adv.*, 2007, **25**, 483–514.
12 K.-F. K. Arndt, D. Kuckling and A. Richter, *Polym. Adv. Technol.*, 2000, **11**, 496–505.
13 S. Park, D. Kim, S. Y. Ko, J.-O. Park, S. Akella, B. Xu, Y. Zhang and S. Fraden, *Lab Chip*, 2014, **14**, 1551–1563.
14 D. Kim and D. J. Beebe, *Lab Chip*, 2007, **7**, 193–198.

15 D. J. Beebe, J. S. Moore, J. M. Bauer, Q. Yu, R. H. Liu, C. Devadoss and B. Jo, *Nature*, 2000, **404**, 588–590.
16 M. Chen, H. Huang, Y. Zhu, Z. Liu, X. Xing, F. Cheng and Y. Yu, *Appl. Phys. A Mater. Sci. Process.*, 2011, **102**, 667–672.
17 M. Czugala, C. O'Connell, C. Blin, P. Fischer, K. J. Fraser, F. Benito-Lopez and D. Diamond, *Sensors Actuators B Chem.*, 2014, **194**, 105–113.
18 J. ter Schiphorst, S. Coleman, J. E. Stumpel, A. Ben Azouz, D. Diamond and A. P. H. J. Schenning, *Chem. Mater.*, 2015, **27**, 5925–5931.
19 T. Satoh, K. Sumaru, T. Takagi and T. Kanamori, *Soft Matter*, 2011, **7**, 8030–8034.
20 G. Filipcsei, K. Sumaru, T. Takagi, T. Kanamori and M. Zrinyi, *J. Mol. Liq.*, 2014, **189**, 63–67.
21 N. Wang, Y. Li, Y. Zhang, Y. Liao and W. Liu, *Langmuir*, 2014, **30**, 11823–11832.
22 M.-M. Russew and S. Hecht, *Adv. Mater.*, 2010, **22**, 3348–3360.
23 E. Merino and M. Ribagorda, *Beilstein J. Org. Chem.*, 2012, **8**, 1071–1090.
24 R. Klajn, *Chem. Soc. Rev.*, 2014, **43**, 148–184.
25 X. D. Sun, M. G. Fan, X. J. Meng and E. T. Knobbe, *J. Photochem. Photobiol. A Chem.*, 1997, **30**, 3–6.
26 H. Gong, C. Wang and M. Fan, *J. Mater. Chem.*, 2001, **11**, 3049–3052.
27 Nobuyuki Otsu, *IEEE Trans. Syst.*, 1979, **9**, 62–66.
28 S. P. Ng, F. E. Wiria and N. Tay, *Procedia Eng.*, 2016, **141**, 130–137.
29 C. Delaney, P. Mccluskey, S. Coleman, J. Whyte, N. Kent and D. Diamond, *Lab Chip*, 2017, **17**, 2013–2021.
30 T. Satoh, K. Sumaru, T. Takagi, K. Takai and T. Kanamori, *Phys. Chem. Chem. Phys.*, 2011, **13**, 7322–7329.
31 B. Ziółkowski, L. Florea, J. Theobald, F. Benito-Lopez and D. Diamond, *J. Mater. Sci.*, 2016, **51**, 1392–1399.
32 S. Coleman, J. ter Schiphorst, A. Ben Azouz, S. Bakker, A. P. H. J. Schenning and D. Diamond, *Sensors Actuators B Chem.*, 2017, **245**, 81–86.

Chapter 4

Photo-responsive passive micromixers based on spiropyran size-tunable hydrogels

Abstract. A light responsive size-tunable hydrogel has been fabricated that can be used to create a passive micromixer. This allows to switch between a mixed and a non-mixed fluid flow in a microchannel. The production process, as well as the characterization is described.

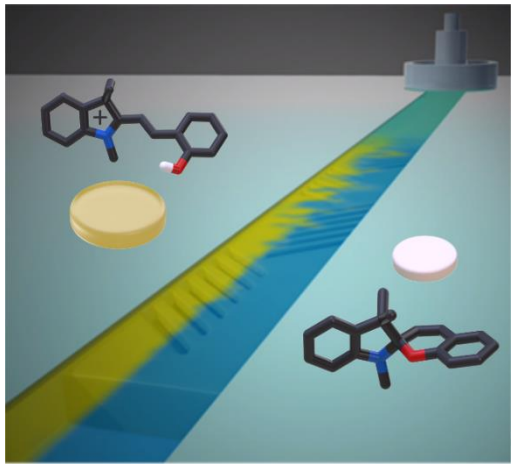

Dedicated to the memory of Giuseppe G. Melpignano who passed away during the completion of this work.

This chapter is partially reproduced from:
'Photo-responsive Passive Micromixers based on Spiropyran Size-Tunable Hydrogels' J. ter Schiphorst, G.G. Melpignano, H. Eslami Amirabadi, H.J.M. Houben, S. Bakker, J.M.J. den Toonder and A.P.H.J. Schenning, *Macromol. Rapid Comm.*, 2018, **39**, 1700086.

4.1 Introduction

Microfluidic devices allow the manipulation of fluids down to the micrometer scale and are receiving a lot of attention for applications where low volumes and high throughputs are required.[1–3] In such devices different fluids often not only need to be transported, but also mixed.[4] However, due to the small size of the micro-channels, laminar flow usually dominates and turbulent flow is non-existent.[5] Within this laminar flow, mixing is predominantly caused by diffusion, which requires long residence times of the fluids, limiting the flow speed and throughput. So-called passive and active micromixers have been developed to obtain mixing of liquids in microfluidic devices through the creation of chaotic laminar flow patterns.[6–12] Active mixers[13] require an external input *e.g.* acoustics,[14] electricity,[15,16] or magnetic fields[17–19] implying complex off-chip setups. Passive mixers cause mixing by structural features inside the microfluidic channel that stretch and fold the liquids to induce shorter path lengths for diffusion.[20–22] One particular example is the slanted groove mixer, consisting of a microchannel with a grooved wall/surface. Since the grooves are slanted with respect to the main flow direction, they induce secondary flow patterns when a liquid is pumped through the channel, resulting in mixing.[7,23] The downside of the passive mixers is that they cannot be manipulated to the user's needs since the structural features are static.[23,24] Therefore, it would be attractive to make such mixers switchable, forming a passive mixer that can be switched between an 'on' and an 'off' state, as this allows to control mixing and to easily clean a microchannel.[25]

Responsive micromixers that change shape using light as a stimulus would be appealing, as it allows to control mixing, in a non-invasive non-contact fashion.[18,26,27] Hydrogels such as poly(N-isopropylacrylamide) (pNIPAM) have received a lot of attention as the shape can be changed from a swollen to a collapsed state with temperature (see also chapter 1).[28–33] This shape change can also be achieved using light by incorporation of a photochromic dye in the polymer hydrogel.[34–38] Upon switching the illumination on and off,[39] the volume of the hydrogel can be switched between two states. By tuning these switching conditions *i.e.* the isomerization rates,[40–42] shape changing hydrogels can be achieved that can be tuned to the user's need.[43,44] However, little is known about tuning the size of the hydrogel, as the photochromic switch is usually converted to only one photostationary state using one light intensity.[38,45,46] Hydrogels having intermediate states would, however, be appealing for a variety of applications in which tunable properties are desired.

Recently, the use of light responsive hydrogels as valves in a microfluidic device have been reported.[30,35,37,47,48] Incorporation of spiropyran[38] and tuning the equilibrium by using a pulsing light source, resulted in an oscillating polymer hydrogel valve having intermediate sizes which was able to regulate the microfluidic flow rate.[49] Light has also been used as a stimulus to mix two oil phases inside a microchannel, using the isomerization of azobenzene dissolved in an aqueous phase, switching from a tubing to drop making state.[50,51] So far, however, the use of light responsive hydrogels as photo-responsive micromixers has not been reported. It is now shown that the size of photoresponsive hydrogel can be tuned by

changing the intensity of the light and these gels can be used to fabricate a passive slanted groove mixer.[21] The mixer can be switched off by light allowing to change from a mixing to a non-mixed state (Figure 4.1).

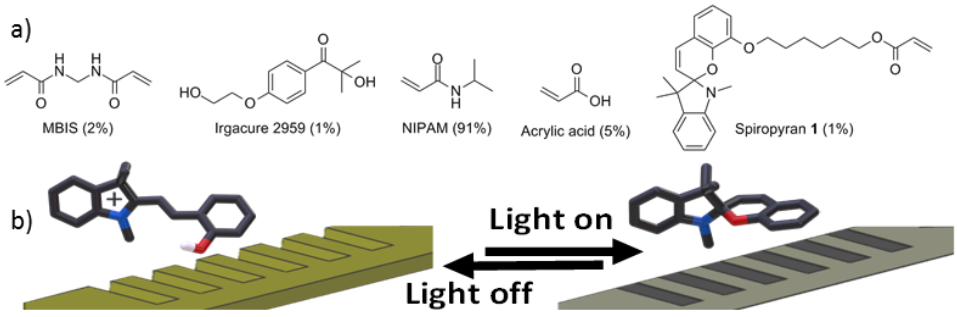

Figure 4.1. a) Chemical structure of the monomers used to fabricate the light responsive hydrogel. b) Schematic representation of the photoresponsive passive micromixers based on a light responsive hydrogel. In the off-state (no illumination, left) the hydrogel is swollen, resulting in a passive mixer, while upon exposure to light, the gel shrinks resulting in a non-mixing flat state (right).

4.2 Experimental

All reagents and chemicals were obtained from commercial sources unless stated otherwise and used without further purification. SU-8 3025 and 2050 (MicroChem) were used for the hydrogel scaffold and PDMS (Sylgard 184; 10: 1 mixing ratio base: curing agent) channel respectively. The used developer for SU-8 is mr-Dev 600. All other chemicals were purchased from Sigma-Aldrich. Spiropyran molecule **1** was synthesized as described in Chapter 2. The scaffold was placed on Thermo Scientific Menzel-Glaser microscope glass slides (76x26 mm). The hydrogel precursor mixture containing a 2:1 dioxane: water mixture with a concentration of monomers of 0.5 mg/µL, was similar to the mixture used in previous chapters.[37] The mixture contains 91 mol% NIPAM, 5 mol% acrylic acid, 2 mol% N,N'-methylenebisacrylamide (MBIS), 1 mol% Irgacure 2959 1 mol% acrylate functionalized spiropyran **1** (Figure 4.1a)

Preparation of the microfluidic device.

The microscope glass slides are cleaned by sonication in ethanol for 20 minutes and dried under a stream of compressed nitrogen. Subsequently they are placed in a UV plasma etcher (Quorum Technologies K1050X) and treated for 5 minutes at 100W, 0.8 mbar O_2 pressure. The glass slides are spincoated (3000 rpm, 30 sec) with a 1:1 mixture of isopropanol: water, containing 1 volume% 3-(trimethoxysilyl)propyl methacrylate, before being placed on a hotplate (100°C) for 15 minutes. For spincoating and curing of SU-8 3025, the following parameters are used: 500 rpm with an acceleration of 100 rpm/s for 10 seconds, followed by 3000 rpm with an acceleration of 300 rpm/s for 45 seconds, followed by a spin down of 10 seconds with a deceleration of 300 rpm/s. The glass slides are transferred to a hotplate

of 65 °C for 1 minute, before being placed on a hotplate of 95 °C for 8 minutes. The samples are allowed to cool down to room temperature. The SU-8 coated glass slides are exposed through a mask (Figure 4.3a) for 25 seconds, 13 mW/cm^2 (325 mJ/cm^2) before being placed on a hotplate of 65 °C for 2 minutes followed by 95 °C for 4 minutes to form the structures. It was found to be crucial to place the sample back on the 65 °C hotplate for 30 seconds before being cooled down slowly to prevent the material from detaching from the glass substrate. The samples are placed in the developer for 10 minutes and rinsed with isopropanol before being dried using compressed nitrogen. The micromixer has an inner channel diameter of 200 um and a length of roughly 3 centimeters. The mixing structure consists of 10 alternating slanted groove pairs consisting of 6 grooves per side. These grooves are under an angle of 45 degree and 130 um in width. The spacing of these grooves is 70 um. The SU-8 around the channel is structured as crosses rather than a uniform layer to prevent the material from cracking and detaching.

The hydrogel precursor mixture is injected in place by hand with the aid of a Leica M80 stereomicroscope using a 5 µl micro syringe (SGE Analytical syringe) with a cone tip under a constant stream of nitrogen to create an inert atmosphere required for the polymerization. The hydrogel precursor is polymerized using an Exfo Omnicure S2000 at full power (~300 mW/cm^2) for 30 seconds.

The PDMS channel is made by forming a negative structure of SU-8 on a silicon wafer. For spincoating and curing of SU-8 2050, the following parameters are used: 500 rpm with an acceleration of 100 rpm/s for 10 seconds, followed by 2000 rpm with an acceleration of 300 rpm/s for 45 seconds, followed by a spin down of 7 seconds with a deceleration of 300 rpm/s. The wafer is transferred to a hotplate of 65 °C for 2 minute, before being placed on a hotplate of 95 °C for 11 minutes. The wafer is allowed to cool down to room temperature before being exposed through a mask for 30 seconds, 13 mW/cm^2 (390 mJ/cm^2). The wafer is transferred to a hotplate of 65 °C for 5 minutes followed by 95 °C for 9 minutes to form the structures. The wafer is placed in the developer for 10 minutes and rinsed with isopropanol before being dried using compressed nitrogen. Sylgard 184 is mixed typically as 40 gram base: 4 gram curing agent (10:1) and degassed under vacuum for at least 30 minutes, until no air bubbles are formed anymore. The mixture is poured over the wafer being taped to the bottom of a glass Petridis, forming a layer of roughly 3-4 mm. After pouring, the material is degassed again and left to cure for at least 72 hours at room temperature, as elevated temperatures resulted in thermal shrinkage and mismatch of the two components. When cured, the PDMS is cut to size and covered using Scotch tape to keep clean. The PDMS is transferred to a plasma etcher (Diener Femto PCCE). The chamber is flushed for 15 minutes with nitrogen before generating a nitrogen plasma (75W) for 5 minutes. The modified PDMS is directly placed on the hydrogel filled SU-8 scaffold and placed in an oven at 60 °C for 24 hours. Before measuring the device, the channel is first flushed with water for at least an hour to ensure a swollen state of the hydrogel and removal of any residual non-reacted monomer.

In microfluidics, the flow usually is laminar, as can be expressed by Reynolds number Re. In channel or pipe flow, for Re <2300, the flow can be considered always laminar, while above this value, the flow can become turbulent. In a laminar flow, only diffusion is a driving force for mixing. Re is defined as:

$$Re = \rho u L/\mu, \quad (1)$$

where ρ = density (water = 1000kg/m^3), u = characteristic velocity, which depends on the flow rate within the channel (0.73 m/s for 1000 µl/min in our channel with rectangular cross section 200x114 um), L the characteristic length of the channel (145 µm for the 200x114 um rectangular channel) and μ the dynamic viscosity of water (0.001 kg/m · s). Using this equation shows that with the fastest flow rate used in this research (1000 µl/min), Re is roughly 100, which is still far below the 2300 threshold for turbulent flow, confirming that the mixing in this device will be caused by diffusion only. To calculate the channel length required for complete mixing by diffusion, the Peclet number is used, which represents diffusive effects over convection.

$$Pe = Lv/D \quad (2)$$

in which D is the diffusion coefficient, which is roughly $0.7 \cdot 10^{-9}$ m^2/s for the used dye methylene blue[52] in water. This results in Pe = $6 \cdot 10^4$. The required length for mixing is $L_m \sim Pe \cdot L$, resulting in 9 meters for complete mixing in the case of a flow rate of 400 µl/min. More realistic values used for the flow rate used in this research are 5-25 µl/min, resulting in a Peclet number of 530 – 2650. For complete mixing trough diffusion at a flow rate of 5 µl/min, still a channel of 7 cm would be required. This illustrates the need of micromixers.

4.3 Results and Discussion

First the degree of swelling, shrinking and the possibilities to tune the hydrogel size using various light intensities is studied. The hydrogel used, is based on poly(N-isopropylacrylamide) containing a crosslinker, acrylic acid as internal proton donor and spiropyran as light responsive moiety (Figure 4.1a). The acrylic acid ensures that the equilibrium of spiropyran is towards the polar protonated merocyanine[31] form, resulting in a swollen gel when not illuminated. Upon exposure to blue or white (LED) light, the polar protonated merocyanine isomerizes to the apolar spiropyran, causing a release of water and shrinkage of the hydrogel (Figure 4.1b). To determine the volume change of the hydrogels, free standing polymer hydrogel disks are prepared having an initial diameter of roughly 1.2 mm and thickness of 200 µm. The hydrogel is obtained after photopolymerization of the acrylate monomer mixture in the presence of a photoinitiator. After adding deionized water the hydrogel disk swells by a factor 3.2 and becomes yellow (Figure 4.2a). The yellow color

indicates the presence of the protonated mercocyanine species.[37] Upon exposure to white light the gel shrinks 23%, which is 2.5 times the size of the dry state and becomes colorless pointing to the conversion of the protonated merocyanine to the spiropyran form (Figure 4.2). The progress of shrinking and swelling takes place in roughly 30 minutes, is fully reversible and the response and degree of shrinking and swelling are similar to earlier observations using comparable light responsive hydrogels with similar white light sources.[32,37]

In order to investigate whether the size of the gel can be tuned, a blue LED (Kingbright HD Blue 450 nm 600mW, 3.5V) is used and the intensity is varied, by adjusting the applied current (Figure 4.2b). First the hydrogel disk is illuminated for 20 min to reach the minimal size of 2.13 μm^2, 94% of the initial size. The gel can be kept at this size for at least 20 minutes by continuous illumination (Figure 4.2b). Subsequently the illumination intensity is halved resulting in an increase in hydrogel size. After 25 minutes the size stabilizes at 2.19 μm^2, 97% of the initial size, and can be maintained for another 25 minutes, illustrating that the size of the hydrogel can be tuned using light. After halving the LED intensity again the gel size increases further to 2.22 μm^2 and after switching the LED off the initial swollen gel size of 2.25 μm^2 is obtained within 10 minutes. These data show that the photo stationary state of the spiropyran - protonated merocyanine equilibrium can be tuned by the intensity of the light *i.e.* the population of these two isomers determines the size of the gel and can therefore be controlled by using different light intensities. It should be noted that it takes 30 minutes to swell the fully shrunken gel to the fully swollen state at room temperature in the absence of light.

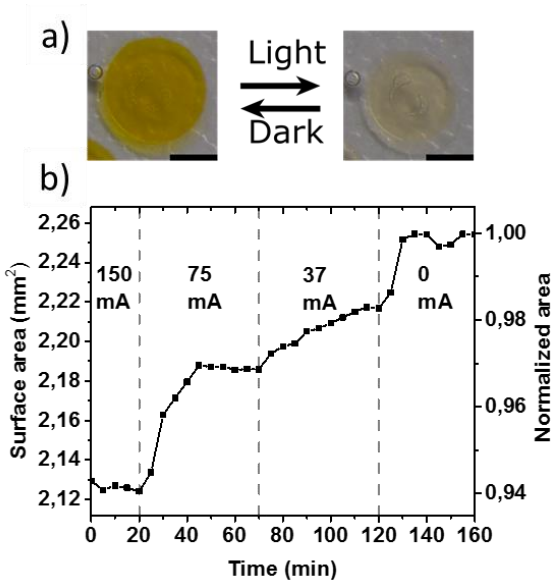

Figure 4.2. a) Hydrogel in the swollen state (before illumination) and the shrunk state (after white light illumination). The yellow color indicates the presence of protonated merocyanine. The scale bar is 1 mm. b) Size of the hydrogel measured in time as a function of the LED driving current.

Fabrication of the photo responsive passive micromixers.

For the fabrication of the microfluidic chip containing the photo-responsive hydrogel passive micromixer, two components are fabricated (Figure 4.3). The bottom component contains the light responsive slanted groove mixer (Figure 4.3b) and the top component contains the micro channel (Figure 4.3c). Two inlets and one outlet are present in the top component, allowing 2 different fluids to be brought in contact before passing over the micromixer structure and subsequently leaving the device. The bottom component is 25 µm in height having 10 alternating sets of slanted grooves, each set consisting of 6 grooves (Figure 4.3). These grooves are under an angle of 45 degree and 130 µm in width. The spacing of these grooves is 70 µm. Building up the microfluidic chip in this way allows to modify the dimensions and conditions of the two components separately.

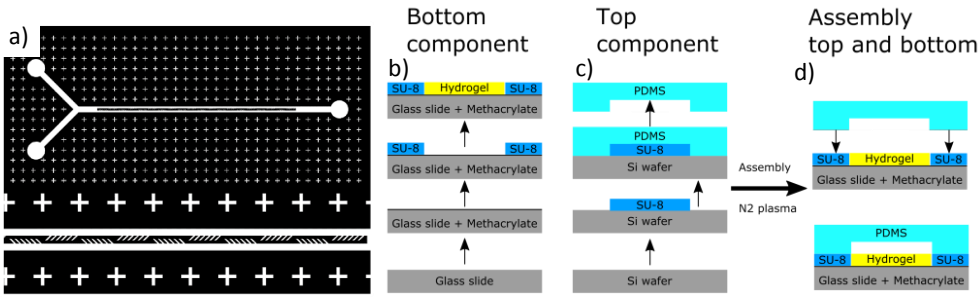

Figure 4.3. a) Lithography mask used to form the channel in the bottom component. The channel is 3 cm in length and 200 µm in width. b-d) Fabrication of the photo-responsive passive micromixers in a microfluidic device. b) Formation of the bottom part, whereby a glass slide is modified with a methacrylate for covalent attachment of the hydrogel, followed by formation of the SU-8 slanted groove scaffold with lithography using the mask shown in a, followed by deposition of the hydrogel inside the channel. c) Formation of the top part, where SU-8 is deposited on the surface and patterned through lithography, followed by replica molding the structure with poly(dimethyl siloxane) PDMS. d) Assembly of the top component to the bottom component to fabricate the microfluidic device, whereby covalent attachment is achieved by modifying the PDMS surface with a N_2 plasma.[53]

The light responsive passive micromixer is made by depositing a dioxane-water solution containing the hydrogel acrylate precursor mixture inside the slanted groove bottom component using a 5 µl cone tipped syringe (Figure 4.3b). Two approaches are used: depositing of droplets, which resulted in complete filling of the entire scaffold, and moving a droplet over the surface, which resulted only in filling the groove cavities by capillary forces. After filling and polymerization, a height of roughly 21 µm was obtained after complete filling, while in case of filling only the grooves, a height of 15 µm was achieved.[54] Subsequently, the light responsive behavior of the slanted groove hydrogel is investigated. When the bottom component containing the completely filled slanted groove hydrogel is placed directly in water, the gel becomes yellow and bulges over the edge of the scaffold, indicating successful swelling.[54] After illumination for 5 minutes, the gel becomes pale, indicating photoisomerization of the protonated mercocyanine to the spiropyran form,

accompanied by shrinkage of the gel, as the color is similar as the hydrogel disk after illumination (Figure 4.4 versus Figure 4.2). The color change for the groove filled mixer is less visible, since the film is thin. The light responsive behavior of both hydrogel system is reversible as the color changes are repeatedly observed upon turning the light on and off. Based on the hydrogel disk measurements using white light (*vide supra*), the completely filled hydrogel scaffold will have a height difference with the scaffold of 42 µm in the swollen state, but upon shrinkage by light, a residual height of 27 µm will remain. The groove filled structure will have a mixing structure of 23 µm fins in the swollen state and 12 µm in the shrunk state. Since the formed channel depth of the top component is 114 µm, and a 20% height difference is found to be optimal for inducing mixing,[23] it is expected that at least for the groove filled structure the passive hydrogel mixer can be switched off (*vide infra*).

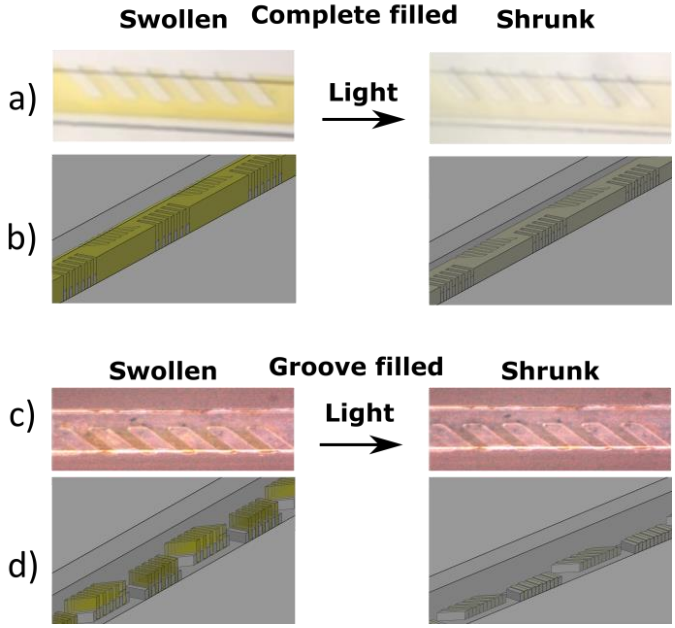

Figure 4.4. Overview of the two configurations of the micromixer used. The gray material is the SU-8 scaffold and the yellow material the hydrogel. a) Photograph of a part of the completely filled hydrogel micromixer before illumination (swollen gel), and after illumination (shrunk gel) with white light, showing the difference in color. b) Schematic representation of the height difference of the completely filled hydrogel mixer before and after light exposure, showing that the material does not return to a flat surface. c) Photograph of a part of the groove filled hydrogel micromixer before and after illumination. Contrast of the image was enhanced for visibility. d) Schematic representation of height difference of the groove filled hydrogel mixer before and directly after light exposure.

Mixing behavior of the photoresponsive micromixer.

Preliminary experiments are performed to investigate if a photoresponsive passive micromixer can be created in a microfluidic device that allows to switch between a mixed and a non-mixed fluid flow in a microchannel. The microfluidic devices are fabricated by

placing the modified PDMS top component on the hydrogel filled SU-8 bottom component and curing in an oven at 60 °C for 24 hours.[53] Before measuring the device, the channel is first flushed with water for at least one hour to ensure a swollen state of the hydrogel and removal of any residual non-reacted monomer. Two syringes connected to pumps, filled with deionized water and deionized water containing methylene blue as contrast agent, respectively, are connected to the two inlets of the chip. It is found that the completely filled scaffold resulted in an always on state of the mixer, showing that the gel is not capable to shrink sufficiently to achieve a completely flat surface (vide supra). Therefore, only experiments with the groove filled micromixer are performed and its efficiency was first evaluated in the absence of light. Hereby, the flow rate was varied between 10 and 60 µL/minute, as in this regime passive mixers are required since mixing by diffusion is not sufficiently fast. An almost homogeneous color distribution across the microchannel cross section is observed for all flow speeds (Figure 4.5), indicating that the mixing is efficient, and close to complete mixing is achieved. This illustrates that the scaffold containing the hydrogel is capable of mixing fluid streams.

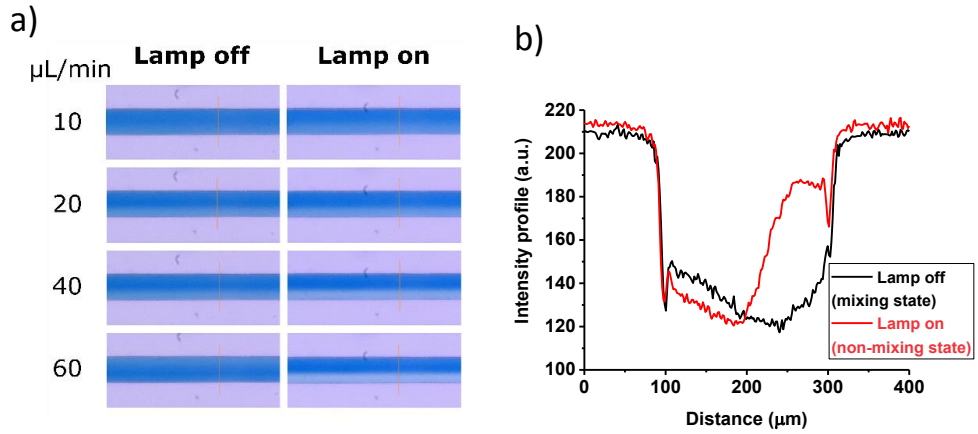

Figure 4.5. a) Micrographs of the end of the channel of the micromixer, past the part where the micromixer is present, measured at a flow rate ranging from 10 to 60 µL per minute in the mixing state (lamp off) and the non-mixing state (lamp on). b) Profile plot of the color intensity across the width of the microchannel (200 µm) measured at the orange line in a), at a 60 µL per minute flow rate while the lamp is off (mixing state) or on (non-mixing state).

In order to investigate if the micromixer can be switched off, the hydrogel mixer is illuminated with white light. Interestingly, at the flow rate of 60 µL/minute (Figure 4.5a), separation between the non-colored and colored water flow indeed becomes visible. This behavior is similar to a microchannel with completely flat walls,[54] confirming that the hydrogel passive mixer can be switched off with light. However, some mixing still occurs which might be due to the residual height present when illuminating (*vide supra*). Upon lowering the flow rate a gradual increase in mixing is observed as the residence time becomes longer and diffusion takes place. In the case of 10 µL/min, almost complete mixing

is observed and little difference between the non-exposed and exposed microfluidic devices.[54] The measured color intensity profiles prove quantitatively the difference between mixing (lamp off) and no mixing (lamp on) for higher flow rates (Figure 4.5b).

4.4 Conclusion

In this chapter, photo-responsive hydrogels of which the size can be tuned by simply changing the intensity of light are presented. Such hydrogels are appealing for applications in which tunable shape changes are desired such as valves and mixers in microfluidic devices. The tunable light responsive hydrogels can be integrated in grooved surfaces of microfluidic channels. Preliminary experiments show the possibilities of switching off the passive micromixer using light. Tuning the mixing in a microchannel will be the next step and will open new possibilities for multi-purpose microfluidic devices where mixing can be tuned depending on the user's need.

4.5 References

1 G. M. Whitesides, *Nature*, 2006, **442**, 368–373.
2 I. E. Araci and P. Brisk, *Curr. Opin. Biotechnol.*, 2014, **25**, 60–68.
3 D. Sinton, *Lab Chip*, 2014, **14**, 3127–3134.
4 V. Hessel, H. Löwe and F. Schönfeld, *Chem. Eng. Sci.*, 2005, **60**, 2479–2501.
5 A. A. S. Bhagat, E. T. K. Peterson and I. Papautsky, *J. Micromechanics Microengineering*, 2007, **17**, 1017–1024.
6 C.-Y. Lee, C.-L. Chang, Y.-N. Wang and L.-M. Fu, *Int. J. Mol. Sci.*, 2011, **12**, 3263–3287.
7 H. E. H. Meijer, M. K. Singh, T. G. Kang, J. M. J. den Toonder and P. D. Anderson, *Macromol. Symp.*, 2009, **279**, 201–209.
8 L. Falk and J. M. Commenge, *Chem. Eng. Sci.*, 2010, **65**, 405–411.
9 E. A. Mansur, M. Ye, Y. Wang and Y. Dai, *Chinese J. Chem. Eng.*, 2008, **16**, 503–516.
10 Y. K. Suh and S. Kang, *Micromachines*, 2010, **1**, 82–111.
11 N.-T. Nguyen and Z. Wu, *J. Micromechanics Microengineering*, 2005, **15**, R1–R16.
12 J.M. Ottino, *The kinematics of mixing: Stretching, Chaos, and Transport*, Cambridge University Press, 1989.
13 T. J. Ober, D. Foresti and J. A. Lewis, *Proc. Natl. Acad. Sci.*, 2015, **112**, 2–7.
14 R. H. Liu, J. Yang, M. Z. Pindera, M. Athavale and P. Grodzinski, *Lab Chip*, 2002, **2**, 151–157.
15 V. V. Khatavkar, P. D. Anderson, J. M. J. den Toonder and H. E. H. Meijer, *Phys. Fluids*, 2007, **19**, 83605.
16 J. den Toonder, F. Bos, D. Broer, L. Filippini, M. Gillies, J. de Goede, T. Mol, M. Reijme, W. Talen, H. Wilderbeek, V. Khatavkar and P. Anderson, *Lab Chip*, 2008, **8**, 533–541.
17 T. G. Kang, M. A. Hulsen, P. D. Anderson, J. M. J. den Toonder and H. E. H. Meijer, *Phys. Rev. E*, 2007, **76**, 1–11.
18 A. K. Agarwal, S. S. Sridharamurthy and D. J. Beebe, *J. Microelectromechanical Syst.*, 2005, **14**, 1409–1421.
19 Y. Gao, A. Van Reenen, M. A. Hulsen, A. M. De Jong, M. W. J. Prins and J. M. J. den Toonder, *Microfluid. Nanofluidics*, 2014, **16**, 265–274.
20 A. D. Stroock, S. K. W. Dertinger, A. Ajdari, I. Mezic, H. A. Stone and G. M. Whitesides, *Science*, 2002, **295**, 647–652.
21 J. Marschewski, S. Jung, P. Ruch, N. Prasad, S. Mazzotti, B. Michel and D. Poulikakos, *Lab Chip*, 2015, **15**, 1923–1933.
22 S. Hossain and K.-Y. Kim, *Springerplus*, 2016, **5**, 794.
23 T. van Schijndel, M. K. Singh, M. Gillies, N. Kahya, A. Kharin and J. M. J. den Toonder, *Macromol. Mater. Eng.*, 2011, **296**, 373–379.
24 C.-P. Jen, C.-Y. Wu, Y.-C. Lin and C.-Y. Wu, *Lab Chip*, 2003, **3**, 77–81.
25 J. B. Prettyman and D. T. Eddington, *Sensors Actuators, B Chem.*, 2011, **157**, 722–726.
26 L. Dong and H. Jiang, *Soft Matter*, 2007, **3**, 1223–1230.
27 D. Baigl, *Lab Chip*, 2012, **12**, 3637–3653.

28 J. ter Schiphorst, M. van den Broek, T. de Koning, J. N. Murphy, A. P. H. J. Schenning and A. C. C. Esteves, *J. Mater. Chem. A*, 2016, **4**, 8676–8681.
29 B. Ziółkowski, L. Florea, J. Theobald, F. Benito-Lopez and D. Diamond, *J. Mater. Sci.*, 2016, **51**, 1392–1399.
30 L. Florea, D. Diamond and F. Benito-Lopez, *Macromol. Mater. Eng.*, 2012, **297**, 1148–1159.
31 B. Ziółkowski, L. Florea, J. Theobald, F. Benito-Lopez and D. Diamond, *Soft Matter*, 2013, **9**, 8754–8760.
32 J. E. Stumpel, B. Ziółkowski, L. Florea, D. Diamond, D. J. Broer and A. P. H. J. Schenning, *ACS Appl. Mater. Interfaces*, 2014, **6**, 7268–7274.
33 K. Otake, H. Inomata, M. Konno and S. Saito, *Macromolecules*, 1990, **23**, 283–289.
34 A. Szilágyi, K. Sumaru, S. Sugiura, T. Takagi, T. Shinbo, M. Zrínyi and T. Kanamori, *Chem. Mater.*, 2007, **19**, 2730–2732.
35 S. Sugiura, K. Sumaru, K. Ohi, K. Hiroki, T. Takagi and T. Kanamori, *Sensors Actuators A Phys.*, 2007, **140**, 176–184.
36 S. Sugiura, A. Szilágyi, K. Sumaru, K. Hattori, T. Takagi, G. Filipcsei, M. Zrínyi and T. Kanamori, *Lab Chip*, 2009, **9**, 196–198.
37 J. ter Schiphorst, S. Coleman, J. E. Stumpel, A. Ben Azouz, D. Diamond and A. P. H. J. Schenning, *Chem. Mater.*, 2015, **27**, 5925–5931.
38 R. Klajn, *Chem. Soc. Rev.*, 2014, **43**, 148–184.
39 P. K. Kundu, S. Das, J. Ahrens and R. Klajn, *Nanoscale*, 2016, **8**, 19280–19286.
40 K. Kumar, C. Knie, D. Bléger, M. A. Peletier, H. Friedrich, S. Hecht, D. J. Broer, M. G. Debije and A. P. H. J. Schenning, *Nat. Commun.*, 2016, **7**, 11975.
41 C. Knie, M. Utecht, F. Zhao, H. Kulla, S. Kovalenko, A. M. Brouwer, P. Saalfrank, S. Hecht and D. Bléger, *Chem. - A Eur. J.*, 2014, **20**, 16492–16501.
42 H. K. Bisoyi and Q. Li, *Chem. Rev.*, 2016, **116**, 15089–15166.
43 Q. Li, *Intelligent Stimuli-Responsive Materials: From Well-Defined Nanostructures to Applications*, Wiley, 2013.
44 D. Bléger and S. Hecht, *Angew. Chemie*, 2015, **54**, 11338–11349.
45 T. Satoh, K. Sumaru, T. Takagi and T. Kanamori, *Soft Matter*, 2011, **7**, 8030–8034.
46 T. Satoh, K. Sumaru, T. Takagi, K. Takai and T. Kanamori, *Phys. Chem. Chem. Phys.*, 2011, **13**, 7322–7329.
47 F. Benito-Lopez, R. Byrne, A. M. Răduță, N. E. Vrana, G. McGuinness and D. Diamond, *Lab Chip*, 2010, **10**, 195–201.
48 S. R. Sershen, G. A. Mensing, M. Ng, N. J. Halas, D. J. Beebe and J. L. West, *Adv. Mater.*, 2005, **17**, 1366–1368.
49 S. Coleman, J. ter Schiphorst, A. Ben Azouz, S. Bakker, A. P. H. J. Schenning and D. Diamond, *Sensors Actuators B Chem.*, 2017, **245**, 81–86.
50 A. Venancio-Marques, F. Barbaud and D. Baigl, *J. Am. Chem. Soc.*, 2013, **135**, 3218–3223.
51 L. Nurdin, A. Venancio-Marques, S. Rudiuk, M. Morel and D. Baigl, *Comptes Rendus Chim.*, 2015, **19**, 199–206.
52 D. G. Leaist, *Can. J. Chem.*, 1988, **66**, 2452–2457.
53 Z. Zhang, P. Zhao, G. Xiao, B. R. Watts and C. Xu, *Biomicrofluidics*, 2011, **5**, 1–8.
54 J. ter Schiphorst, G. G. Melpignano, H. E. Amirabadi, M. H. J. M. Houben, S. Bakker, J. M. J. den Toonder and A. P. H. J. Schenning, *Macromol. Rapid Commun.*, 2018, **39**, 1700086.

Chapter 5

Dual responsive cotton fabric functionalized with a surface-grafted spiropyran–NIPAM hydrogel

Abstract. A dual-responsive cotton fabric functionalized with a spiropyran–NIPAM hydrogel, capable of dimensional changes upon irradiation with visible light or upon a temperature stimulus is reported. These volume changes are due to absorption and release of water, from and into the air, by increasing temperature above the LCST in the dark, and/or by irradiation with sunlight or white light from artificial sources. The material is obtained via grafting photo- and temperature-responsive monomers directly from the cotton fibers, using a controlled polymerization method, ARGET-ATRP.

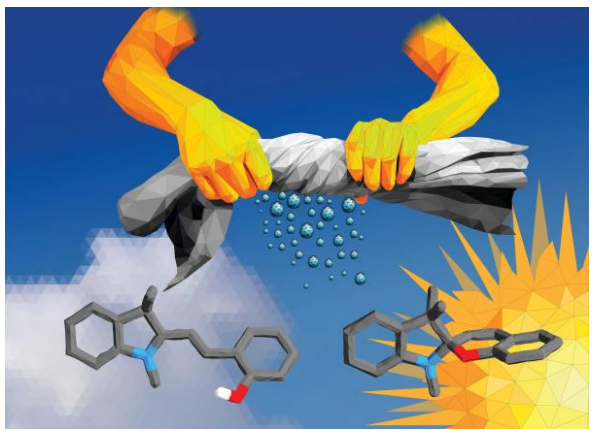

This chapter is partially reproduced from:
'Dual light and temperature responsive cotton fabric functionalized with a surface-grafted spiropyran–NIPAAm-hydrogel' J. ter Schiphorst, M. van den Broek, T. de Koning, J. N. Murphy, A. P. H. J. Schenning and A. C. C. Esteves, *J. Mater. Chem. A*, 2016, **4**, 8676–8681.

5.1 Introduction

Smart polymeric materials that change their functional properties in response to changes in environmental variables, such as temperature,[1] humidity,[2] light,[3,4] and pH,[5] are currently the subject of widespread interest. Feedback from responsive polymers can take the form of changes in physical characteristics such as shape,[6] reflectivity, color,[7] or porosity[8] and are of great interest in the field of sustainable energy,[9] water management,[6,10] and personal comfort.[11] In particular, light as a stimulus is appealing, as light is easily accessible and non-invasive, *i.e.*, it does not require direct contact between source and substrate resulting in minimal impact on both material and surroundings.[12] Natural materials are interesting as substrates for these polymers, as they enable production from sustainable sources.[9,13,14] When light triggering can be combined with bio-based fibers, responsive advanced materials become available that can, as an example, be applied in the textile industry.[1,13,15,16] However, such materials have been scarcely explored to date. Only a few papers have reported light-responsive, cotton-based materials,[17–21] none of which present reversible shape changes based on interaction with humid air or on the uptake and release of water, as reported here.

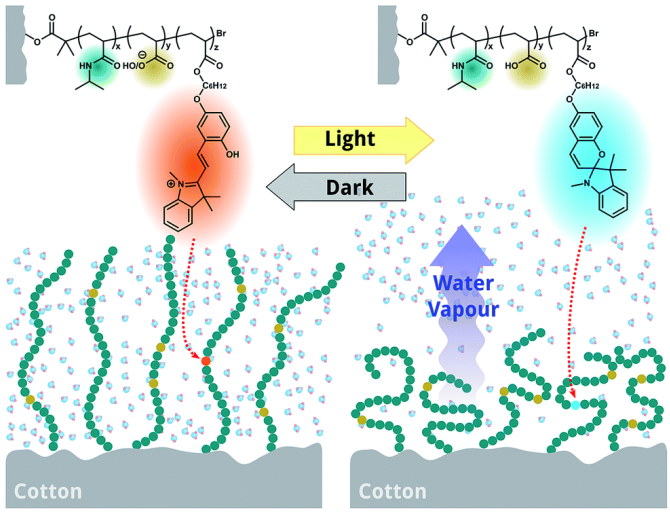

Figure 5.1. Schematic representation of the polymer-grafted cotton fibers. A random distribution of the monomers in the polymer, with monomers incorporated in proportion of the relative feed (x=95, y=5, z=1) is expected. The McH^+ chromophore depicted in orange (left) results from the abstraction of a proton from the copolymerized acrylic acid units, isomerizing to a hydrophilic species, which triggers the uptake of water by the hydrogel. Subsequent illumination with white light isomerizes the chromophore back to the hydrophobic state (right), expelling the absorbed water.

Recently, a cotton fabric functionalized with a N-isopropylacrylamide (NIPAM) hydrogel was developed, that was able to absorb a large amount of water from humid air, which could be subsequently released with a temperature trigger above the lower critical solution temperature (LCST) of the polymer.[2] This behavior was repeatable for several cycles and was attributed to a combined effect of the intrinsic phase transition of pNIPAM around the

LCST and the change between the extreme superhydrophilic/superhydrophobic morphologies of the hydrogel layer directly grafted from the cotton fibers.

We have also fabricated light-responsive hydrogels using spiropyran-based derivatives (see also previous chapters).[6] When copolymerized with a spiropyran-NIPAM hydrogel, acrylic acid serves as an internal proton donor[22] for the spiropyran isomerization to hydrophilic merocyanine-H^+ (McH^+), resulting in water uptake. The hydrophobic spiropyran (Sp) isomer can be reversibly formed upon illumination with white light, resulting in release of water.[3,23]

In this chapter, a cotton-fabric is reported, functionalized with a dual-responsive hydrogel that changes thickness by absorbing and releasing water from humid air (Figure 5.1) in the presence of a light or temperature stimulus. This dimensional change is reversible and repeatable and can be triggered by both stimuli.

To generate the functional textile, surface initiated activators regenerated by electron transfer atom transfer radical polymerization (SI-ARGET-ATRP) is used. This method is particularly attractive for future up-scaling and industrial processing, since the synthetic conditions are quite accommodating, *i.e.*, it is tolerant to the presence of small amounts of oxygen; complex experimental apparatus are not required and in general, minimal amounts of copper catalyst can be used.[24–26]

5.2 Experimental

The cotton fabric obtained from Textile Innovators Division of SDL ATLAS was functionalized with an ATRP bromide initiator as previously reported by Yang *et al.*[2] The spiropyran based molecule was synthesized according to the procedure reported previously.[27] *N*-isopropylarcylamide (NIPAM, Aldrich 97%) was recrystallized in n-heptane and dried under vacuum at 40°C for 24 hours, to remove the present inhibitor. α-bromoisobutyrylbromide (BiB, Aldrich 99%), triethylamine (TEA, Aldrich 99.5%), copper(II)bromide ($CuBr_2$, Aldrich 99%), sodium acrylate (NaAc, Acros 97%), ascorbic acid (Aldrich), *N*,*N*,*N*′,*N*′,*N*″-pentamethyldiethylenetriamine (PMDETA, Aldrich, 99%), 4-(dimethylamino)-pyridine (DMAP, Aldrich, 99%), methanol (Biosolve) and dichloromethane (Biosolve) were used without further purification. Tetrahydrofuran was dried and the stabilizer was removed using a MB-SPS-800 drying system.

Typically, 30 mg of the initiator functionalized cotton fibers, 1 mL of copper-complex solution (10.5 µL/mL PMDETA, 5.70 mg/mL copper(II)bromide ($CuBr_2$) solution in water), *N*-isopropylacrylamide (NIPAM, 1.07*g*, 9.50 mmol) and NaAc (47.5 mg, 0.50 mmol) were added to a round bottom flask. The flask was sealed with a rubber stopper and 8 mL distilled water was added. The spiropyran acrylate (**2**) derivative (44.5 mg, 0.10 mmol) was dissolved in 10 mL methanol and added to the mixture, which was then flushed with nitrogen for several hours. Ascorbic acid (44 mg, 0.25 mmol) was dissolved in 0.5 mL distilled water and added to 0.5 mL of a 0.1 M NaOH aqueous solution. The mixture was flushed with argon for several hours to remove a large part of the oxygen.

To start the reaction, the ascorbic acid aqueous solution was added to the round bottom flask containing the mixture of all the other reagents via a nitrogen purged syringe, through the rubber seal. The reaction took place at 0 °C for the first 2 hours and then for 24 hours at room temperature, after which the reaction was stopped by opening the round flask and exposing the mixture to air.

The cotton piece was removed from the flask and rinsed with methanol, ethanol and water consecutively, for three times. Next it was Soxhlet extracted three times with 50 ml warm methanol for 1 hour. Subsequently, the material was dried in vacuum at 40°C overnight.

For the reference experiments, where either sodium acrylate or spiropyran were absent in the copolymers, procedures similar to the ones described above were used. The amount relative to the monomers absent was replaced by similar molar additions of NIPAM. Furthermore, the reaction with NIPAM only and NIPAM-NaAc only, were carried out with 2.1 μL PMDETA, 1.14 mg $CuBr_2$ and 8.8 mg ascorbic acid. The full description of the equipment and procedures used for the characterization of the materials can be found elsewere.[28]

5.3 Results and Discussion

Materials preparation.

The fibers of a woven piece of cotton fabric are first functionalized with an ATRP initiator, by reacting the cellulose-hydroxyl functionalities with α-bromoisobutyrylbromide (BiB) (Figure 5.2), according to procedures previously reported.[2] The presence of the initiator on the fiber surface is confirmed by X-ray photoelectron spectroscopy (XPS) with a characteristic signal of the bromine at 184 eV and 71 eV.[28]

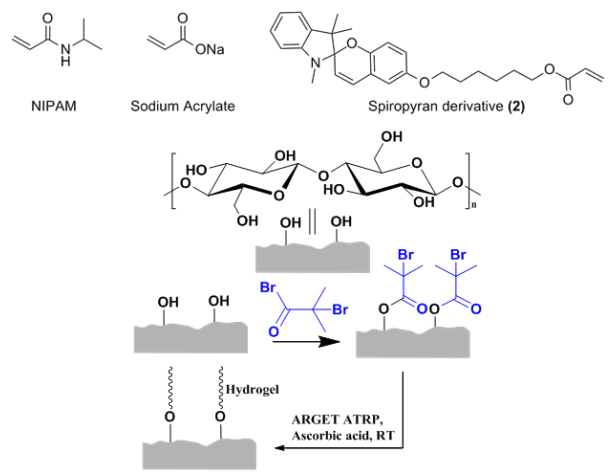

Figure 5.2. Illustration of the functionalization of the cotton fiber. In the first step, the hydroxyl groups on the fibers are functionalized with an ATRP initiator. In the second step, (co)polymers are grafted from the surface of the cotton fiber using ARGET-ATRP, and the monomers.

Subsequently, to introduce the light-responsive properties, the monomers NIPAM, acrylic acid (in the form of sodium acrylate) and an acrylate functionalized spiropyran **2**, are grafted from the cotton fibers by ARGET-ATRP (Figure 5.2). The BiB-functionalized cotton was cut in small pieces of typically 30 mg and immersed in a 1:1 methanol:water mixture (20 mL), containing NIPAM [N], sodium acrylate [P], spiropyran acrylate [S], copper bromide [Cu], ligand (PMDETA) [L] and ascorbic acid (reducing agent) [R] in a ratio of [N]:[P]:[S]:[Cu]:[L]:[R] = 95:5:1:0.25:0.5:2.5. The polymerization under these conditions is particularly challenging, as deactivation of the copper catalyst might take place by the acrylic acid and merocyanine.[29] Therefore the reaction is carried out at pH = 9 and the sodium salt of the acrylic acid monomer was used.[30] A relatively high content of methanol was necessary to dissolve the spiropyran derivative. The total monomer concentration for all experiments is 0.5 mol/L. Furthermore for the ARGET ATRP, relatively higher concentrations of the copper catalyst and ascorbic acid are used, as compared to typical polymerizations by this technique,[29] to obtain higher grafting yields.

Materials analysis.

Following the polymerization, carried out at room temperature for 24 hours, the material is washed with warm methanol and water to extract non-reacted monomers and/or non-grafted polymers.[28] Upon drying, the material becomes stiffer and faintly yellow in color. Gravimetric analysis reveals that the overall weight of the dried material increased considerably, up to 123 % increase compared to the unmodified fabric, indicating the successful grafting of the copolymer and a dense coverage of the fibers surface, as compared to previous reports on cotton modified by ARGET-ATRP.[26]

Scanning electron microscopy (SEM) analysis of the fibers extracted from the functionalized cotton fabric confirms the large and near-complete coverage of the fibers with a polymer layer, showing a rough surface with small aggregates of the polymer (Figure 5.3). When compared with the bare cotton fibers, the surface is irregular and an increase in the diameter of roughly 7 μm is found. This is in agreement with the weight increase and the morphology of the polymer layer is similar to what was previously reported for pNIPAM-fibers functionalized by direct SI-ATRP.[2] The fibers re further characterized by infrared spectroscopy (Figures 5.3e). The vibration peaks around 1733 cm^{-1} and 1486 cm^{-1}, indicate the presence of the spiropyran moiety, while the peaks at 1639 cm^{-1} and 1542 cm^{-1}, correspond to pNIPAM, and the peak at 1386 corresponds to acrylic acid.[5]

When the hydrogel functionalized cotton fabric is immersed in water, it slowly turns yellow/orange, clearly revealing the presence of the hydrophilic McH^+ isomer (see also Chapter 2).[6] It should be noted that a grafted cotton reference sample, lacking the acrylic acid moiety, exhibits barely any color change.[28]

Differential scanning calorimetry (DSC) confirms the presence of an LCST (~34 °C),[28] similar to pNIPAM, although it widens and is not as clear as in the case of cotton fibers

functionalized with pNIPAM only.[31–33] These results confirm the successful grafting of the sodium acrylate, spiropyran and pNIPAM monomers from the cotton fibers surface.

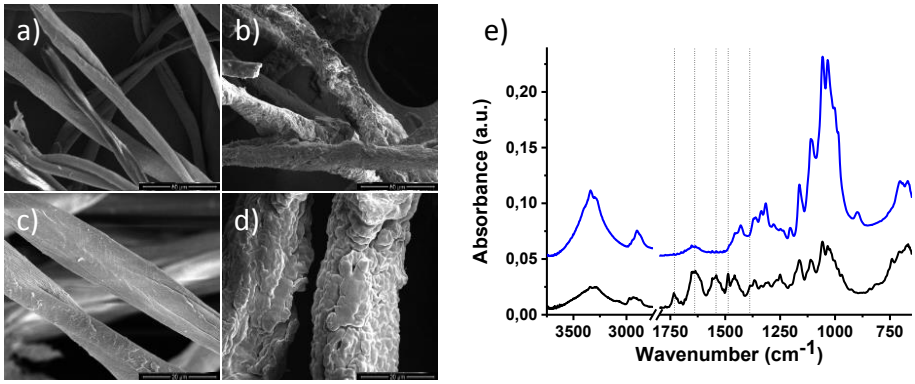

Figure 5.3. SEM images of a cotton fiber with surface attached initiator before (a,c) and after ARGET-ATRP (b,d) of NIPAM, sodium acrylate and spiropyran acrylate at different magnifications (scale bar represents 20 µm (b,d) or 50 µm (a,c). ATR-IR spectra e) of the cotton fibers without (blue) and with (black) hydrogel functionalization.

The exact monomer composition of the hydrogel polymer is, however, not possible to quantify in view of the difficulty to ungraft the polymers from the surface without decomposing or changing the properties of the initial materials.[2,34] Furthermore, the relatively low feed concentrations of both spiropyran and acrylic acid makes analysis of the polymers by routine polymer characterization techniques challenging. Nevertheless, based on earlier results, a random copolymer is expected.[27]

In order to investigate the light responsive properties, the functionalized cotton fabric is immersed in water, upon which it turns yellow/orange, as it isomerizes to the McH^+ form. Further on, it is remarkable that within 1 minute of exposure to bright sunlight this material completely loses the yellow color (Figure 5.4).

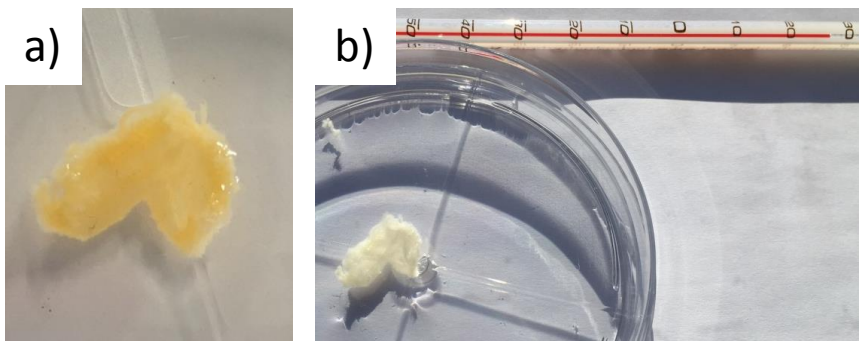

Figure 5.4. The functionalized cotton in the laboratory (under fluorescent tube light) showing the yellow/orange color a) corresponding to protonated merocyanine formed after immersion in water. The cotton was placed in sunlight b) (behind a glass window) and within 60 seconds the material completely lost its color. The cotton piece is roughly 2 cm in size. The temperature is roughly 27°C, which still below the LCST.

In a similar way, the yellow/orange-colored cotton (Figures 5.4a and 5.5a) is illuminated with a white lamp inside the laboratory, at 20 °C for 5 minutes. During exposure, the material turns completely white, indicating that the McH^+ isomerizes to the colorless spiropyran derivative (Figure 5.5a,b).[6] The material subsequently recovers its original yellow/orange color when placed in the dark, in a similar time frame as shown in previous chapters (roughly 30 minutes), as illustrated in Figure 5.5a-d.

After drying, the functionalized cotton fabric was placed in a highly humid environment (~97% RH) and kept in the dark for several days at 20 °C. The material weight was measured gravimetrically revealing an increase of approximately 50%, which indicates the ability to absorb a significant amount of water from a highly humid environment, with no direct contact with liquid water. Since the material is woven (*i.e.*, a piece of fabric is used) and contains only a surface-layer of hydrogel, no effect on the overall size of the cotton fabric is visually detected (with the naked eye).

Light responsive behavior.

To analyze the volume changes in detail, cotton fibers are pulled at random from the woven material and placed in a high humidity environment (~97% RH inside a chamber of a Linkam cell) at 20°C, a temperature below the LCST of pNIPAM. For each measurement series, a common region of the fiber is isolated to ensure consistency.

In the absence of light, the fiber is swollen and has an average diameter of ~40 μm (Figure 5.5e). Upon exposure to white light for 5 minutes, the fiber's average diameter shrinks to ~33 μm (Figure 5.5f). After switching off the light, the fibers re-swell to their original diameter. It should be noted that the large standard deviations result from the highly variable fiber widths; the standard deviation of the swelling/shrinking ratios, when comparing identical points along the length of the fiber, no overlap is found.[28] Distributions of both width and swelling/shrinking ratios, for all fibers, show that the width changes occur uniformly along the fiber, roughly in proportion to the diameter. Additionally, it is noted that the hydrogel is capable of bending the fiber, as revealed by detailed image analysis of the fibers. At a position where the material bulges on one side, a pivot point is observed, likely resulting from imbalanced forces, where the fiber reversibly bends by ~10°.[28]

These results reveal that the fibers are capable of increasing ~ 25% in diameter, indicating efficient uptake of water from the air in the measured time frame of 5 minutes of recovery (Figure 5.5g). These procedures were repeated for at least 5 consecutive cycles, resulting in a repeatable shrinking of the fibers diameter with irradiation, and consistent spontaneous swelling and recovery to the original diameter occurs each time the light was switched off (Figure 5.5g).

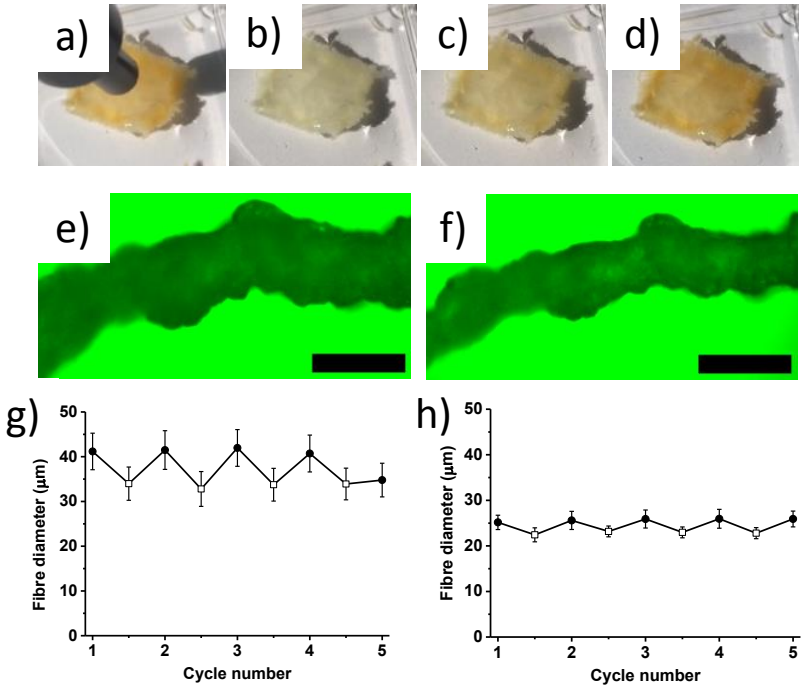

Figure 5.5. Photographs of the functionalized cotton immersed in water: a) before and b) directly after exposure; c) 5 minutes recovery and d) 30 minutes recovery, after white light illumination. Optical micrographs of representative cotton fibers: e) before and f) after white light illumination. The scale bar represents 50 µm. Note: the green background is caused by a filter used in order to prevent isomerization of the chromophore by the microscope white lamp. A series of these images are used to estimate average diameters. The graphs show the fiber's average diameter in response to cycles of illumination (open squares), followed by recovery in the dark (closed circles) with g) and without h) acrylic acid.

These results clearly show that the cotton fibers are capable of absorbing and releasing a significant amount of water in response to light, due to McH^+ - SP isomerization. It should also be noted that the reference cotton fibers functionalized without the acrylic acid moiety, which cannot form the hydrophilic McH^+ derivative efficiently, only show very small volume changes (Figure 5.5h).

Temperature responsive behavior.

The temperature responsiveness of the functionalized hydrogel-cotton is also investigated (Figure 5.6). By increasing the temperature above the LCST of pNIPAM (up to 50 °C) in the absence of white light, the fiber diameter decreases, transitioning from an average of ~42 µm at 15 °C to ~31 µm at 50 °C, indicating the release of water (Figure 5.6 black line). This process is repeated for 5 cycles of 15-50 °C, illustrating the reversible water adsorption and release behavior of the hydrogel functionalized fibers (Figure 5.6).

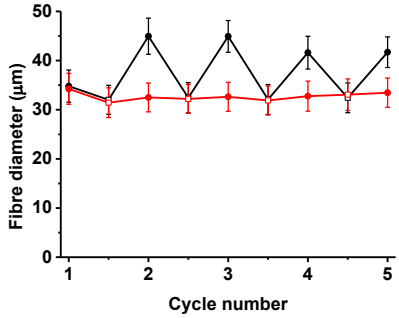

Figure 5.6. Temperature-responsive behavior of the functionalized cotton fiber through 5 consecutive temperature fluctuation cycles of 15°C (closed circles) and 50°C (open squares), in the dark (absence of white light, black curve) and under continuous white light irradiation (red curve).

Remarkably the temperature-induced response is similar to the light-induced switching behavior, suggesting comparable changes of the pNIPAM hydrogel induced by both temperature and light. However, when the functionalized hydrogel-cotton is constantly illuminated with white light and similar temperature cycles are performed, the average diameter of the fiber is constant and consistent with the diameter of the material above the LCST of pNIPAM (Figure 5.6 red line). This indicates that in the presence of light, the sole presence of the spiropyran in the closed hydrophobic form, seems to inhibit or drastically hinder the temperature-triggered transition of the pNIPAM molecules towards a water-absorbing state.

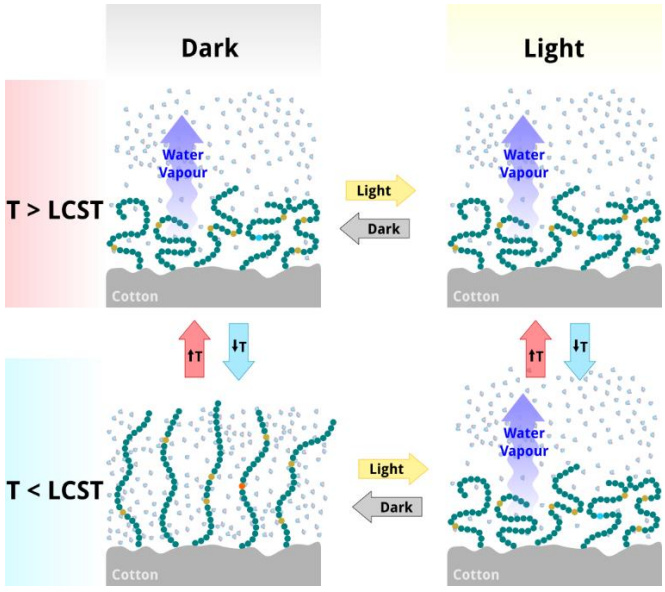

Figure 5.7. Schematic of the cotton material (gray) in response to the combination of light (left versus right) and temperature (top versus bottom) stimuli, depicting the dual responsiveness of the material. The extended brushes illustrate the material in the swollen state where the water molecules are between the brushes. Upon applying a stimulus, the material shrinks (contracted brushes) and water is expelled.

Basically, for water uptake, this material effectively functions as an AND gate (Figure 5.7), in which humidity absorption only occurs when dark AND low temperature (below LCST) conditions are combined. On the other hand, for water release, three situations are possible, either low temperature (below LCST) and irradiating with light, or increasing the temperature (above LCST) both in absence of presence of light.

5.4 Conclusions

A novel hydrogel functionalized cotton fabric that is dual responsive is developed. It can be actuated by a light or temperature stimulus, to reversibly and repeatable change volume and shape by absorbing and releasing water from humid environments. This is achieved with a facile and versatile surface-initiated controlled polymerization method, ARGET-ATRP,[24] used to graft monomers of NIPAM, acrylic acid (as sodium acrylate) and a spiropyran-derivative directly from the surface of the cotton fibers.

This polymerization method enables the functionalization of cotton fibers with several other stimuli-responsive polymers,[35] as long as they are compatible with the experimental conditions, *e.g.*, being non-reactive towards the copper (or other metal) catalysts used. This may be extended to the functionalization of other natural and synthetic fibers. The reaction conditions are rather simple and in principle easy to scale-up, making industrial application feasible.[25,36,37]

This volume/shape changing hydrogel-cotton shows a potential for water extraction from air, which could have a high impact in areas where potable water sources are scarce,[38] *e.g.*, coastal deserts and foggy mountains. These responsive fibers may also find opportunities in other technological applications, such as breathable textiles and agricultural purposes. Finally, the faint but observable color change during illumination, whether by fluorescent light or sunlight, provides a simple visual indicator of the optically-induced humidity absorption/release process.

5.5 References

1 H. Yang, A. C. C. Esteves, H. Zhu, D. Wang and J. H. Xin, *Polymer*, 2012, **53**, 3577–3586.
2 H. Yang, H. Zhu, M. M. R. M. Hendrix, N. J. H. G. M. Lousberg, G. de With, A. C. C. Esteves and J. H. Xin, *Adv. Mater.*, 2013, **25**, 1150–4, 1149.
3 R. Klajn, *Chem. Soc. Rev.*, 2014, **43**, 148–184.
4 T. Ueki, R. Usui, Y. Kitazawa, T. P. Lodge and M. Watanabe, *Macromolecules*, 2015, **34**, 5928–5933.
5 Z. Li, J. Shen, H. Ma, X. Lu, M. Shi, N. Li and M. Ye, *Mater. Sci. Eng. C. Mater. Biol. Appl.*, 2013, **33**, 1951–1957.
6 J. ter Schiphorst, S. Coleman, J. E. Stumpel, A. Ben Azouz, D. Diamond and A. P. H. J. Schenning, *Chem. Mater.*, 2015, **27**, 5925–5931.
7 J. E. Stumpel, D. J. Broer and A. P. H. J. Schenning, *Chem. Commun.*, 2014, **50**, 15839–15848.
8 B. Ziółkowski, L. Florea, J. Theobald, F. Benito-Lopez and D. Diamond, *J. Mater. Sci.*, 2016, **51**, 1392–1399.
9 V. A. Ganesh, A. Baji and S. Ramakrishna, *RSC Adv.*, 2014, **4**, 53352–53364.
10 F. Benito-Lopez, R. Byrne, A. M. Răduţă, N. E. Vrana, G. McGuinness and D. Diamond, *Lab Chip*, 2010, **10**, 195–201.
11 L. Florea, D. Diamond and F. Benito-Lopez, *Macromol. Mater. Eng.*, 2012, **297**, 1148–1159.

12 S. Sugiura, A. Szilágyi, K. Sumaru, K. Hattori, T. Takagi, G. Filipcsei, M. Zrínyi and T. Kanamori, *Lab Chip*, 2009, **9**, 196–198.
13 J. Hu, H. Meng, G. Li and S. I. Ibekwe, *Smart Mater. Struct.*, 2012, **21**, 53001.
14 A. Bashari, N. Hemmati Nejad and A. Pourjavadi, *J. Text. Inst.*, 2013, **104**, 1145–1155.
15 D. Jocic, A. Tourrette, P. Glampedaki and M. M. C. G. Warmoeskerken, *Mater. Technol. Adv. Perform. Mater.*, 2009, **24**, 1–10.
16 T. Chen, Q. Fang, Q. Zhong, Y. Chen and J. Wang, *Polymers*, 2015, **7**, 909–920.
17 W. Tian and J. Tian, *Langmuir*, 2014, **30**, 2–6.
18 K. Arai and T. Ohyama, *J. Mater. Chem.*, 1996, **6**, 11–14.
19 Y. Wang, L.-O. Heim, Y. Xu, G. Buntkowsky and K. Zhang, *Adv. Funct. Mater.*, 2015, **25**, 1434–1441.
20 O. Grigoray, H. Wondraczek, E. Heikkilä, P. Fardim and T. Heinze, *Carbohydr. Polym.*, 2014, **111**, 280–287.
21 A. Duval, H. Lange, M. Lawoko and C. Crestini, *Biomacromolecules*, 2015, **16**, 2979–2989.
22 B. Ziółkowski, L. Florea, J. Theobald, F. Benito-Lopez and D. Diamond, *Soft Matter*, 2013, **9**, 8754–8760.
23 J. E. Stumpel, B. Ziółkowski, L. Florea, D. Diamond, D. J. Broer and A. P. H. J. Schenning, *ACS Appl. Mater. Interfaces*, 2014, **6**, 7268–7274.
24 W. Jakubowski, K. Min and K. Matyjaszewski, *Macromolecules*, 2006, **39**, 39–45.
25 S. Hansson, A. Carlmark, E. Malmström and L. Fogelström, *J. Appl. Polym. Sci.*, 2015, **132**, 41434.
26 X. Dong, H. Bao, K. Ou, J. Yao, W. Zhang and J. He, *Fibers Polym.*, 2015, **16**, 1478–1486.
27 J. E. Stumpel, D. Liu, D. J. Broer and A. P. H. J. Schenning, *Chemistry*, 2013, **19**, 10922–10927.
28 J. ter Schiphorst, M. van den Broek, T. de Koning, J. N. Murphy, A. P. H. J. Schenning and A. C. C. Esteves, *J. Mater. Chem. A*, 2016, **4**, 8676–8681.
29 K. Matyjaszewski and J. Xia, *Chem. Rev.*, 2001, **101**, 2921–2990.
30 X. Deng and J. Lahann, *J. Appl. Polym. Sci.*, 2014, **131**, 40176.
31 H. Feil, Y. H. Bae, J. Feijen and S. W. Kim, *Macromolecules*, 1993, **26**, 2496–2500.
32 A. E. Ivanov, N. L. Eremeev, P. O. Wahlund, I. Y. Galaev and B. Mattiasson, *Polymer*, 2002, **43**, 3819–3823.
33 K. Sumaru, M. Kameda, T. Kanamori and T. Shinbo, *Macromolecules*, 2004, **37**, 4949–4955.
34 S. Hansson, P. Antoni, H. Bergenudd and E. Malmström, *Polym. Chem.*, 2011, **2**, 556–558.
35 S. Hansson, E. Östmark, A. Carlmark and E. Malmström, *ACS Appl. Mater. Interfaces*, 2009, **1**, 2651–2659.
36 K. Matyjaszewski, W. Jakubowski, K. Min, W. Tang, J. Huang, W. A. Braunecker and N. V Tsarevsky, *P. Natl. Acad. Sci. USA*, 2006, **103**, 15309–15314.
37 K. Matyjaszewski, D. Hongchen, W. Jakubowski, J. Pietrasik and A. Kusumo, *Langmuir*, 2007, **23**, 4528–4531.
38 K. C. Park, S. S. Chhatre, S. Srinivasan, R. E. Cohen and G. H. McKinley, *Langmuir*, 2013, **29**, 13269–13277.

Chapter 6

Light-responsive hierarchically structured liquid crystal polymers for cell manipulation

Abstract. Light-responsive liquid crystal polymer networks are used for their adaptive and programmable nature to form hybrid surfaces, presenting micrometer scale topographical cues and changes in nanoscale roughness at the same time to direct cell migration. This chapter describes the characterization and implementation of these materials for cell culturing. It is shown that the cell speed and migration patterns are strongly dependent on the height of the (light-responsive) micrometer scale topographies and differences in surface nanoroughness. Furthermore, switching cell migration patterns upon in situ temporal changes in surface nanoroughness, points out the ability to dynamically control cell behavior on these surfaces. Finally, the possibility is shown to form photo-switchable topographies, appealing for future studies where topographies can be rendered reversible on demand.

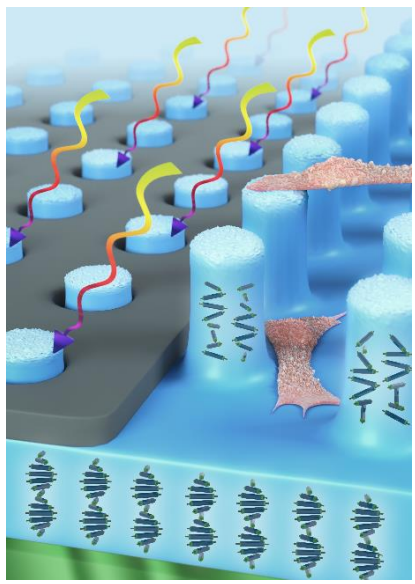

This chapter is partially reproduced from:
'Light-Responsive Hierarchically Structured Liquid Crystal Polymer Networks for Harnessing Cell Adhesion and Migration' G. Koçer, J. ter Schiphorst, M. Hendrikx, H. G. Kassa, P. Leclère, A. P. H. J. Schenning and P. Jonkheijm, *Adv. Mater.*, 2017, **29**, 1606407.

6.1 Introduction

Control over size (from the nano to micron scale) and arrangement of topographical features are known to greatly influence cell adhesion, spreading, migration and differentiation, and tissue organization.[1–7] Therefore, both in situ (*i.e.* in presence of cells) and ex situ reversible and irreversible changes of a natural matrix is highly interesting for the generation of new biomaterials. Several studies on dynamic topographies have used strain-responsive buckling of plasma oxidized poly dimethyl siloxane (PDMS) thin films,[8,9] thermally activated shape-memory polymer (i.e. ε-polycaprolactone (PCL)),[10,11] and strain-responsive liquid crystal elastomers[12] in dynamic control of (stem) cell alignment, spreading, and differentiation.

However, the possibility to use and actuate these materials in situ is underexposed and challenging. Generally, light offers flexibility and remote control, non-invasiveness, and physiological compatibility, *i.e.* when tuned in correct doses and wavelength, to generate changes in surface or bulk properties of biomaterials.[13,14] The conceivable benefits of employing light responsive systems are recognized and encourage utilization to advance dynamic surface topographies across larger areas.[15,16] Yet, there are only a few examples where light has been used to form (re)configurable topographies in polymer systems consisting of photo-switchable molecules in order to control cell spreading and alignment while challenges regarding in situ studies still remain.[15–17] Furthermore, materials often used are hydrogel based soft materials, sensitive to small changes in the environment (see also Chapter 1). In a very recent example, Netti and coworkers elegantly showed in situ spatio-temporal control of topography to direct cell alignment on azopolymers.[18] However, so far no study has documented of in situ light-induced changes (*i.e.* temporal changes) in surface structure effects cell migration, which is one of the essential processes in tissue remodeling and wound healing, as well as in colonization of biomaterials by desired cell types for successful implantation.[7,19,20] Here, we employ the adaptive and programmable nature of light responsive liquid crystal polymer network (LCN) coatings[21] to achieve new spatially arranged patterned bio interfaces for in situ temporal control of surface properties to guide cell behavior. These azobenzene based LCN systems can operate, in contrast to the hydrogels used in previous chapters, in solvent free environments and present a versatile way to change surface topography both in a reversible and irreversible fashion.[21–25] It is shown that these LCNs are biocompatible and can be used as bio-instructive responsive materials to control cell adhesion and migration. Furthermore, we exploit these materials to induce in situ temporal changes (permanent in this case) in hierarchical formed surface structural properties (*i.e.* roughness) to control cell migration.

6.2 Experimental

Preparation of light responsive liquid crystal networks (LCNs).

All reagents and chemicals were obtained from commercial sources and used without further purification and the molecular structures are given in Figure 6.1. A3MA (1) was synthesized by Syncom (Groningen, the Netherlands). LC756 (2) was obtained from BASF. RM83 (3), RM23 (4) and RM105 (5) were obtained from Merck. Irgacure 819 (6) was obtained from Ciba Specialty Chemicals Inc. 4-Methoxyphenol (7) was obtained from Sigma-Aldrich. For the fabrication of the liquid crystal polymers, a mixture of A3MA (2.0 wt%), LC756 (3.2 wt%), RM83 (18.3 wt%), RM23 (29.7 wt%), RM105 (40.7 wt%), Irgacure 819 (1.7 wt%) and 4-methoxyphenol (4.4 wt%) was dissolved in 4 mL tetrahydrofuran (THF), resulting in a concentration of 0.25 g monomer/mL THF.

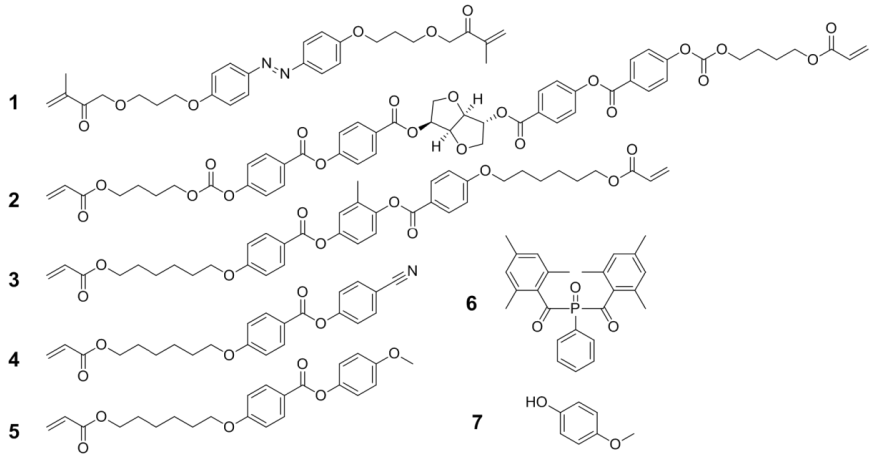

Figure 6.1. Molecular structure of the materials that were used for preparing the light-responsive liquid crystal polymer (compounds are 1: light responsive azobenzene, 2: chiral dopant, 3-5: nematic hosts, 6: photo-initiator, 7: chain stopper/inhibitor).

Thin films of the light-responsive liquid crystalline polymers were prepared and attached to a quartz glass slide. The internal surface of the bottom slide of this cell was functionalized with 3-(trimethoxysilyl)propyl methacrylate to ensure covalent attachment of the liquid crystal polymer (see also chapter 2). 50 µL of the monomer mixture in THF was placed on the functionalized surface and heated to 70°C for 10 min to evaporate the solvent. For easy removal of the top quartz glass slide, the corresponding quartz glass slide was functionalized with a fluorinated compound (*1H,1H,2H,2H*-perfluorodecyl-triethoxysilane). Before closing the cell, the sample is allowed to cool down to room temperature to induce the cholesteric liquid crystalline phase. The cell was closed by placing the top slide on the bottom slide and subsequently the slides are sheared to induce planar cholesteric alignment of the liquid crystal, resulting in samples of roughly 8-12 µm in thickness. Subsequent exposure to UV-light results in a polymerized sample. After 5 min of illumination using an Exfo Omnicure

S2000 light source and a cut-off filter (Edmund Industrial Optics Stock No. 54516) to prevent isomerization of the azobenzene moiety, the sample was heated to 90°C and illuminated an additional 10 min to ensure full polymerization of the film. The fluorinated glass slide was removed and the substrate was ready for use.

Forming the structures.

To form a patterned structure on the liquid crystal, a chromium oxide mask was used. The samples were heated to 60°C to pass the glass transition temperature (T_g) and illuminated for 1 h using an Exfo Omnicure S2000 light source, whereby 57% of the light intensity has a wavelength of 395-445 nm and 43% is 320-390 nm with a total intensity between 400 and 800 mW/cm^2, depending on the desired height of the structure. Subsequently the samples were cooled to room temperature. The height of the structures depends on the initial sample thickness and illumination intensity. Flat surfaces were prepared with the same illumination parameters but in the absence of a mask. In the case of the flat non-illuminated sample, the same treatment is performed, but the sample was partially covered to prevent light to reach the sample during the illumination step, allowing direct comparison between illuminated and non-illuminated samples.

Characterization of LCN surfaces.

Surface profiles were measured using a Sensofar PLμ 2300 optical profilometer in confocal mode equipped with a 50x objective. UV-Vis measurements were performed on a Perkin Elmer Lambda 750 UV-Vis-NIR spectrophotometer equipped with a 150 mm integrating sphere containing a lead sulfide (PbS) and photomultiplier tube (PMT) detector. Contact angle measurements were performed on a Dataphysics OCA 30 at room temperature using deionized water as the probe liquid.
Roughness measurements were performed either on an Asylum Research MFP-3D-Bio or NT-MDT Solver P47 Pro atomic force microscope (AFM) equipped with a Bruker NCHV tip (f_0 = 320 kHz, k = 42 N/m) in non-contact/tapping mode to measure the topography (height and phase); scanning by tip. Data analysis was performed using Gwyddion software and the roughness measured as the root mean square (RMS) height variation in the measured area. Intermodulation AFM (ImAFM) was performed on a Dimension Icon AFM (Bruker Corp.), coupled with an external multi-frequency lock-in amplifier (Intermodulation Products AB) to analyze the nano-mechanical properties of the samples, performed by Hailu G. Kassa. A silicon cantilever (Bruker RTESPA-30) with a stiffness of 40 N/m and a resonance frequency (ω) of 300 kHz was used. The resolution of all ImAFM images taken are 512 x 512 pixels. The working principle of ImAFM and the methodology[26–30] we used to extract the nanoscale mechanical properties can be found elsewhere.[31]

In situ roughness modulation.

All biological cell experiments were performed by G. Koçer. For in situ switching experiments on flat surfaces (where permanent changes were induced on the surface roughness in the presence of cells), cells were seeded on a non-illuminated surface and cultured for 1 day. Before illumination of the surface, live cell imaging was performed in order to derive cell speed and cell migration patterns. The sample was illuminated from the bottom continuously for 10 min at room temperature where light penetration measurements indicated that cells were exposed to 390-440 nm light (blue light) at 35 mW cm^{-2}. Then, cells were again brought to normal culture conditions and monitored, in order to derive cell migration behavior. In order to analyze cell migration patterns and speed after illumination, cells were monitored for 12h for their viability and then 1h trajectories of individual cells were determined (for 6 cells).

Reversible and irreversible structures.

To measure the topographies during illumination, digital holographic microscopy (DHM, Reflection DHM® Lyncée Tec) was used. For illumination, two LED's (Thor labs, 365 nm, UV 675 mW/cm^2 and blue 455 nm, 57 mW/cm^2) were used. The UV-illumination was performed from the bottom using an UV-mirror (Thor Labs) to direct the light to the sample. This light is not collected by the DHM, since there is a cut-off filter (<400nm) in place. The blue light illumination was performed under an angle from the top, as this part is not filtered from the DHM.

6.3 Results and discussion

The preparation of the responsive LCN coatings (Figure 6.1) is given in Figure 6.2a. A mixture of (meth)acrylate functionalized azobenzene and liquid crystalline monomers (Figure 6.1) are used to create a chiral nematic phase that is subsequently aligned in plane by shear forces and then photo-polymerized. Mask illumination of the films leads to local *trans* to *cis* isomerization of azobenzene molecules in the network resulting in a local formation of structures (volume generation) in the illuminated areas yielding (hierarchical) topographical cues for cells (Figure 6.2).[25,32] These surface topographies can be rendered permanent by modifying the LC mixture.[32] Cell adhesion and migration was studied either on surfaces with pre-defined (fixed) microscale topographical cues or on surfaces where at a specific point in time the surface structure is changed in situ. By using a mask containing a hexagonal pattern, hexagonally arranged pillars (HP) are formed. The height of the HPs is determined for cellular studies in the micrometer scale by conveniently varying the illumination dose (intensity). A series of surfaces is prepared with pillars ranging in height from 0.2 to 1.6 μm, having a diameter of 20 μm and spaced 20 μm from each other as is verified using optical profilometry (Figure 6.2 b,c), abbreviated as HP-x μm, where HP

denotes the orientation (hexagonal pillars) and the number of µm the height of the pillars. Other patterns re achieved using other masks, such as circular patterns (CP) of *e.g.* 15 µm in width and separation and with a height of 0.3 µm (CP-0.3), demonstrating the versatility of this method to fabricate topographical polymeric biointerfaces (Figure 6.2d). As control surfaces to the films with microscale topographies, 'flat' (with respect to microscale) LCN surfaces are used that are or are not entirely illuminated (Flat_i or Flat_ni). Upon illumination the morphology of the film alternates, which is verified by a change in the absorbance properties of the polymer films, as can be found elsewhere.[31]

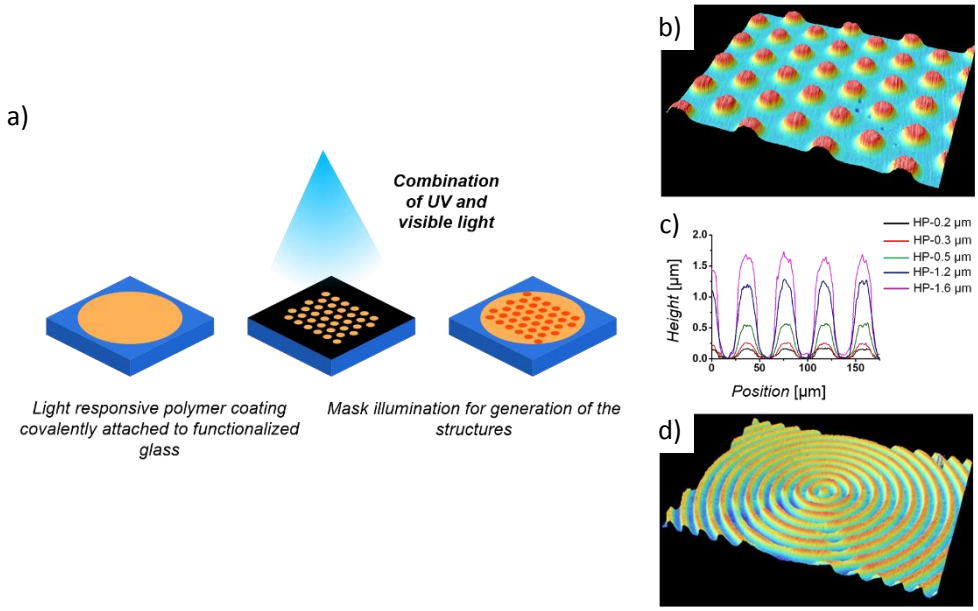

Figure 6.2. Encoding topography in films using light in LCNs to harness cell behavior. a) Schematic representation of the method to fabricate HP topographies in LCN films by using a patterned mask and b) 3D representation of a HP surface. c) Height profiles of the used HP surfaces. d) 3D representation of the CP surface.

To identify the effect of illumination in the absence of a mask, AFM measurements on Flat_ni and Flat_i surfaces are performed and reveal an increase in surface roughness on the illuminated areas changing from 9.9 ± 0.9 nm to 18.2 ± 0.4 nm showing that the nanoscale topography is changed upon illumination (Figure 6.3 d,e). It should be noted that the formation of pillars further increase the nanoroughness (*vide infra,* Figure 6.3). The surfaces are hydrophobic irrespective of illumination with contact angles of 88 ± 1° and 101 ± 4° for Flat_ni and Flat_i, respectively. In order to facilitate protein adsorption and hence cell adhesion on these surfaces, all the LCN films are incubated and coated with serum proteins overnight before performing the cell experiments.

To measure the effect of cell adhesion on the surfaces, the well-established cell lines of NIH3T3 fibroblasts is used, as it is informative in revealing adhesion related cellular processes.[3,18] Adhered NIH3T3 fibroblast cells and their supported growth on all the

fabricated LCN surfaces validate the biocompatibility of these LCN films similar to polystyrene, which is commonly used for cell cultures. From time-lapse imaging experiments, single cell migration behavior and the mean cell migration speed (total distance covered per time of measurements) is determined (Figure 6.3g). A decrease from the initial mean cell migration speed of 0.85 µm/min on flat LCN films to 0.32 µm/min on flat illuminated surfaces is observed, while qualitatively no changes in cell morphology is visible.[31] These observations can be related to the increase in nanoscale surface roughness upon illumination, as measured using AFM (9.9 ± 0.9 nm vs. 18.2 ± 0.4 nm, for Flat_ni vs. Flat_i, respectively, Figure 6.3 d,e). It is known that cells are able to sense nanoscale features down to 8 nm and distinguish the size of the features by their nanopodial extensions. Yet, studies also show that in general cell attachment is also influenced by changes in mechanical properties.[3,7,33] Therefore, the mechanical properties of the surface is also measured. This is both performed for a Flat_ni, Flat_i and structured surface and described in the next paragraph.

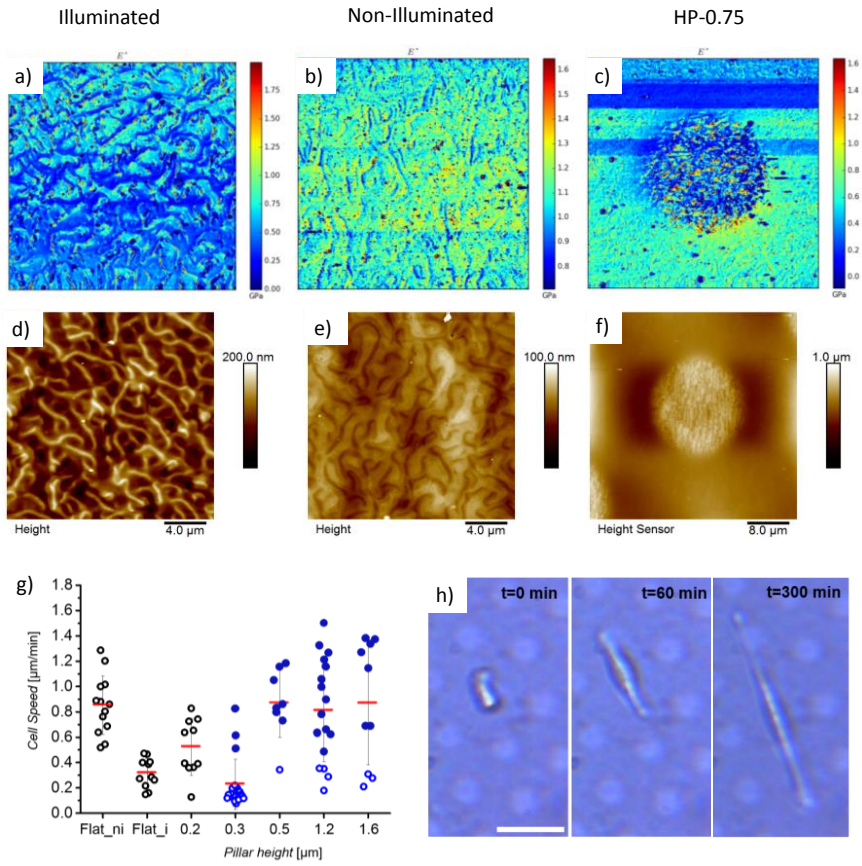

Figure 6.3. (a-c) Intermodulation AFM measurements and surface profile AFM measurements (d-f) of the illuminated (a,d), non-illuminated (b,e) and pillared structure (c,f), showing the difference in stiffness and roughness. g) Overview of the cell speed at the various formed surface structures. h) Single cell measured for 300 minutes spreading on a 0.3 µm pillar, showing aligning of a cell over this structure.

To gain more insight in the nanoscale topographical and mechanical properties of the pillars and surrounding areas, a hierarchical structured HP-0.75 µm film is imaged using intermodulation atomic force microscopy (ImAFM) (Figure 6.3 a-f). Height and roughness on top of the pillars and in their surrounding areas are determined and compared to flat_i surfaces. Illumination of flat films results in a ca. 20 nm nanoscale roughness. The surfaces of illuminated pillars are found also more rough (55 nm) compared with the non-illuminated surrounding areas (10 nm). These results verified that we have fabricated hybrid interfaces presenting light-induced topographical patterns with significantly increased nanoscale roughness. ImAFM inspections also reveal simultaneously the nanoscale mechanical properties of the surface of the pillars and their surrounding areas (Figure 6.3). Figure 6.3c is a typical effective elastic modulus map showing an average effective elastic modulus (ca. 0.5-0.75 GPa) of the surfaces of illuminated pillars, which is lower than non-illuminated surrounding areas (ca. 1.2 GPa). Even though the elastic modulus decreased upon illumination, we believe that both illuminated and non-illuminated areas present stiff matrices to cells to a similar extent due to their high elastic modulus (in GPa) compared to elastic natural matrix (elastic modulus ranging from a few hundred Pa to a few hundred kPa). Forces generated by cells are in the range of 1-5 nN μm^{-2} and cells would need to pull against and deform the underlying substrate to be able to sense and respond to stiffness. Therefore, our hierarchical interfaces allow us to relate the effect of nanoscale roughness and micron scale topographical cues independently of the stiffness of the surfaces.

The derived mean cell migration speeds on LCN films with the HP topographical cues reveal that surfaces with 0.3 µm high pillars (HP-0.3 µm) induced a significantly lower mean cell speed of 0.23 µm/min when compared to the HP-0.5, HP-1.2 and HP-1.6 surfaces, which have a mean cell speed of 0.87, 0.81 and 0.87 µm/min, respectively (Figure 6.3g). Interestingly, the latter topographies induce cell speeds in the same range as observed on the non-illuminated flat LCN films while the cell speed observed on the HP-0.3 topography is similar to that on the illuminated flat LCN films. The mean cell speed of 0.52 µm/min observed on HP-0.2 topographies represents an intermediate case (vide infra). As a control surface for cell adhesion and migration, a speed of 0.55 µm/min is observed on classical tissue culture polystyrene surfaces, which lies in between the values observed for both flat LCN surfaces.

Most notable are the consequences for cell migration behavior when switching from flat surfaces to a HP-0.3 topography. Cells on HP-0.3 topographies are adherent and residing only on the pillars, mainly elongating over the pillars for extended periods of up to 5h (see Figure 6.3h and corresponding article),[31] in agreement with the observed contact of cellular protrusions on the rougher pillars. In contrast, cells on the flat LCN surfaces, irrespective of illumination, are spreading, but not elongated, which is typical for cell morphologies on 2D surfaces.[31] This clearly points towards topography guided cell morphology, which is known to influence cell motility.[1,5–7] Interestingly, even though cells are residing on illuminated parts of the topographic films, presumably due to increased roughness, the mean

cell migration speed of the cells on HP-0.3 significantly drops further to 0.15 μm/min when comparing to the cell migration speed of 0.32 μm/min on flat, illuminated films (Figure 6.3g). The migration pattern plots for HP-0.3 topographies reveal that this category of cells become even more static with lower and less frequent changes observed in cell speed.[31] In strong contrast, cells on HP-1.2 topographies yielded a dramatic shift in the cell migration pattern to a highly dynamic behavior with increasing frequencies and magnitudes of changes in cell migration speed over time.

Next to the HP topographic patterned films, single cell behavior is also imaged and analyzed on the CP topographies of comparable heights and spacing as the HP patterns (Figure 6.2d). This analysis similarly reveals that cells aligning on the patterns of 0.3 μm in height and 15 μm spacing.[31] These results show that cell adhesion and migration speed is guided on a different surface geometry indicating that the observations are generic, although the speed on these structures is slightly higher (0.6 μm/min), likely caused by several outliers in the mean cell speed. When correcting for this, a mean speed of again 0.3 μm/min is observed. These results demonstrate also the versatility of employing light responsive LCN films as new biointerfaces to direct cell movement and migration speed.

To explore the possibility to guide cell migration and collect these migrating cells in local spots, the following surface topographic pattern is designed. Films are prepared with flat, non-illuminated areas surrounded by HP-1.1 topographies, achieved by a hand-made chromium mask (Figure 6.4a-b). With previous results in mind, one could expected that the cells have similar speed do not show a preference for either the flat or the pillared surface, as the speed was similar. However, much to our surprise, the majority of the cells (82%, 9 out of 11 cells that are monitored for 4h) starting from the pillar area, entered the flat area and remained in this area with a spread morphology (Figure 6.4c). This shows that not only roughness, but a hierarchical structured surface is required for both cell adhesion and alignment, showing both the possibility to control the localization and adhesion of the cell population through cell migration on these surfaces, which has important implications in colonization of cells on biomaterials to enhance their performance.[19,20]

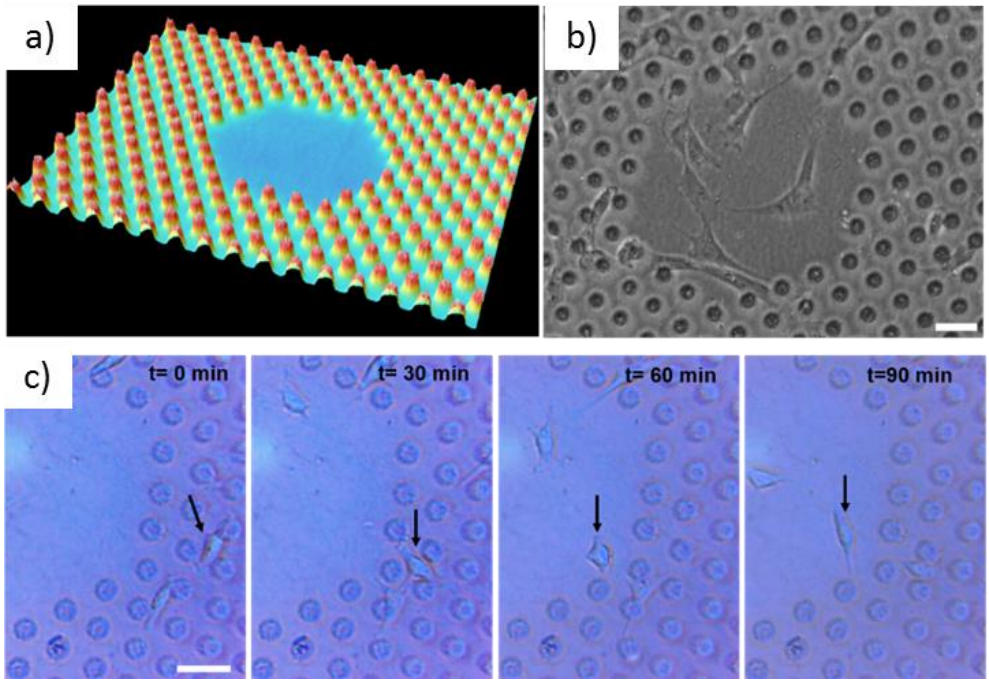

Figure 6.4. Spatial and temporal switches in cell behavior on the same LCN surface. a) 3D representation of the mixed surface with a Flat_ni region surrounded by HP-1.1 topographies b) Phase contrast image of NIH3T3 cells on LCN surfaces presenting a flat not illuminated area surrounded by 1.1 μm high HPs after 3 days of culture. c) Live cell imaging for a representative cell going from the pillar area to the flat area (scale bar: 50 μm).

Previous experiments are all performed by first forming the surface structure, followed by cell culturing. However, cells strongly respond to dynamic surfaces, which requires in situ modulation of the surface. Therefore we also investigated response of cells to dynamic surfaces. Before seeding the cells on the surface, the roughness of the unexposed material is measured. Subsequently the cells are seeded and illuminated. For this type of experiments, a critical consideration is the biocompatibility of the illumination dose.[13] Illuminating the film from the bottom in presence of the cells and performing light penetration measurements using an intensity detector showed no UV penetration through the samples to the cells indicating that the UV light is absorbed by the film. According to this measurement, the films are exposed to light of λ = 390-440 nm for 10 min (35 mW cm^{-2}). After removal of the biological material, AFM is performed to measure the effect of the illumination. According to AFM measurements on this sample an increase in surface roughness from 9.0±1.2 to 11.1±2 nm occurs,[31] indicating that a change in cell migration can be expected.[3,7,34]

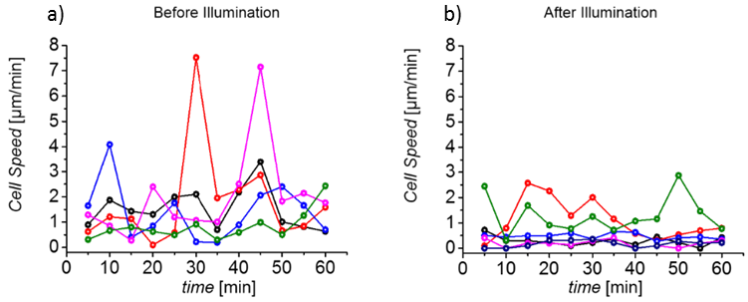

Figure 6.5. In situ switch in cell migration patterns on flat LCN surfaces as change in single cell speed at every 5 min before illumination a) and after illumination b). Cells are present on the sample during illumination.

After illumination of the sample in presence of the cells, the sample is monitored for 12h before measuring the cell migration speed, to observe and confirm their viability after illumination. Live cell imaging data reveals that 87% of the cells remain viable within this time. Changes in cell migration speed occur less frequent and to a smaller extent with a decrease in mean cell speed from 1.21 to 0.54 µm/min after illumination showing. This shows a shift towards a more static behavior (Figure 5 a,b). These observations are in accordance with the ex-situ experiments where speed decreases when increasing the roughness.

In order to study reversibility of light responsive topographies on LCN films, patterned polymer films are made containing hexagonal patterned cholesteric liquid crystal (CLC) pillars embedded in isotropic surrounding, forming a preprogrammed surface, as there is a difference in expansion between CLC and isotropic regions. As stated before, changing the composition (Figure 6.1, molecule 7), more specifically the inhibitor concentration, reversible and irreversible light switchable topographies are made, either with 0% or 4.4% inhibitor by a 2 step polymerization, as shown by Liu *et al.*[32] To form the preprogrammed surface, a hexagonal patterned mask is placed directly on the non-polymerized monomeric liquid crystal mixture. The sample is polymerized for 6 s to form the cholesteric pillars. Then the sample is flipped, placed on a heating stage of 120°C and again illuminated to polymerize the isotropic matrix for 1 minute. The mask was removed using a razorblade. Initial heights in the structure of 130 nm are observed, as this is a negative print of the hexagonal chromium pattern on the mask (Figure 6.6a). Polymerization induced diffusion is observed, as can be seen by the presence of the typical "bunny ear structures"

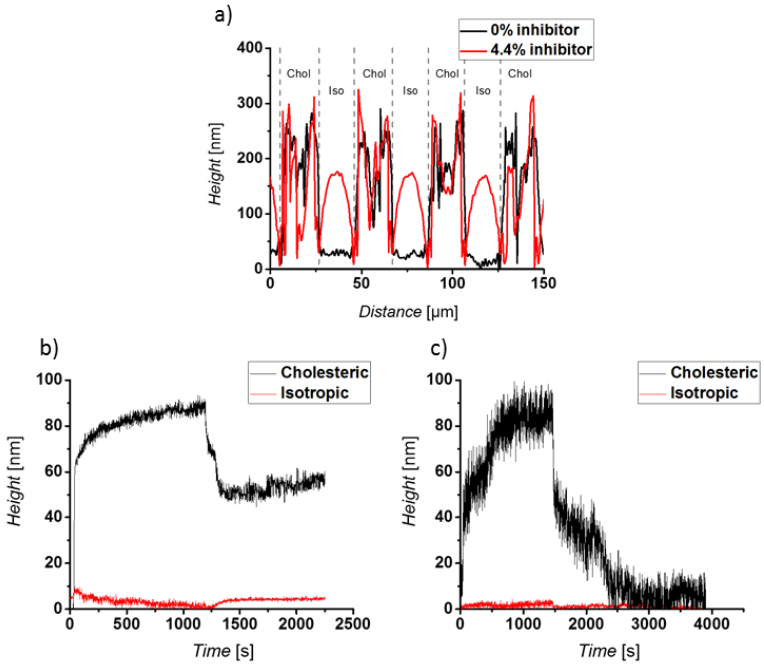

Figure 6.6. a) Height differences of the samples containing 0% and 4.4% inhibitor before light induced structure formation. The low parts are isotropic (iso) regions, while the high parts are cholesteric (chol) pillars. The height difference of a sample where simultaneously a cholesteric (black) and isotropic (red) part of the sample is measured on a permanent sample (b) and a reversible sample (c). After reaching a plateau, the UV lamp (365 nm) is switched off (first dip in the height) and several minutes later the blue LED (455 nm), resulting in a drop in height in both cases.

For these experiments a different light source is used, as the Exfo Omnicure S2000 lamp is not compatible with the DHM set-up. Therefore, a 365 nm and a 405 nm LED is used instead. The surface is monitored for 30 seconds before switching on the LEDs. When switching on both LEDs, a rapid increase in the surface height difference is observed for the cholesteric pillars, while the isotropic matrix stays constant.[35,36] A "plateau" is reached at roughly 600 s, where the rapid grow starts to diminish (Figures 6.6 b,c). In both cases, the height difference is roughly 90 nm. When the 365 nm LED is switched off, in both cases a decrease in height is observed. When switching off the 405 nm LED, a further decrease in height is observed. In case of the film containing inhibitor a permanent topography is obtained with a height difference of roughly 55 nm (Figure 6.6b), while for the film without inhibitor the sample goes back to its initial topography (Figure 6.6c). This shows that in principle these materials are capable of forming reversible structures which are of interest for cell culturing. However, at this point in time, the used wavelengths and doses are in conflict with the biocompatibility.

6.4 Conclusion

In conclusion, liquid crystalline polymer networks form an interesting material to generate hierarchical structured surfaces. Not only does this study results in more insight of hierarchical structures and mechanical properties, it is also found that cell motility patterns can be switched from static to highly mobile by increasing the height of the pillars or from dynamic to moderately static by increasing the nanoscale roughness. In situ temporal experiments further demonstrate the effect of nanoscale changes. Preliminary experiments on patterned LCN surfaces show that it is also possible to form photo-switchable (reversible) topographies on demand at the nanoscale which is another important step for in situ control of cell behavior. These results demonstrate a new approach in engineering bio-instructive light responsive surface structures. Future experiments should aim at in situ reversible studies as well as manipulation of microscale topographies where light responsive elements that are switchable at longer wavelengths can be used to match the volume generation properties with cytocompatible illumination doses.[37] The freedom that is offered in this system will enable scientists to generate materials that are more closely recapitulating the dynamic natural microenvironment not just giving better insights in fundamental biological processes but will also enable us to enhance biomaterial performance for regenerative medicine applications.

6.5 References

1 M. Nikkhah, F. Edalat, S. Manoucheri and A. Khademhosseini, *Biomaterials*, 2012, **33**, 5230–5246.
2 M. J. Dalby, N. Gadegaard, R. Tare, A. Andar, M. O. Riehle, P. Herzyk, C. D. W. Wilkinson and R. O. C. Oreffo, *Nat. Mater.*, 2007, **6**, 997–1003.
3 M. J. Dalby, N. Gadegaard and R. O. C. Oreffo, *Nat. Mater.*, 2014, **13**, 558–569.
4 J. Le Digabel, A. Richert, P. Hersen and M. Ghibaudo, *Biophys. J.*, 2009, **97**, 357–368.
5 F. Viela, D. Granados, A. Ayuso-sacido and I. Rodríguez, *Adv. Funct. Mater.*, 2016, **26**, 5599–5609.
6 B. D. Kim, C. Seo, K. Han, K. W. Kwon, A. Levchenko and K. Suh, *Adv. Funct. Mater.*, 2009, **742**, 1579–1586.
7 R. J. Petrie, A. D. Doyle and K. M. Yamada, *Nat. Rev. Mol. Cell Biol.*, 2009, **10**, 538–549.
8 M. Guvendiren and J. A. Burdick, *Adv. Healthc. Mater.*, 2013, **2**, 155–164.
9 M. T. Lam, W. C. Clem and S. Takayama, *Biomaterials*, 2008, **29**, 1705–1712.
10 D. M. Le, K. Kulangara, A. F. Adler, K. W. Leong and V. S. Ashby, *Adv. Mater.*, 2011, **23**, 3278–3283.
11 T. Gong, K. Zhao, G. Yang, J. Li, H. Chen and Y. Chen, *Adv. Healthc. Mater.*, 2014, **3**, 1608–1619.
12 A. Agrawal, O. Adetiba, H. Kim, H. Chen, J. G. Jacot and R. Verduzco, *J. Mater. Res.*, 2015, **30**, 453–462.
13 A. M. Rosales and K. S. Anseth, *Nat. Rev. Mater.*, 2016, **1**, 15012.
14 M. J. Salierno, A. J. García and A. Campo, *Adv. Funct. Mater.*, 2013, **23**, 5974–5980.
15 C. M. Kirschner and K. S. Anseth, *Small*, 2013, **9**, 578–584.
16 C. Rianna, A. Calabuig, M. Ventre, S. Cavalli, V. Pagliarulo, S. Grilli, P. Ferraro and P. A. Netti, *ACS Appl. Mater. Interfaces*, 2015, **7**, 16984–16991.
17 R. Barillé, R. Janik, S. Kucharski, J. Eyer and F. Letournel, *Colloids Surfaces B Biointerfaces*, 2011, **88**, 63–71.
18 C. Rianna, L. Rossano, R. H. Kollarigowda, F. Formiggini, S. Cavalli, M. Ventre and P. A. Netti, *Adv. Funct. Mater.*, 2016, **26**, 7572–7580.
19 D. A. Lauffenburger and A. F. Horwitz, *Cell*, 1996, **84**, 359–369.
20 X. Yao, R. Peng and J. Ding, *Adv. Mater.*, 2013, **25**, 5257–5286.
21 T. J. White and D. J. Broer, *Nat. Mater.*, 2015, **14**, 1087–1098.
22 D. Liu, C. W. M. Bastiaansen, J. M. J. den Toonder and D. J. Broer, *Angew. Chemie*, 2012, **51**, 892–896.
23 J. E. Stumpel, D. Liu, D. J. Broer and A. P. H. J. Schenning, *Chemistry*, 2013, **19**, 10922–10927.
24 D. Liu, C. W. M. Bastiaansen, J. M. J. den Toonder and D. J. Broer, *Langmuir*, 2013, **29**, 5622–5629.
25 D. Liu and D. J. Broer, *Nat. Commun.*, 2015, **6**, 1–7.

26 D. Platz, E. A. Tholén, D. Pesen and D. B. Haviland, *Appl. Phys. Lett.*, 2008, 3–5.
27 D. Forchheimer, D. Platz, E. A. Thol and D. B. Haviland, *Phys. Rev. B*, 2012, **85**, 195449.
28 D. B. Haviland, D. Platz, D. Forchheimer and E. A. Thole, *Nat. Commun.*, 2013, **4**, 1360.
29 D. Platz, D. Forchheimer, E. A. Tholén and D. B. Haviland, *Beilstein J. Nanotechnol.*, 2013, **4**, 45–56.
30 D. Platz, D. Forchheimer, E. A. Thol and D. B. Haviland, *Nanotechnology*, 2012, **23**, 265705.
31 G. Koçer, J. ter Schiphorst, M. Hendrikx, H. G. Kassa, P. Leclère, A. P. H. J. Schenning and P. Jonkheijm, *Adv. Mater.*, 2017, **29**, 1606407.
32 D. Liu, C. W. M. Bastiaansen, J. M. J. den Toonder and D. J. Broer, *Macromolecules*, 2012, **45**, 8005–8012.
33 L. E. Mcnamara, T. Sjöström, K. Seunarine, D. Meek, B. Su and M. J. Dalby, *J. Tissue Eng.*, 2014, **5**, 1–5.
34 I. Biol, D. Moratal, R. O. C. Oreffo, M. J. Dalby and M. Salmero, *Integr. Biol.*, 2012, **4**, 531–539.
35 M. Hendrikx, A. P. H. J. Schenning and D. J. Broer, *Soft Matter*, 2017, **13**, 4321–4327.
36 M. Hendrikx, A. P. H. J. Schenning, M. G. Debije and D. J. Broer, *Crystals*, 2017, **2**, 1–20.
37 N. Q. Balaban, U. S. Schwarz, D. Riveline, P. Goichberg, G. Tzur, I. Sabanay, D. Mahalu, S. Safran, A. Bershadsky, L. Addadi and B. Geiger, *Nat Cell Biol*, 2001, **3**, 466–472.

Chapter 7

Technology assessment

Abstract. This chapter describes the technological assessment of the developed light responsive polymers, ranging from applications to scope and limitations of the materials described in this thesis, followed by future recommendations. For example, light-responsive materials have found their use in microfluidic systems, allowing precise control over the flow speed, but have also demonstrated limitations, such as the requirement of neutral and clean water. Furthermore, light-responsive liquid crystals have shown their uses in structured surfaces, but actuation requires harsh illumination conditions.

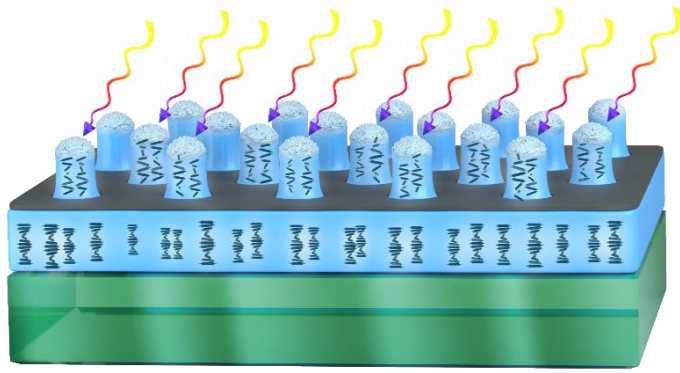

This chapter is partially reproduced from:

'Light-responsive polymers for microfluidic applications' J. ter Schiphorst, J. Saez, D. Diamond, F. Benito-Lopez and A.P.H.J. Schenning, *Lab Chip*, 2018, **18**, 699-709.

7.1 Introduction

A number of light responsive polymers were discussed in this thesis. The molecule to device approach utilizing the entire chain of knowledge is used as a strategy to reach new components both on the molecular level, by making new light responsive triggers, as well as developing new devices and principles, such as the oscillating light responsive hydrogels (Figure 7.1).

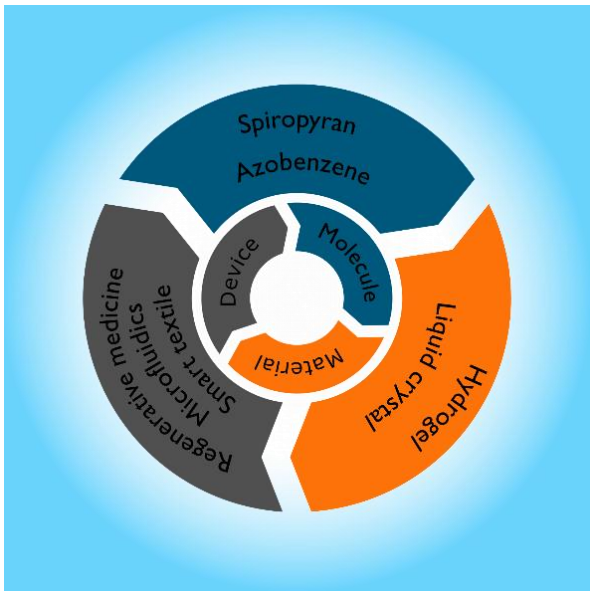

Figure 7.1. Schematic representation of the molecule to device approach applied in this thesis, showing a symbiotic interplay between the molecules (blue), materials (orange) and devices (gray). The results of the device study is used as a new input for development of new molecules. The outer ring summarizes the molecules, materials and devices that were created and described in this thesis.

During this research, new molecules and materials are generated and applied. By designing new spiropyran-based molecules containing acrylates, photoswitches that alternate from a ring opened to a ring closed structure and *vice versa*, the isomerization kinetics are brought into balance. The ring closing and opening are now on the same time scale. This is in great contrast to previous systems, where there was a significant mismatch between these two events. By tuning the molecular kinetics, several properties of the material are improved including the swelling kinetics, which are reduced from hours to minutes/seconds.[1–3] This switching can be further improved by further tuning the isomerization kinetics. However, several more fundamental limitations of responsive shape changing materials remain. With hydrogels, soft materials are achieved with high volume changes based on the absorption and release of solvents, while on the other end of the spectrum, glassy liquid crystal materials with low volume changes generated by order/disorder are employed. There seems to be an inherent difficulty in achieving a material with high volume change without the use

of a solvent. Finding a balance in this material paradox will be interesting for a large range of applications, both in microfluidics as well as many other possible disciplines.
In this technology assessment, first microfluidic systems will be discussed as this is the main application of light responsive polymers used in this thesis. Then the combination of responsive polymers with common polymers is discussed. Finally, the challenge for the next generations of light responsive polymers are discussed. Two main challenges will be discussed; the first being actuation without solvent while having large deformations (*vide infra*). The second challenge will be the use of visible light and bistable properties in photo responsive polymers.

7.2 Microfluidic systems

Microfluidic devices allow the manipulation of fluids and their embedded analytes with high precision and consistency throughout the network of channels. However, external components are often required to run these delicate processes, including pumps, valves and mixers. It is shown that several of these components can be simplified using light responsive hydrogels. Using these materials, valves and mixers are created that allow flow control of individual channels, which can be extended to large parallel processes, where multiple of these components are required for a single system.
The challenge is to create microfluidic systems with much more sophisticated functionality than current approaches, but at an affordable or ideally dramatically reduced unit cost. We believe that this can be achieved with light responsive polymers and that they will play an important part in microfluidic devices. The ability to use a non-contact form of stimulation and control events in the fluidic system is very attractive as it is inherently non-invasive, and could simplify fabrication. Hereby the main field of interest is expected to form itself around low cost large scale applications, where inspiration should be drawn from biomimetic systems. Reliability will be key to generate these large scale applicability and idealistically a system that is self-aware of its conditions, and can autonomously self-maintain, repair and regulate, would appear to be needed.
Light responsive materials might find difficulties to compete to existing mechanical components in means of mechanical stability, but will excel in their use for mass parallel systems. The possibility to combine computational platforms with cheap LED technology, and precise control over the gel size is exciting and a field of research that is currently under-exposed. To develop the next generation of analytical devices, a molecule to device approach should be used. New molecules are designed to fulfil the requirements of a material. These materials are integrated into a (microfluidic) device. Hereby the main topics are represented as materials, sensing, microfluidics and integration. These fields are currently experiencing a dramatic rate of continuous innovation and provide the highest potential of forthcoming breakthroughs for a technological revolution. Big steps towards truly developing these devices and in-field employment will only continue when there is close collaboration between scientists in various scientific disciplines and commercial

entities to create the next generation of light responsive microfluidic devices.
As stated in Chapter 1, there is a drive to produce cheap and widely employable valves to create a network of sensors that are in contact with each other to communicate the quality of our environment. Major steps towards creating these systems are made, as it is shown that inexpensive hydrogel valves can be generated. Cheap and small LEDs are used as a trigger for light responsive microvalves, requiring both minimal capital investment and energy input for maximal accuracy. Despite the tremendous improvements in valves that operate in minutes/seconds rather than hours with both high accuracy and full control over flow speed described in chapters 2 to 4, there are still limitations. For instance, the requirement of water and absorption of the analytes used for the tests limits the use of these materials for precise analytic systems. To overcome these problems, additional technological break-troughs are required, which can be achieved by decoupling the valve from the material that is being analyzed by placing a flexible protective layer such as a membrane, for instance. Combining this membrane with the valve would allow the normal swelling and shrinking needed for flow manipulation, while utilizing an externally located reservoir for the hydration of the material. The valve is demonstrated to be integratable in a laboratory test set-up, but further steps to achieve a higher technology readiness level are required to form a market-implementable device followed by market introduction. At this stage, the focus should be on stability, reproducibility and development of a production process that may be automated and is scalable.
Light responsive hydrogels have also shown their use in micromixers. With these first steps, the principle of a switchable mixer is shown. However, there are also several possibilities for improvement, especially in the manufacturing process. Currently these devices are generated one at a time, using a laborious and time-intensive multi-step fabrication process. With the knowledge that this device is not yet developed enough for implementation, further research on manufacturing this device consistently would be appealing. This will allow for a mixer that can be tuned to the same degree as the current microvalve, where full control over the behavior of the device is achieved using pulsating light.

7.3 Common polymers combined with light responsive polymers

A new application of light responsive polymers is shown in Chapter 5, where spiropyran containing hydrogels are grafted from a surface for water collection. For this application, the mechanical characteristics of the device is less problematic than the valves. In this thesis it is shown that light responsive cotton can be made and used for absorbing and releasing humidity. These materials are of interest for both water collection, as well as humidity control. When grafting these materials onto either natural or polymeric fibers or woven materials, a hybrid material combining the mechanical properties of the carrier with the responsive properties of the hydrogel is formed. As these materials are based on the absorption of water, they might find their use in water harvesting, the extraction of pollution from water (such as ions, dyes, or other chemicals) or as a humidity control element for

interior spaces. Furthermore, these systems could, for instance, find use where irrigation of wine is strictly controlled, such as in the Duoro valley of Portugal. In such regions, the temperature range and humidity are high enough that the natural fog can be collected and used for grape crop growth.

7.4 Light responsive materials having large deformations

A method to achieve materials that show large deformations, which is not based on absorption and release of a solvent is the use of liquid crystalline elastomers.[4] Incorporation of spiropyran in liquid crystal elastomers would be very interesting, as the liquid crystal elastomers are mechanically more stable than hydrogels, but are capable of deforming more than a glassy network. In case of the isomerization of spiropyran, a large change in polarity takes place, which is in contrast to azobenzene based systems, where an order/disorder mechanism is dominating. This might lead to large deformations of the elastomer. Initial experiments are performed with spiropyran-based structures designed with both a flexible spacer as well as a rigid core, expected to be compatible with liquid crystals (Figure 7.2 a).

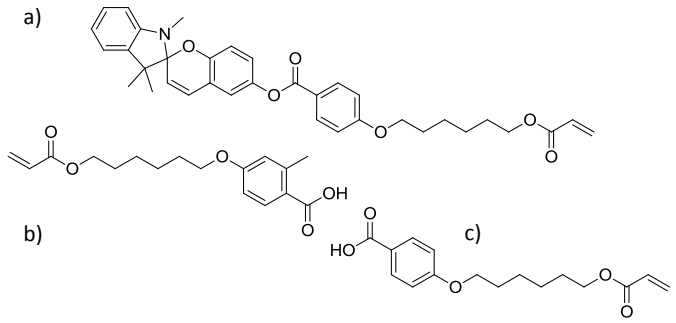

Figure 7.2. a) Spiropyran based molecule with compatibility in liquid crystalline structures, as it contains a rigid core as well as flexible spacer. (b,c) 6OBAM b) and 6OBA c), liquid crystalline monomers containing a carboxylic acid group used as proton donor.

This spiropyran molecule (Figure 7.2 a) is incorporated in a liquid crystal matrix (Figure 7.2 b,c), where the carboxylic acid groups from the molecules are used as internal proton donors to stabilize the protonated merocyanine form.[5] However, it is found that the sole presence of these acid containing moieties in a glassy liquid crystal is not sufficient to stabilize the protonated merocyanine form. As a proof of principle, trifluoroacetic acid in tetrahydrofuran is used to open the spiropyran in this network and switching with light becomes possible. These initial results are promising making materials where a change in charge is required, or where longer wavelengths are required to trigger actuation of the material.

7.5 Visible light responsive and bistable polymers

For hydrogels, spiropyran is most commonly used, since hydrogels are found to respond stronger to a polarity change, which is limited in azobenzenes. However, in the case of liquid crystals, azobenzene is the most used molecule to induce light responsive behavior. It can be aligned in the liquid crystal network, copolymerized as a crosslinker and actuated using polarized light, as the absorption in an oriented network is polarization selective. The current challenge is to activate these materials with light of lower intensity and longer wavelengths, to create materials that can be used, but are not limited to biological applications.

Currently, harsh illumination conditions are often required to form surface protrusions, using UV irradiation with intensities up to 1 W/cm^2.[6–8] These intensities can damage the polymer and limit the applicability of these materials in, for instance, biomedical applications, as living cells often are unable to withstand these kind of conditions. Furthermore, the thermal component required to initiate actuation of these materials often is significant, as shown in the recent work of Gelebart *et al.*,[9,10] where oscillation and movement of objects by LC-based actuators could be accomplished at specific illumination conditions by transforming the incident light into heat. To overcome these limitations caused by using highly intense UV sources, illumination with less intense light sources and longer, more biological-friendly wavelengths are desired.

Furthermore, in biological applications a single experiment can take several hours. It is therefore of great interest to achieve bistable structures, meaning that in the timeframe used for an application, a structure can be written or erased using two different stimuli, which do not need to remain 'on' during the time required to perform the experiment. This can be two wavelengths of light, for instance, where the first wavelength is used to form the structures and a second wavelength is used to erase the structures. This is in line with current research where fluorinated azobenzenes are used as a material showing two stable isomers. As shown by Bleger *et al.*,[11] visible light switches using long-lived *z* isomers are available, and in this work they are used for the first time in a liquid crystalline network to form bistable surface protrusions. These azobenzenes show a bathochromic shift in the *trans* absorption wavelength, compared to the *cis* isomer, allowing isomerization with wavelengths in the visible light spectrum. Therefore, *trans* to *cis* isomerization is achieved using green light (530 nm), while *cis* to *trans* isomerization is achieved using blue light (405-455 nm).

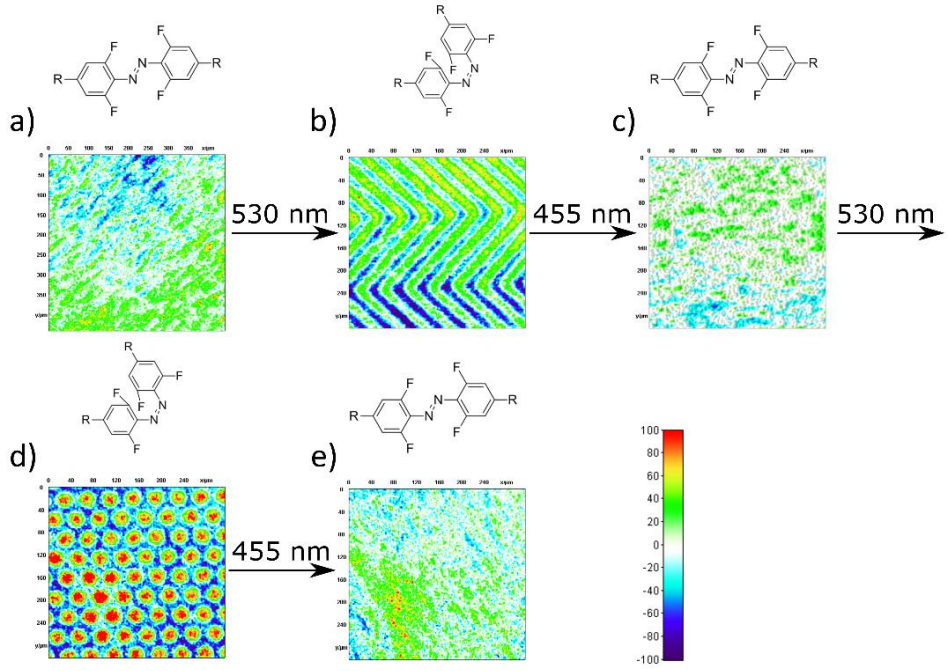

Figure 7.3. Digital holographic microscope image (250x250 μm^2) of a flat cholesteric liquid crystal film containing a fluorinated azobenzene a) before illumination, b) after mask exposure with green light, c) after exposure to blue light, d) after exposure with a different mask and e) after blue light exposure, showing the reversibility and rewritability of this material. The scale bar is the height in nanometers, where red is +100 nm, white is 0 nm and blue is -100 nm.

When combining a liquid crystalline network similar to that used in Chapter 6 with the fluorinated azobenzene, formation of structures is achieved using less than 10 mW/cm^2 green light, while erasing is achieved with less than 1 mW/cm^2 blue light (Figure 7.3). The future recommendations would be to expand the possibilities of this system. To date, only small surface structures have been generated, as a large part of the thermal component necessary for generating large structures is absent. With only order/disorder differences to form structures, 200 nm architectures are generated. This may not appear significant, but these height changes appear to be in the same range as described in Chapter 6, where large effects on cell behavior are found for structures between 0 and 300 nm. Therefore, these materials may be used for biological applications, where biocompatible doses of light are required to understand the effect of a changing matrix on living cells. Liquid crystalline elastomers may result in larger deformations, while remaining the biocompatible illumination conditions, as they show large dimensional changes while remaining harder than a hydrogel.[4]

7.6 Conclusions

In conclusion, light responsive polymers in this thesis present a unique opportunities to create materials and devices, reducing the costs and size tremendously. By further developing these polymers as discusses in this chapter, the next generation of these materials will lead to new applications for a bright future and proved that light can be used to set matter in motion. Given the impact of these polymers, an exciting continuation in this field of science and commercialization is foreseen. I hope this thesis will inspire scientists working in the fields of mechanical engineering, materials science, analytical and organic chemistry, and microfluidics to work together and deliver creative solutions to these issues, and thereby greatly expand the possibilities for light responsive polymers in the future.

7.7 References

1 C. Delaney, P. Mccluskey, S. Coleman, J. Whyte, N. Kent and D. Diamond, *Lab Chip*, 2017, **17**, 2013–2021.

2 S. Coleman, J. ter Schiphorst, A. Ben Azouz, S. Bakker, A. P. H. J. Schenning and D. Diamond, *Sensors Actuators B Chem.*, 2017, **245**, 81–86.

3 J. ter Schiphorst, S. Coleman, J. E. Stumpel, A. Ben Azouz, D. Diamond and A. P. H. J. Schenning, *Chem. Mater.*, 2015, **27**, 5925–5931.

4 T. J. White and D. J. Broer, *Nat. Mater.*, 2015, **14**, 1087–1098.

5 L. T. de Haan, J. M. N. Verjans, D. J. Broer, C. W. M. Bastiaansen and A. P. H. J. Schenning, *J. Am. Chem. Soc.*, 2014, **136**, 10585–10588.

6 G. Koçer, J. ter Schiphorst, M. Hendrikx, H. G. Kassa, P. Leclère, A. P. H. J. Schenning and P. Jonkheijm, *Adv. Mater.*, 2017, **29**, 1606407.

7 D. Liu, C. W. M. Bastiaansen, J. M. J. den Toonder and D. J. Broer, *Angew. Chemie*, 2012, **51**, 892–896.

8 D. Liu, C. W. M. Bastiaansen, J. M. J. den Toonder and D. J. Broer, *Macromolecules*, 2012, **45**, 8005–8012.

9 A. H. Gelebart, D. J. Mulder, M. Varga, A. Konya and G. Vantomme, *Nature*, 2017, **546**, 632–636.

10 A. H. Gelebart, G. Vantomme, E. W. Meijer and D. J. Broer, *Adv. Mater.*, 2017, **29**, 1606712.

11 C. Knie, M. Utecht, F. Zhao, H. Kulla, S. Kovalenko, A. M. Brouwer, P. Saalfrank, S. Hecht and D. Bléger, *Chem. - A Eur. J.*, 2014, **20**, 16492–16501.

Curriculum Vitae

Jeroen was born on April 4th, 1990, in Arnhem. After finishing HAVO at the Jeroen Bosch College in 's-Hertogenbosch, he studied Chemistry at Fontys University of Applied Science. After an internship at MagnaMedics B.V. and a graduation project at Eindhoven University of Technology, he graduated in 2011. Subsequently, he started the master program Chemical Technology at Eindhoven University of Technology, specializing in the Molecular Engineering track and finished his master thesis in 2014 in the Functional Organic Materials and Devices group chaired by Prof. dr. Dick Broer and Prof. dr. Albertus Schenning. During this course of time, he was employed by Merck (former Peer+) twice during the summer holidays. From 2014 he started a PhD project at the Technische Universiteit Eindhoven in the Functional Organic Materials and Devices group under the supervision of Prof. dr. Albertus Schenning. The most important results of this research are described in this thesis. Concurrently, in 2017 Jeroen co-founded "Lusoco B.V.", a TU/e spin-off company focusing on the development of high-tech printed Luminescent Solar Concentrators for aesthetic energy harvesting. In his role as Chief Technology Officer (CTO) he focusses on the development of the ink and electronics.

Publications related to this work

- *Light-responsive Materials for Microfluidic Applications.*
  ter Schiphorst, J., Saez, J., Diamond, D., Schenning, A.P.H.J. & Benito-Lopez, F. (2018), Lab on a Chip, 18, 699-709 (review).
- *Photoresponsive Polymer Hydrogel Coatings that Change Topography.*
  Stumpel, J.E., ter Schiphorst, J. & Schenning, A.P.H.J. (2017), Wiley-WCH, Book chapter 7, 159-173. ISBN: 978-3-527-33869-6.
- *Tuning microfluidic flow by pulsed light oscillating spiropyran-based polymer hydrogel valves.*
  Coleman S., ter Schiphorst, J., Ben Azouz, A., Bakker, S., Schenning, A.P.H.J. & Diamond, D. (2017), Sensors and Actuators, B: Chemical, 245, 81-86.
- *Photoresponsive passive micromixers based on spiropyran size-tunable hydrogels.*
  ter Schiphorst, J., Melpignano, G.G., Eslami Amirabadi, H., Houben, H.J.M., Bakker, S., den Toonder, J.M.J. & Schenning, A.P.H.J. (2017), Macromolecular Rapid Communications, 39, 1700086 (cover article).
- *Light-Responsive Hierarchically Structured Liquid Crystal Polymer Networks for Harnessing Cell Adhesion and Migration.*
  Koçer, G., ter Schiphorst, J., Hendrikx, M., Kassa, H.G., Leclère, P., Schenning, A.P.H.J. & Jonkheijm, P. (2017), Advanced Materials, 29, 1606407 (cover article).
- *Dual light and temperature responsive cotton fabric functionalized with a surface-grafted spiropyran-NIPAAm-hydrogel.*
  ter Schiphorst, J., van den Broek, M., de Koning, T., Murphy, J.N., Schenning, A.P.H.J. & Esteves, A.C.C. (2016), Journal of Materials Chemistry A, 4(22), 8676-8681 (cover article).

- *Molecular design of light-responsive hydrogels, for in situ generation of fast and reversible valves for microfluidic applications.*
  ter Schiphorst J., Coleman, S., Stumpel, J.E., Ben Azouz, A., Diamond, D. & Schenning, A.P.H.J. (2015), Chemistry of Materials, 27(17), 5925-5931 (cover article).

Non-related work

- *Rapid energy transfer enabling control of emission polarization in perylene bisimide donor-acceptor triads.*
  Menelaou, C., ter Schiphorst, J., Kendhale, A.M., Parkinson, P., Debije, M.G., Schenning, A.P.H.J. & Herz, L.M. (2015), The Journal of Physical Chemistry Letters, 6(7), 1170-1176.
- *Effect of the ortho-alkylation of perylene bisimides on the alignment and self-assembly properties.*
  Dasgupta, D., Kendhale, A.M., Debije, M.G., ter Schiphorst, J., Shishmanova, I.K., Portale, G. & Schenning, A.P.H.J. (2014), ChemistryOpen, 3(4), 138-141.
- *Dichroic perylene bisimide triad displaying energy transfer in switchable luminescent solar concentrators.*
  ter Schiphorst, J., Kendhale, A.M., Debije, M.G., Menelaou, C., Herz, L.M. & Schenning, A.P.H.J. (2014), Chemistry of Materials, 26(13), 3876-3878.

Acknowledgement

Congratulations. You have managed to reach the last section of this thesis. Thank you for reading it from the start, and I hope you enjoy and appreciate the work described. The final pages of this thesis will be used to thank the large group of people that I collaborated with, worked with, and mostly, with whom I enjoyed my PhD.

Allereerst wil ik prof. Albert Schenning bedanken voor al zijn steun en advies. Rond 2011 ben ik als HBO student bij SFD begonnen en vervolgens niet meer weg gegaan. Hiermee zit ik bijna even lang bij SFD als jijzelf. Ik wil je bedanken voor de mogelijkheid een PhD onderzoek in deze groep te doen. Ook voor alle grappen en nieuwe benamingen voor moleculen (bakstenen) en het overnemen van mijn vocabulaire voor hoge intensiteit lampen (bouwlampen). Als al het andere faalt, kunnen we altijd nog op de bouw aan de gang, aangezien we het vak jargon al goed beheersen. Al denk ik dat jij vooral "adviseert" en ik het fysieke werk mag uitvoeren (ja, m'n kapstok hangt eindelijk en ook nog eens waterpas).

Ik wil prof. Dick Broer bedanken voor de mogelijkheid altijd binnen te wandelen met vragen en de bereidheid de tijd te nemen om deze onderwerpen te bespreken. Ik denk niet dat er iemand is die meer kennis heeft op het gebied van vloeibare kristallen en die dit zo helder en gedetailleerd kan uitleggen. Ook wil ik je bedanken voor de correcties van mijn proefschrift.

Ik wil prof. Jaap den Toonder bedanken voor alle samenwerking en mij te verwelkomen in zijn groep alsof ik een van zijn eigen promovendi was. Ik wil je bedanken voor alle keren dat ik uitgenodigd ben om mee te gaan naar Glow en de groepsuitjes. Ook wil ik je bedanken voor alle discussies die geleid hebben tot het afronden van hoofdstuk 4 en de bijbehorende publicatie.

I would like to thank prof. Dermot Diamond first of all for being a great project coordinator. I believe that the entire NAPES project would not have gone as smooth as it did without your coordination. Also, I would like to thank you for providing a very open and welcome atmosphere whenever I visited your group, bringing me to the Gravediggers, and providing me with enough Guinness! I also would like to provide you the last chance (Angela, please convince him!) to finally bring your fiddle, the legendary instrument that was spoken about so often, but until now I've never been able to listen to. Angela Lally, thank you for coordinating the project and helping me during the visits at Dublin. I appreciate all the nice dinners and talks.

Ik wil Luc Scheres bedanken voor zijn bereidheid deel te nemen in mijn promotie commissie. Ook wil ik je bedanken voor de introductie bij SFD en de praktische vaardigheden die ik vandaag de dag nog steeds gebruik. Ook wil ik Jan van Geldrop bedanken, die mij bij Luc heeft geïntroduceerd.

I would like to thank dr. Rafal Klajn for his willingness to participate in my committee. Your work has been a great inspiration during my PhD work and your review was an excellent starting point for me on this new topic.

I would like to thank dr. Danqing Liu for the fruitful discussions regarding responsive liquid crystalline materials, as well as being part of my promotion committee.

Ik wil prof. Nico Sommerdijk bedanken voor het voorzitten van mijn promotie zitting.

I would like to thank dr. Catarina de Carvalho Esteves for the supervision and guidance of the students Tom and Merijn. Also I would like to thank you for being part of my promotion committee.

To all members of the NAPES project, I would like to thank you for all nice discussions, trips and scientific collaboration. In particular Simon Coleman, Aymen Ben Azouz, Colm Delaney and Peter McCluskey, with whom I collaborated closely resulting in the development of the microfluidic set-up used in chapter 2 and 3. Simon, a special word of thank to you, for the friendship that was built during the last years. I would also like to thank Fernando Benito-Lopez and Janire Saez for all the great times and our latest accomplishment in the form of a nice review.

To Gülistan Koçer and Pascal Jonkheijm, thank you for the biological experiments resulting in Chapter 6. Gülistan, your hard work and precision is of admirable quality. It resulted in a close collaboration which I hope continues between our groups after finishing my research.

To Hailu Kassa and Philippe Leclère, thank you for the AFM measurements and interpretation, resulting in the figures displayed in Chapter 6. It has greatly improved the quality of the publication and chapter, as well as giving new insight for the mechanism of the cell adhesion.

Ellen en Matthew, bedankt voor de samenwerking resulterend in de zichtbaar licht responsieve materialen die naar voren komen in hoofdstuk 7.

Cees Bastiaansen, Johan Lub, and Michael Debije, thank you for your guidance over the years and ensuring that the quality delivered by the group is always high. To Michael, thank you for the corrections in my thesis, and your guidance and discussions on LSCs. We are glad to have you as an advisor and will make sure that this device finally gets commercialized.

I also would like to thank all current and past members of SFD and microsystems, who made my PhD a great experience. I will not make a list of names, since I know myself too well and I will most likely forget people, but you all know who I'm talking about. Thank you for your help, discussions and collaborations.

A special word of thank to Jelle, Monali and Wei with whom I've shared the office with great pleasure for the last four years. Jelle, bedankt voor de afgelopen jaren. Je bent een zeer uniek en wonderbaarlijk persoon in alle positieve manieren van deze

woorden. Bedankt voor de hulp aan vooral het begin van mijn onderzoek. Monali, it has been a great pleasure to talk about both work and non-work related topics. I wish you all the best for your defense short after. Wei, thank you for sharing your visits to China and I would also like to wish you all the best with your PhD research.

Eveneens wil ik de studenten die onder mijn supervisie een project hebben uitgevoerd bedanken. Anouk, Hao-Liang, Menno en Sterre, bedankt voor jullie hulp op het gebied van hydrogels, resulterend in de hoofdstukken 2 t/m 4 en de bijbehorende publicaties. Merijn en Tom, bedankt voor jullie hulp met het project om hydrogels op katoen te graften resulterend in hoofdstuk 5 en de bijbehorende publicatie. Zonder de hulp van jullie allen was dit proefschrift er niet geweest. Lex, Marx, Maxime en Renee, bedankt voor jullie hulp op het gebied van LSCs. Zonder jullie input, was de technologische vooruitgang bij lange na niet zo voorspoedig verlopen.

Marjolijn, bedankt voor te veel om op te noemen. Enkele voorbeelden zijn: de mogelijkheid om altijd binnen te lopen met werk gerelateerde vragen, het altijd bereid zijn te helpen, het geven van advies, het beoordelen of een cover wel of niet mooi is en het draaiend houden van de groep. Ik wil je hiervoor oprecht bedanken.

Bardo en Tom, Ik wil jullie bedanken voor jullie rol als paranimf. Ik wil jullie ook persoonlijk bedanken voor de vriendschap van de afgelopen jaren, alle discussies over auto's en motoren en het sporten. Ook de rit in Limburg op de motor moeten we zeker nog een keer over doen.

Henk Eding, jij hebt zeker een plekje in mijn dankwoord verdient. Ooit heeft Luc mij de eerste keer meegenomen en op het hart gedrukt, dat 's-ochtends bij jou koffie drinken van essentieel belang is. Dit heeft geleid tot een ritueel waar ik elke dag naar uit kijk. Bedankt voor alles wat er besproken is. Bardo, Bas, Bas, Margot, Rene en Robin, jullie ook bedankt hiervoor. Er is geen betere start van de dag.

Giuseppe, ondanks dat ik weet dat je dit nooit zal lezen, wil ik je toch bedanken. In een korte tijd zijn we vanuit een samenwerking van collega's tot vrienden uitgegroeid. Ik zal je vriendelijkheid, bereidheid te helpen, intelligentie en goede gesprekken nooit vergeten. We hebben het wel eens over onze toekomstplannen gehad om een eigen bedrijf te beginnen en ik ga de stap wagen. Ik zou willen dat jij hier ook bij geweest zou zijn.

Teun Wagenaar, bedankt dat je samen met mij het avontuur aan wil gaan en Lusoco wil opzetten. Henry Sprenkels, bedankt dat je bij dit team hoort en we gaan er iets fantastisch van maken.

Mijn ouders, Alex en Susan, bedankt voor alles wat ervoor gezorgd heeft dat ik de persoon ben die ik nu ben. Aan mijn broers Tom en Nick, hun vrouwen Joyce en Lucienne en natuurlijk mijn neefje Tim. Bedankt voor alles, voor alle keren dat ik bij jullie ben komen eten en alle support. Zonder jullie had ik dit niet voor elkaar gekregen.